Regulation of CP12-mediated carbon metabolism by NTRC during cold acclimation

Dissertation

Zur Erlangung des Grades eines Doktors der Naturwissenschaften

an der Fakultät für Biologie

der Ludwig-Maximilians-Universität München

vorgelegt von

Jing Tsong Teh

München, 09 August 2021

Erstgutachter: Prof. Dr. Joerg Nickelsen

Zweitgutachter: Prof. Dr. Peter Geigenberger

Tag der Einreichung: 09 August 2021

Tag der mündlichen Prüfung: 22 November 2021

TABLE OF CONTENT

ABSTRACT

In plant and algal chloroplasts redox regulation is essential for the rapid adaptation of metabolism in response to changing light conditions. NADPH-dependent thioredoxin reductase C (NTRC) is known as an alternative to the classical ferredoxin-thioredoxin system mediating these regulatory processes. By deriving reducing potential from NADPH, NTRC can function in both light and dark conditions, unlike the ferredoxin-thioredoxin system which is obligately light-dependent. Despite extensive studies of NTRC have been carried out in higher plants, not much is known in algae.

In this study, the role of NTRC in the green alga *Chlamydomonas reinhardtii* during cold acclimation which was previously attributed to the chaperone functions of NTRC was scrutinized (Moon et al., 2015). The site-specific mutation analyses of the redox-active site of NTRC, however, revealed that the cold-sensitive phenotype displayed by *ntrc* loss-of-function mutants is redox-dependent instead. By means of co-immunoprecipitation and mass spectrometry, a redox- and cold-dependent binding of the Calvin Cycle Protein 12 (CP12) to NTRC was identified. The study was then extended to the vascular plant *Arabidopsis thaliana* and demonstrated via *in vitro* redox activity analyses that recombinant NTRC from *C. reinhardtii* reduces CP12 of both *C. reinhardtii* and *A. thaliana* and vice versa.

CP12 is a scaffold protein joining two Calvin cycle enzymes, namely the phosphoribulokinase (PRK) and the glyceraldehyde-3-phosphate dehydrogenase (GAPDH), to form an auto-inhibitory supracomplex of around 550 kDa. Therefore, the complex integrity in the *ntrc* knockout mutant was studied. Although *NTRC* deletion caused no detectable changes in the complex integrity in *C. reinhardtii*, dissociation of the PRK/CP12/GAPDH complex was impeded in *A. thaliana*. Further, *in vitro* treatment of *C. reinhardtii* lysate with NADPH-activated recombinant NTRC also demonstrated that the enzyme induces dissociation of the complex. A more direct evidence is provided by the less pronounced cold-induced elevation of GAPDH enzyme activity in *C. reinhardtii ntrc* knockout and cysteine-substituted mutants, in comparison to the wild type. Taken together, these results demonstrate that NTRC reduces CP12 and hence triggers the dissociation of the PRK/CP12/GAPDH complex. This is crucial under cold stress to release the enzymes for catalytic activities and regenerate $NADP^+$ for the removal of excess electrons from the photosynthetic electron transport chain (ETC). Doing so can prevent reactive oxygen species (ROS) formation via the Mehler reaction wherein electrons from the ETC are accepted by oxygen.

Next, *C. reinhardtii cp12* knockout mutants were generated using CRISPR/Cas9 technique to study CP12 directly. As observed for the *ntrc* knockout mutant, the generated mutants also exhibited a cold-sensitive phenotype. Surprisingly, knockout of *CP12* led to robust decreases in both PRK and GAPDH protein accumulations implying a protein protection effect of CP12 besides inhibiting the

enzymes activities. Both functions are critical for CP12 to prepare a repertoire of enzymes which are protected from degradation and simultaneously poised to spontaneous activation in response to environmental changes.

Additionally, the *C. reinhardtii cp12* knockout strains also exhibited a defect in growth during the light-dark cycle. Time course PRK and GAPDH enzyme activity analyses demonstrated that *cp12* knockout mutants experienced a delay in suppressing the Calvin cycle during the dark phase. However, as *ntrc* knockout and cysteine-substituted mutants did not display a growth defect in the light-dark cycle, a regulation of CP12 by NTRC during the diurnal rhythm is highly unlikely. Instead, redox-regulation of CP12 during the diurnal cycle can be taken over by the ferredoxin-thioredoxin

In conclusion, this study discovered that contrary to previous studies, NTRC-mediated cold acclimation is redox-dependent. Further, CP12 was identified as a redox target of NTRC which was previously undiscovered. Although NTRC and CP12 have both been previously described independently to be involved in cold acclimation, the molecular mechanisms behind this have not been fully understood. This is the first report demonstrating interactions between these two proteins, and the regulation of the Calvin cycle enzymes by NTRC under cold stress, via CP12.

ZUSAMMENFASSUNG

In Pflanzen- und Algenchloroplasten ist die Redoxregulation essentiell für eine schnelle Anpassung des Stoffwechsels als Reaktion auf wechselnde Lichtbedingungen. Die NADPH-abhängige Thioredoxin-Reduktase C (NTRC) ist als eine Alternative zum klassischen Ferredoxin-Thioredoxin-System bekannt, durch das diese Regulationsprozesse vermittelt werden. Im Gegensatz zum Ferredoxin-Thioredoxin-System, dass obligat lichtabhängig ist, ist die NTRC durch Nutzung des Reduktionspotentials des NADPHs sowohl unter Licht- als auch unter Dunkelbedingungen funktional. Obwohl umfangreiche Studien über die NTRC in höheren Pflanzen vorliegen, ist in Algen nicht viel über dieses Enzym bekannt.

In dieser Studie wurde die Rolle der NTRC in der Grünalge *Chlamydomonas reinhardtii* während der Kälteakklimatisierung untersucht, welche zuvor auf die Chaperonfunktion der NTRC zurückgeführt wurde (Moon et al., 2015). Ortsspezifische Mutationsanalysen des aktiven Zentrumsder Thioredoxin-Domäne der NTRC zeigten jedoch, dass der kälteempfindliche Phänotyp, den *ntrc loss-of-function* Mutanten aufweisen, stattdessen redox-abhängig ist. Mit Hilfe von Co-Immunopräzipitation und Massenspektrometrie wurde die redox- und kälteabhängige Bindung des Calvin-Zyklus-Proteins 12 (CP12) an die NTRC nachgewiesen. Anschließend wurde die Studie auf *A. thaliana* ausgeweitet und mittels *in vitro* Redox-Aktivitätsanalyse gezeigt, dass die NTRC aus *C. reinhardtii* sowohl das CP12 Protein aus *C. reinhardtii* als auch in *A. thaliana* reduziert und umgekehrt.

CP12 ist ein Gerüstprotein, das zwei Calvin-Zyklus-Enzyme, nämlich die Phosphoribulokinase (PRK) und die Glyceraldehyd-3-Phosphat-Dehydrogenase (GAPDH), zu einem autoinhibitorischen Suprakomplex von etwa 550 kDa verbindet. Daher wurde die Integrität des Komplexes in *ntrc-knockout*-Mutante untersucht. Obwohl der Verlust der NTRC in *C. reinhardtii* keine nachweisbaren Veränderungen der Komplexintegrität verursachte, war die Dissoziation des PRK/CP12/GAPDH-Komplexes in *A. thaliana* beeinträchtigt. Weiterhin zeigte die *in vitro* Behandlung von *C. reinhardtii* Lysat mit NADPH-aktivierter rekombinanter NTRC, dass das Enzym die Dissoziation des Komplexes induziert. Einen direkteren Beweis liefern die beobachteten Abnahmen der kälteinduzierten Erhöhungen der GAPDH-Enzymaktivitäten in *C. reinhardtii ntrc-knockout* und Cystein-substituierten Mutanten im Vergleich zum Wildtyp. Zusammengenommen zeigen diese Ergebnisse, dass die NTRC CP12 reduziert und damit die Dissoziation des PRK/CP12/GAPDH-Komplexes auslöst. Dies ist unter Kältestress entscheidend, um die Enzyme für katalytische Prozesse freizusetzen und $NADP^+$ für den Abtransport von überschüssigen Elektronen aus der photosynthetischen Elektronentransportkette (ETC) zu regenerieren. Dadurch kann die Bildung von reaktiven Sauerstoffspezies (ROS) über die Mehler-Reaktion, bei der Elektronen aus der ETC von Sauerstoff aufgenommen werden, verhindert werden.

Zur weiteren Untersuchung des CP12 Proteins aus *C. reinhardtii* wurden mit Hilfe der CRISPR/Cas9-Technik *cp12-knockout*-Mutanten erzeugt. Die generierten Mutanten zeigten ebenso wie die *ntrc-knockout*-Mutant einen kälteempfindlichen Phänotyp. Überraschenderweise führte die Abwesenheit von CP12 zu einer starken Abnahme der PRK- und GAPDH-Proteinakkumulation, was neben der Hemmung der Enzymaktivitäten auf einen Proteinschutz-Effekt von CP12 hindeutet. Beide Funktionen sind entscheidend dafür, dass CP12 ein Repertoire an Enzymen bereitstellt, die einerseits vor Abbau geschützt und andererseits für eine spontane Aktivierung als Reaktion auf Umweltveränderungen bereit sind.

Zudem wurde bei den *C. reinhardtii cp12 knockout*-Stämmen ein Wachstumsdefekt im Licht-Dunkel-Zyklus festgestellt. Zeitverlaufsanalysen der PRK und GAPDH Enzymaktivitäten zeigten, dass *cp12-knockout*-Mutanten eine Verzögerung bei der Unterdrückung des Calvin-Zyklus während der Dunkelphase erfahren. Nichtsdestotrotz zeigten *ntrc-knockout* und Cystein-substituierte Mutanten keinen Wachstumsdefekt im Tagesrhythmus, was die Regulation von CP12 während des Tagesrhythmus unwahrscheinlich macht. Stattdessen kann die Redox-Regulation von CP12 während des Tageszyklus durch das Ferredoxin-Thioredoxin-System erfolgen. Zusammenfassend konnte in dieser Studie abweichend von früheren Studien festgestellt werden, dass die NTRC-vermittelte Kälteakklimatisierung redoxabhängig ist. Darüber hinaus wurde CP12 als Redoxpartner der NTRC identifiziert, was bisher unentdeckt war. Obwohl sowohl für die NTRC als auch für CP12 eine voneinander unabhängige Rolle in der Kälteakklimatisierung beschrieben wurde, sind die zugrundeliegenden molekularen Mechanismen dieser Vorgänge noch nicht vollständig verstanden. Dies ist der erste Bericht, der Interaktionen zwischen diesen beiden Proteinen und die Regulierung der Calvin-Zyklus-Enzyme unter Kältestress durch die NTRC über CP12 zeigt.

I. INTRODUCTION

I.1. Photosynthetic CO_2 Assimilation

Oxygenic photosynthesis allows green organisms comprising plants, algae, and cyanobacteria to convert light energy into chemical energy which can be stored in organic compounds. The process takes place in chloroplasts of plants and algae or at plasma membrane infoldings of cyanobacteria. The endosymbiosis theory of the chloroplast origin has been widely accepted; the theory proposed that the chloroplast was originated from a cyanobacterium-like cell engulfed by a eukaryotic ancestor host cell happened 1.2-1.5 billion years ago (Mereschkowsky, 1905; Martin & Kowallik, 1999; for a review on endosysbiosis, read Gould et al., 2008). Sharing the same evolutionary origin (McFadden & van Dooren, 2004), photosynthesis, the key function of chloroplast and its mechanism are highly conserved across the green species.

Photosynthesis consists of a series of reactions which can be divided into two parts: light-dependent reactions and light-independent (or dark) reactions. The light-dependent reactions are carried out basically by light-harvesting complexes (LHCs) and the photosynthetic electron transport chain (ETC) composed of multi-protein complexes embedded in the thylakoid membrane of chloroplast (Nelson & Junge, 2015). Solar energy is absorbed by antenna pigments in the LHCs which then transfer the energy to the photosystem II (PSII) reaction center where an electron is excited and donated from a chlorophyll-*a* molecule. This initiates an electron flow from PSII to plastoquinone, the cytochrome b_6/f complex, plastocyanin and lastly photosystem I (PSI). It is vital to take note that the PSI core can also be excited by a photon from the LHC leading to a second release of an electron. In PSI, the electron is then accepted by a ferredoxin. In the other end, electrons lost from chlorophylls in PSII are eventually compensated from water molecules (H_2O) which get photolyzed by the oxygen evolving complex of PSII and release dioxygen (O_2), protons (H^+) and electrons (Shen, 2015).

There are two products of utmost importance generated from this electron flow. The first one is the cellular energy currency – adenosine triphosphate (ATP). When the electron flow along the ETC, protons are relocated from the stroma into the thylakoid lumen, generating a proton gradient across the thylakoid membrane. This electrochemical potential, as known as proton motive force (pmf), is later utilized by the ATP synthase complex to drive the endergonic phosphorylation reaction of adenosine diphosphate (ADP) to generate ATP (Hahn et al., 2018). The second product is NADPH, a molecule with high reducing potential. Reduced ferredoxins in the photosynthetic ETC can be re-oxidized by $NADP^+$ molecules which turn into NADPH. This process is catalysed by ferredoxin-$NADP^+$ reductase (FNR; Mulo, 2011). Both ATP and NADPH are essential to fuel the Calvin-Benson-Bassham cycle which represents the light-independent reactions of photosynthesis, to synthesize carbohydrates.

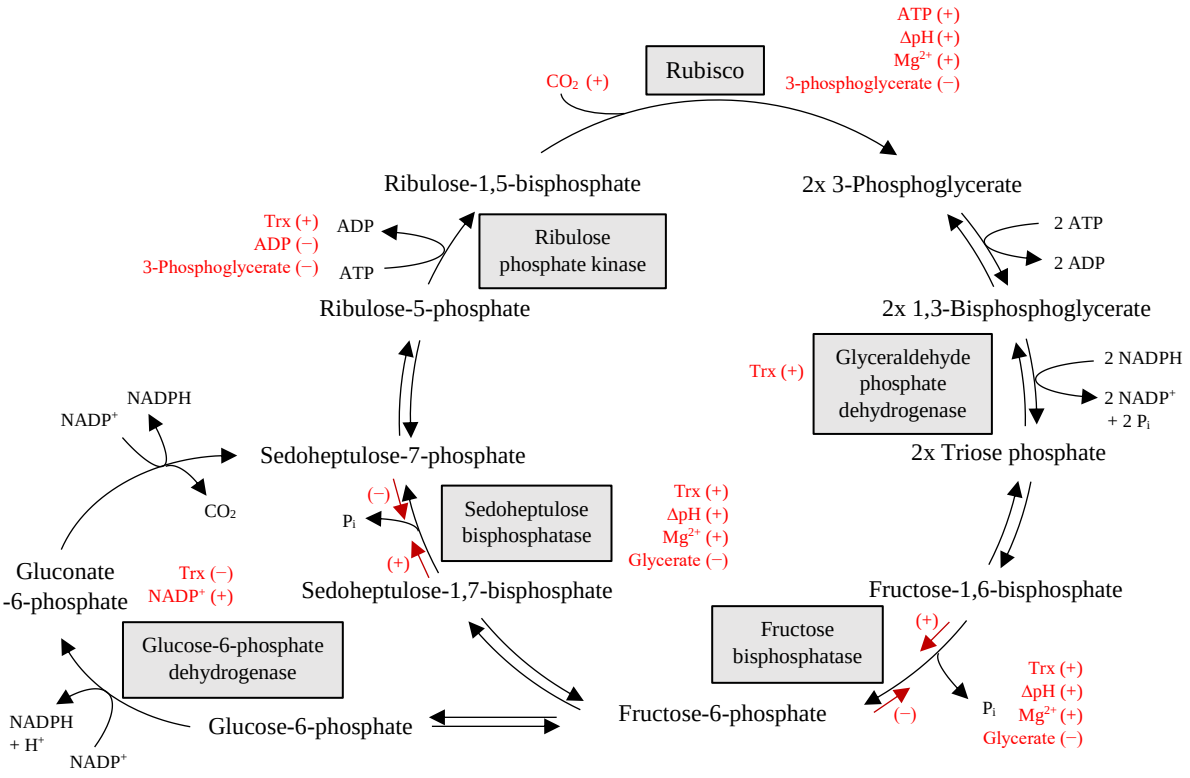

Figure 1: Overview of the Calvin cycle and oxidative pentose phosphate pathway (OPPP). The simplified scheme is a redrawn version from Heldt & Piechulla (2011). The main circle shows the Calvin cycle reactions, while the semicircle branched out from the cycle depicts the OPPP. Enzymes catalysing the reactions are enclosed in grey boxes, whereas regulators such as reduced thioredoxin (Trx), magnesium ions (Mg^{2+}), light-dependent alkalization (ΔpH) and metabolites are written in red. (+) and (−) denote activation and inhibition of enzymes respectively. Red arrows represent product feedback inhibition or substrate feedforward activation.

The Calvin-Benson-Bassham cycle, or simply Calvin cycle, takes place in the stroma of the chloroplast. It was first described in 1950 and named after the discoverers (Bassham et al., 1950). The reactions start from the carboxylation of ribulose-1,5-bisphosphate (RuBP), a 5-carbon compound, by carbon dioxide (CO_2), catalysed by the Ribulose-1,5-bisphosphate carboxylase-oxygenase (Rubisco). This leads to the production of an extremely unstable 6-carbon compound called 2-carboxy-3-keto-1,5-bisphosphoribotol (CKABP) which immediately splits into two molecules of 3-phosphoglycerate (3PGA), a 3-carbon compound. 3PGA is then phosphorylated into 1,3-bisphosphoglycerate (1,3BPGA) which in turn gets reduced into glyceraldehyde-3-phosphate (GAP). The reactions are catalysed by phosphoglycerate kinase (PGK) and glyceraldehyde-3-phosphate dehydrogenase (GAPDH) respectively, consuming ATP and NADPH molecules generated during the light-dependent reactions mentioned above. The resulted GAP can either be converted into glucose or undergo a series of enzyme catalysed reactions to replenish RuBP as shown in Figure 1 (Heldt & Piechulla, 2011). This RuBP regeneration gives the reactions a cyclical nature as denoted in its name (reviewed in Buchanan, 2016).

I.2. Redox Regulators in the Chloroplast

One of the main regulatory mechanisms to adapt enzyme activities in the chloroplast is by altering the interchangeable disulphides and thiol groups of cysteine residues of a target protein (König et al., 2012; Pérez-Pérez et al., 2017). This redox reaction leads to changes in the conformation and hence the activity of the protein thioredoxin (Trx) which is an oxidoreductase catalysing this reaction. There are two major Trx systems in the chloroplast, categorized based on their sources of reducing potentials – ferredoxin or NADPH. These are the ferredoxin-thioredoxin system and the NADPH-thioredoxin reductase-thioredoxin system as overviewed below in Figure 2.

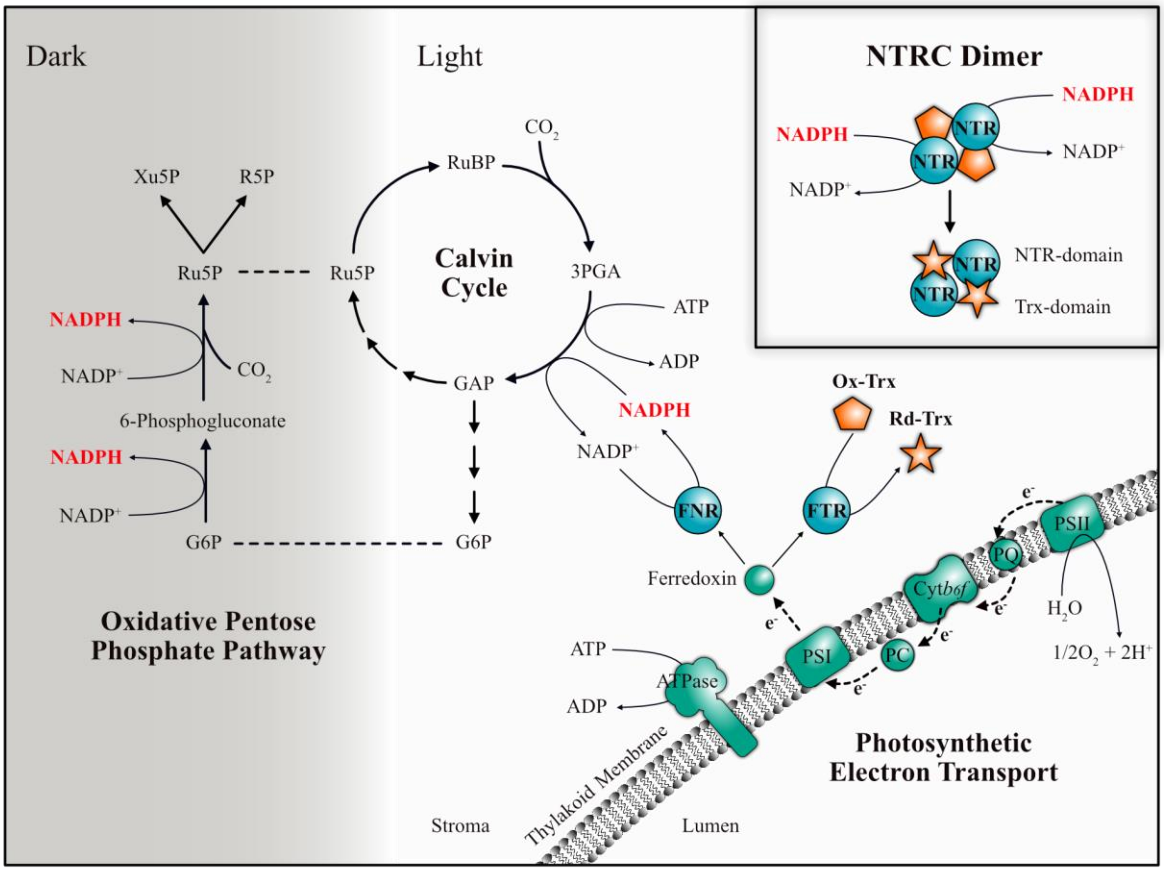

Figure 2: Schematic overview of redox regulators in the chloroplast – versatile thioredoxins and NTRC retrieving their reducing potentials. In the light, electron flow along the photosynthetic ETC, generating reduced ferredoxins. The reduced ferredoxin in turn reduces either a $NADP^+$ molecule or a versatile thioredoxin (Trx) protein via ferredoxin- $NADP^+$ reductase (FNR) or ferredoxin-thioredoxin reductase (FTR), respectively. NADPH molecules generated from the ETC during the light reactions of photosynthesis are either consumed by the Calvin cycle or utilized by the NTRC dimer as reducing power to serve its role as a redox regulator. NADPH are also generated in OPPP in dark allowing NTRC to function light-independently. Box in the upper right corner showing NTRC forms catalytic active dimer with each subunit consists of a $NADP^+$-thioredoxin reductase (NTR) domain and a thioredoxin domain. Antiparallel arrangement of the subunits enables cross-reduction activity between the subunits.

I.2.1. The Ferredoxin-Thioredoxin System

Redox regulations in the chloroplast are carried out by the ferredoxin-thioredoxin system via versatile thioredoxins (Laurent et al., 1964; Moore et al., 1964), a group of universal, small proteins of approximately 12 kDa in size (Holmgren & Bjornstedt, 1995; Collet & Messens, 2010). There are five isoforms of free thioredoxins in the chloroplast namely *f*, *m*, *x*, *y*, and *z* types, which reduce different sets of target enzymes. Trx-*x*, -*y* and -*z* are involved mainly in oxidative stress response while Trx-*f* and -*m* regulate a wide range of enzymes catalysing primary metabolic reactions in the chloroplast (Collin et al., 2003; Lemaire et al., 2003; Meyer et al., 2005; Lemaire et al., 2007).

A thioredoxin protein itself bears a disulphide formed by its Cys-Gly-Pro-Cys (CGPC) motif (Holmgren & Bjornstedt, 1995). This motif functions as catalytic active site for the reduction of disulphide bridge(s) in the target enzyme. After that, the thioredoxin regains its reducing potential from a ferredoxin molecule. In the light, electrons that are delivered by PSI lead to the reduction of ferredoxins in the chloroplast. As shown in Figure 2, reduced ferredoxins can then transfer the electrons to either: 1) $NADP^+$ molecules via FNR and generates NADPH as mentioned in section I.1 or 2) thioredoxins via ferredoxin-thioredoxin reductase (FTR) which is the case for Trx-*f*,-*m*,-*x*,-*y* and -*z* (Droux et al., 1987; Huppe et al., 1990).

Most of the downstream targets of chloroplast thioredoxins are redox-activated in the light and deactivated in the dark, correlating to its PSI/ferredoxin-dependent regeneration (Ruelland & Miginiac-Maslow, 1999; Schürmann & Jacquot, 2000; Schürmann & Buchanan, 2008). Hence, the thioredoxin-mediated redox regulation in the chloroplast was thought to be exclusively powered by ferredoxin, until the discovery of NTRC in *Oryza sativa* (rice) and *Arabidopsis thaliana* (Serrato et al., 2004).

I.2.2. The Alternate Redox Regulator – NTRC

NTRC is a nuclear encoded protein of about 55 kDa in size. It is a member of NADPH-thioredoxin reductases (NTR), flavoproteins with a bound FAD cofactor reducing thioredoxins by utilizing reducing power from NADPH instead of ferredoxin. Besides NTRC which presents in the chloroplast, there exist several other isoforms of NTRs in different cellular compartments. For instances, NTRA and NTRB in *A. thaliana* (homologous to NTR1 and NTR2 in *C. reinhardtii*, respectively) exist in the cytosol and mitochondria, reducing *h*-type and *o*-type thioredoxins, respectively (Serrato et al., 2004; Reichheld et al., 2005). A single NTRC encoding gene occurs in all nuclear genomes of higher plants and algae sequenced to date. However, heterogeneity has been observed in cyanobacteria wherein not all species carry the gene (Florencio et al., 2006; Pascual et al., 2011). Worth noting, other than chloroplast, NTRC has also been identified in other non-green plastids such as amyloplasts (Michalska et al., 2009; Kirchsteiger et al., 2012).

Largely different from other NTR proteins, NTRC has a thioredoxin domain at the C-terminus joined to its N-terminal canonical NTR domain (Serrato et al., 2004). Like other free chloroplastic thioredoxins, this thioredoxin domain also has its own set of downstream redox targets. NTRC has been reported in year 2006 to reduce and activate 2-Cys peroxiredoxin (PRX1) which in turn detoxifies hydrogen peroxide (H_2O_2) and protects the chloroplast from oxidative damages (Pérez-Ruiz et al., 2006). Further, when mixing recombinant NTRC variants with active site mutations in either the NTR domain or thioredoxin domain, the reduction activity of NTRC on PRX1 was partially recovered (Perez-Ruiz et al., 2009). Furthermore, native NTRC extracted from *A. thaliana* has been reported forming aggregates which dissociate into catalytic active homodimers in the presence of NAPDH (also in the presence of NADH or DTT; Perez-Ruiz et al., 2009). Together, these results led to the proposed model of autonomous regulatory NTRC homodimers (Figures 2 and 3) in which the two monomers are arranged antiparallelly so that the NTR domain of one monomer can cross-reduce and activate the thioredoxin domain of the other monomer (Perez-Ruiz et al., 2009; Wulff et al., 2011; Toivola et al., 2013).

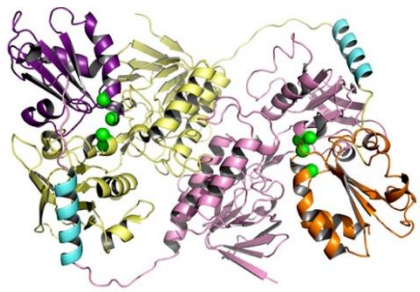

Figure 3: Structure model of *A. thaliana* NTRC homodimer. The model is a predicted homology model retrieved from Toivola et al. (2013) and was constructed by the authors based on reported crystal structure of the NTR-TRX complex of *Escherichia coli* (Lennon et al., 2000). The subunits are orientated anti-parallelly to each other so that the redox active cysteine residues (green) from NTR domains (yellow/ pink) and thioredoxin domains (orange/ purple) are brought in proximity for the reciprocal reduction to happen. Domains within a subunit are joined by an α-helical linker (blue).

I.2.3. Redox Targets of NTRC

Activities of all the versatile thioredoxins in the chloroplast (Trx-*f*, -*m*, -*x*, -*y* and -*z*) depend on FTRs which utilize ferredoxins as reducing powers, and the generation of reduced ferredoxins is solely based on the photosynthetic ETC. This allows the chloroplast to couple many metabolic pathways to its core activity – photosynthesis – via the redox switch of thioredoxins. However, this is a double-edged sword: as being strictly light dependent, the free thioredoxins are unable to perform redox regulations in the dark condition. On the contrary, NTRC is hitherto the only reported "thioredoxin" which derives its reducing potential from NADPH. NADPH is not only generated from photosynthetic ETC activities, but also a product of the light-independent oxidative pentose phosphate pathway (OPPP), unleashing NTRC from irradiance-dependency (Figure 3; Neuhaus & Emes, 2000; Spínola et al., 2008).

A good example of this comes from the redox activation of ADP-glucose pyrophosphorylase (AGPase), a central enzyme in plant starch biosynthesis. NTRC has been found indispensable in the sucrose-dependent redox activation of AGPase in darkened leaves and root tissues of *A. thaliana* (Michalska et al., 2009). Conversely, knockout of Trx-f_1 though attenuated the light activation of AGPase, exerted no effect on AGPase activities in the dark (Thormählen et al., 2013; Thormählen et

al., 2015). These results demonstrate that NTRC is a more flexible redox regulator responsive to other abiotic changes besides light intensity.

Besides AGPase, several other chloroplast enzymes have been identified as redox targets of NTRC. Oxidative stress homeostasis via PRX1 regeneration is the first identified and so far, the most extensively studied function of NTRC (Serrato et al., 2004; Kirchsteiger et al., 2009; Bernal-Bayard et al., 2014; Puerto-Galán et al., 2015; Pérez-Ruiz et al., 2017). Other than that, two independent studies have demonstrated NTRC redox regulation on ATP synthase γ-subunit, a subunit of the ATPase complex in the photosynthetic ETC (Carrillo et al., 2016; Naranjo et al., 2016). This explains the build-up of thylakoid proton gradient and the subsequent elevation of non-photochemical quenching (NPQ) in the *ntrc* knockout plant (Carrillo et al., 2016; Naranjo et al., 2016). These observations were found low light-specific and vanished at higher light where the redox modulation of ATP synthase γ-subunit can be taken over by the ferredoxin-thioredoxin system (Carrillo et al. 2016). Finally, NTRC has also been shown to be involved in the redox regulation of Mg-protoporphyrin IX methyltransferase, an enzyme in the biosynthesis pathway of tetrapyrroles which form the basic skeleton of chlorophylls (Richter et al., 2013; Da et al., 2017).

I.2.4. Chaperone Functions of NTRC

Like what has been reported for versatile thioredoxins such as Trx-*f* and Trx-*m* (Sanz-Barrio et al., 2012), NTRC can also operate *in vitro* as a foldase or holdase chaperone depending on its oligomeric status (Chae et al., 2013). NTRC dimer acts as disulphide reductase and foldase while heat-induced oligomerized NTRC works as a holdase (Chae et al., 2013). A foldase chaperone facilitates the refolding of a partially denatured protein, whereas a holdase binds to a folding intermediate, preventing the protein from non-specific aggregation. The same study also showed that *NTRC* overexpression enhanced thermotolerance in *A. thaliana* whereas knockout of *NTRC* made the plant vulnerable to elevated temperatures (Chae et al., 2013).

Further, an *in vitro* study has revealed a nucleic acid binding property of NTRC's thioredoxin domain which protected RNA and DNA from RNase A and metal triggered oxidative damages (Moon et al., 2015). The authors also demonstrated that NTRC as a holdase, prevented *in vitro* freeze-thaw induced aggregation of malate dehydrogenase, a model substrate which has been extensively used for other protein chaperone studies (Moon et al., 2015). The authors proposed that these two properties could provide cryoprotection to the *NTRC* overexpression line of *A. thaliana* which was found more tolerant to freezing and cold shock than the wild type, whereas the reverse was observed in the knockout mutant (Moon et al., 2015). Additionally, *NTRC* mRNA levels of both *Chlorella vulgaris* and *A. thaliana* were found elevated in response to cold stress, even though the protein levels remained unchanged (Machida et al., 2007; Moon et al., 2015).

I.3. Regulations of the Calvin Cycle

I.3.1. Redox Regulation of Calvin Cycle Enzymes

The Calvin cycle activities need to be coordinated to the photosynthetic electron transport not only to ensure smooth supplies of ATP and NADPH to fuel the Calvin cycle, but also to regenerate $NADP^+$ for the photosynthetic ETC in return. Downregulation of the Calvin cycle could lead to overreduction-associated damages to the photosystems and inhibition of photosynthesis (Hashida & Kawai-Yamada, 2019a). The coordination is mediated via the ferredoxin-thioredoxin redox regulatory system. It has been reported that Trx-*f* and -*m* can reduce and activate thiol-modulated enzymes of the Calvin cycle including GAPDH, phosphoribulokinase (PRK), fructose-1,6-bisphosphatase (FBPase) and sedoheptulose-1,7-bisphosphate (SBPase) in higher plants (Buchanan, 1980, 1991; Buchanan & Balmer, 2005; Michelet et al., 2013). Nonetheless, comparative analysis of amino acid sequences of these enzymes has revealed that all of the four enzymes in cyanobacteria and two of them, GAPDH and SBPase, in algae lack potential thiol-group forming cysteine residues (Takeda et al., 1995; Tamoi et al., 1996a; Tamoi et al., 1996b; Tamoi et al., 1998; Tamoi et al., 2001; Kobayashi et al., 2003; Tamoi & Shigeoka, 2015). Hence, another regulatory mechanism is required and carried out via enzyme aggregation as described in the following section.

I.3.2. Regulatory Aggregation of GAPDH

GAPDH is a ubiquitous enzyme which reversibly converts glyceraldehyde-3-phosphate into 1,3-bisphosphoglycerate (Figure 1). There are two subunits of GAPDH in higher-plant chloroplasts, namely GapA and GapB which form an active A_2B_2-GAPDH heterotetrametric enzyme of about 160 kDa. This A_2B_2-GAPDH heterotetramer can further aggregate to form a $(A_2B_2)_4$-GAPDH hexadecamer complex of around 600 kDa (Pupillo & Piccari, 1973; Cerff, 1982). Interestingly, this aggregation is reversibly controlled by the C-terminal extension (CTE) of the GapB subunit. This CTE is a 30 amino acid extension, absent in the GapA subunit and constitutes the most predominant difference between the two subunits. It contains two cysteine residues allowing the formation of a regulatory disulphide. Genetic deletion of the CTE or reduction of the disulphide by thioredoxins in response to light has been found resulting in the dissociation of the $(A_2B_2)_4$-GAPDH complex, relieving the A_2B_2 tetrameric GAPDH enzyme from this autoinhibitory aggregate (Zapponi et al., 1993; Baalmann et al., 1995; Scheibe et al., 1996; Li & Anderson, 1997; Sparla et al., 2002; Fermani et al., 2007).

Besides the A_2B_2 isoform, it has been found that GAPDH also exists naturally as an A_4 homotetramer in higher plants (Cerff, 1979). Unlike the A_2B_2 isoform, this A_4 isoform with the lack of CTE, fails to undergo the autonomous inhibitory aggregation and is therefore insensitive to thioredoxins and other metabolites such as 1,3-bisphosphoglycerate (Baalmann et al., 1996; Scagliarini et al., 1998;

Sparla et al., 2002). Further, the GapB subunit is phylogenetically absent in cyanobacteria, green and red algae; the 'non-regulatory' A_4-GAPDH is the only isoform in these organisms (Petersen et al., 2006; Graciet et al., 2003b; Oesterhelt et al., 2007; Tamoi & Shigeoka, 2015). Despite the unresponsiveness of A_4-GAPDH to reduced thioredoxins, GAPDH catalytic activities in these lower phototrophs have been demonstrated to be modulated by the light (Figge et al., 1999; Lebreton et al., 2003). In fact, the regulation of A_4-GAPDH is conferred by a small protein named Calvin Cycle Protein 12 (CP12) which joins GAPDH and PRK, giving rise to a second mode of regulatory aggregation.

I.3.3. Discovery History of the PRK/CP12/GAPDH complex

CP12 was first identified in 1996 in higher plants by Pohlmeyer and his colleagues (1996), who noticed that its amino acid sequence is highly similar to that of the GapB CTE. In the same report, CP12 was demonstrated interacting with GAPDH (Pohlmeyer et al., 1996). Later on, Wedel and his colleagues identified the PRK as another binding partner of CP12 in *Pisum sativum* (pea) using the yeast two-hybrid approach (Wedel et al., 1997). Further, size exclusion chromatography (SEC) data demonstrated the existence of a 550 kDa stable complex composed of these three proteins in the stroma of *Spinacia oleracea* (spinach) chloroplast (Wedel et al., 1997). Wedel then expanded his studies to the cyanobacterium *Synechocystis sp.* PCC 6803, the moss *Ceratodon purpureus* and *C. reinhardtii*, demonstrating both CP12 and the PRK/CP12/GAPDH complex to be highly conserved in oxygenic photosynthetic organisms (Wedel et al., 1997; Wedel & Soll, 1998).

I.3.4. Heterogeneity of the PRK/CP12/GAPDH complex in higher plants

With the presence of GapB subunit, GAPDH enzymes in higher plants can appear in several forms (Figure 4). First of all, there are two types of active GAPDH tetramers – A_2B_2 and A_4 isoforms. Howard and his colleagues (2011b) did a comprehensive comparison across nine land plants including *A. thaliana* and found that the A_2B_2 tetramer is the major form of GAPDH. Although the A_4 tetramer was identified in *Medicago*, tobacco, potato, and spinach in the study, it appeared to not be the predominant form in these organisms (Howard et al., 2011b). Nevertheless, the A_4 tetramer should not be neglected as it can constitute up to 20 % of the total GAPDH activity as reported for spinach (Scagliarini et al., 1998).

In term of oligomeric aggregation, higher plants can also form two types of supracomplexes – the PRK/CP12/GAPDH complex and the conventional $(A_2B_2)_4$-GAPDH complex. Scheibe and her colleagues demonstrated the coexistence of both in spinach chloroplasts and found that they were under different modes of regulations; the PRK/CP12/GAPDH complex became fully activated by reduction alone while the $(A_2B_2)_4$-GAPDH complex required additional activation by 1,3-bisphosphoglycerate (Scheibe et al., 2002). Nonetheless, the two complexes do not exist in equal proportion. The

PRK/CP12/GAPDH complex was the prevalent one whereas the canonical $(A_2B_2)_4$-GAPDH complex constituted only a minor portion of the GAPDH aggregate pool in all land plant species examined by Howard, except for tobacco and French bean (Howard et al., 2011b).

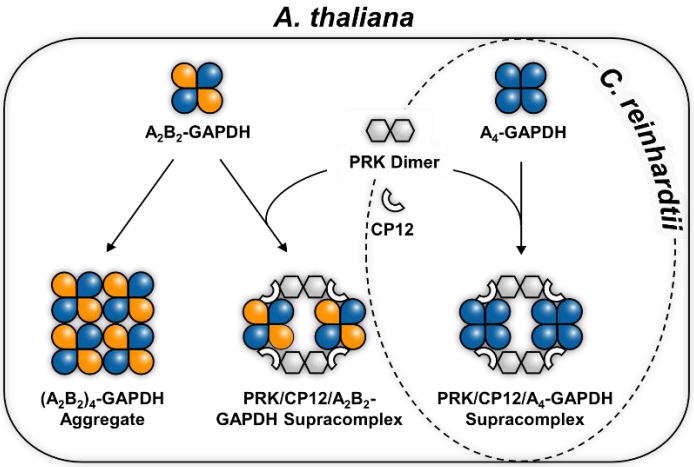

Figure 4: Diagram illustrating various forms of GAPDH supracomplexes. There are two GAPDH isoforms present in the chloroplast of *A. thaliana* which further aggregate into three different types of GAPDH homo- or hetero-supracomplexes as framed by the solid line rounded rectangle. Conversely, the A_4-GAPDH homotetramer is the only isoform that exists in *C. reinhardtii* chloroplasts, giving rise to only one form of supracomplex – the PRK/CP12/A_4-GAPDH complex, as bordered by the dashed-line ellipse. Be noted that the A_4 isoform is incapable of self-aggregation.

Another layer of heterogeneity come into account in the question of which isoforms, the A_2B_2 or the A_4 is the one that forms a complex with PRK and CP12. The A_2B_2-GAPDH isoform has been detected in the PRK/CP12/GAPDH complex in most higher plants (Wedel et al., 1997; Scheibe et al., 2002; Howard et al., 2008; Howard et al., 2011b). Nevertheless, the A_4-GAPDH tetramer has also been found forming part of the PRK/CP12/GAPDH complex pool in spinach and *Medicago* (Howard et al., 2011b). Further, in *A. thaliana* and *Nicotiana tabacum* (tobacco), the complex was found hardly detectable (neither in light nor dark conditions) and appears only if the leave extracts were preincubated with NAD^+ (Howard et al., 2011a; Howard et al., 2011b). These variations have raised doubts about the regulations of PRK and GAPDH as the only role of CP12 in higher plants. In fact, CP12 has been reported to have other functions (see section I.3.7 for details).

I.3.5. Regulations of the PRK/CP12/GAPDH Complex

PRK is a dimeric enzyme with one thioredoxin-sensitive disulphide in each subunit (Porter et al., 1988). The disulphide formation itself renders a substantial inhibition to its catalytic activity (Hirasawa et al., 1999; Geck & Hartman, 2000) though incorporation of oxidized PRK into the PRK/CP12/GAPDH complex does cause additional suppression to its enzyme activity (Marri et al., 2005). However, the presence of the supracomplex provides indispensable regulatory alternative to GAPDH activity in cyanobacteria and algae which lack the regulatory GapB subunit (Petersen et al., 2006; Graciet et al., 2003b; Oesterhelt et al., 2007; Tamoi & Shigeoka, 2015).

It has been shown that the assembly of the PRK/CP12/GAPDH complex is accompanied with suppressed GAPDH and PRK enzyme activities as compared to the free GAPDH tetramer and PRK dimer (Avilan et al., 1997; Wedel et al., 1997; Marri et al., 2005; Howard et al., 2008). Moreover, the complex was found dissociated upon treatment with the artificial reducing agent dithiothreitol (DTT), suggesting the complex integrity is redox-sensitive (Avilan et al., 1997; Wedel et al., 1997; Wedel & Soll, 1998). A study in *P. sativum* demonstrated that the complex assembled in dark-adapted leaves while dissociated in leaves which had undergone 30 minutes of illumination (Howard et al, 2008). Besides, the study also demonstrated that Trx-*f* dissociated the complex *in vitro* (Howard et al, 2008). Another study in *A. thaliana* similarly showed that Trx-*f* and Trx-$m_{1/2}$ activated the enzyme activities of reconstituted PRK/CP12/A_4-GAPDH complexes (Marri et al., 2009). These findings suggested the regulation of the complex in response to light intensity by the light-dependent ferredoxin-thioredoxin system.

Additionally, like the $(A_2B_2)_4$-GAPDH aggregate, PRK/CP12/GAPDH complexes also respond to pyridine nucleotides, NADH and NADPH which are both commonly viewed as redox currencies in the cell (Wedel et al., 1997; Wedel & Soll, 1998; Tamoi et al., 2005; Trost et al., 2006). The significance of the complex regulation by pyridine nucleotides was demonstrated by Tamoi and his colleagues who found in cyanobacteria, a higher NADPH/NADH or NADP/NAD ratio prevailing in the light as compared to that measured in the dark; applying NADP(H)/NAD(H) in the same ratio mimicked the light effect and dissociated the complex *in vitro* (Tamoi et al., 2005). In the same study, the cyanobacterial *cp12* knockout mutant grew slower than the wild type when cultured under the light-dark rhythm but not under continuous light, illustrating the importance of CP12 during the transition from light to dark (Tamoi et al., 2005).

I.3.6. Assembly Mechanism of the PRK/CP12/GAPDH Complex

Unlike the CTE of the GapB subunit, CP12 possess a second cysteine pair in its N-terminus in addition to the C-terminal cysteine pair. The N-terminal cysteine pair though is highly conserved but has been reported missing in some photoautotrophic species such as the cyanobacterium *Synechococcus*, the unicellular freshwater algae *Cyanophora* or certain red algae (Tamoi et al., 2005; Petersen et al., 2006; Groben et al., 2010). Intramolecular disulphides formed by these cysteine pairs have been found pivotal for CP12 to interact with GAPDH and PRK. Site-specific mutation studies have revealed that the C-terminal disulphide is involved in the interaction with GAPDH tetramer while the disulphide at the N-terminus is required for PRK dimer binding (Wedel et al., 1997; Lebreton et al., 2006; Marri et al., 2008).

Moreover, the exchange of GAPDH tetramer bindings of NADP(H) to NAD(H) has been suggested as the initial step for the complex assembly (Marri et al., 2005; Marri et al., 2008).

Independent kinetic studies based on *in vitro* reconstitution of PRK/CP12/GAPDH complexes of *C. reinhardtii* and *A. thaliana* illustrated that the PRK dimer does not form a complex directly with CP12 (Graciet et al., 2003a; Graciet et al., 2004; Marri et al., 2005; Marri et al., 2008). Instead, it binds to CP12 only after a CP12-GAPDH binary complex has been formed. These led to the proposed model of complex assembly as shown in Figure 5. In short, the assembly starts from binary complex formation between oxidized CP12 and NADP(H) bound GAPDH tetramers followed by the incorporations of PRK dimers to form the final ternary complex.

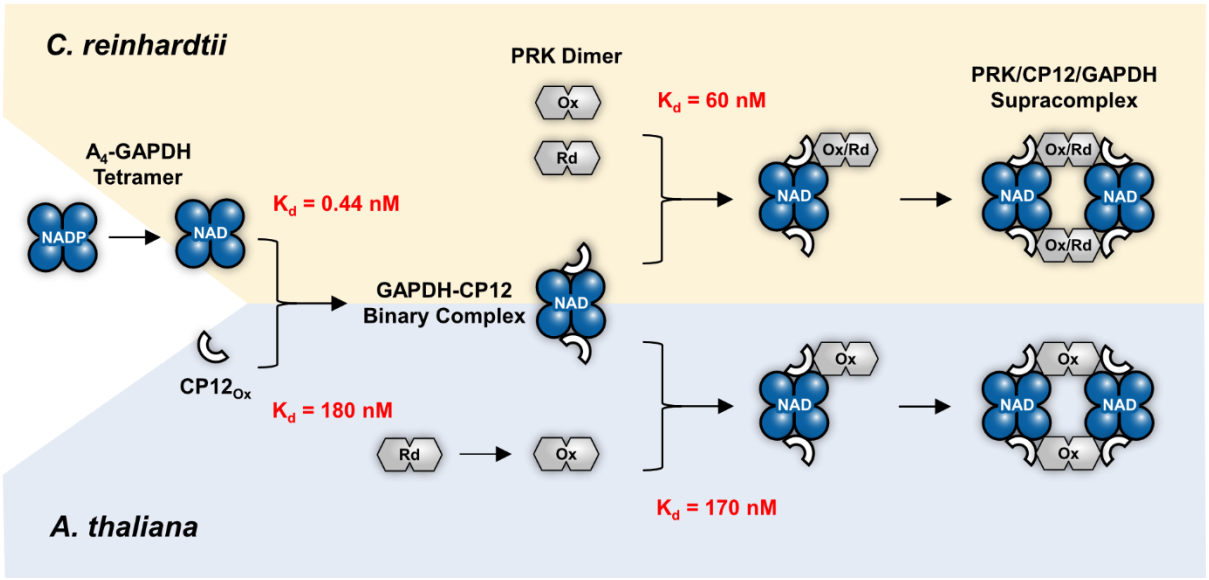

Figure 5. Schematic diagram depicting the assembly mechanism of the PRK/CP12/GAPDH supracomplex in *C. reinhardtii* and *A. thaliana*. The diagram is modified from the complex assembly model of *A. thaliana* published in Marri et al. (2008) incorporating findings in *C. reinhardtii* reported in Graciet et al. (2003a). The complex assembly in both organisms starts with pyridine nucleotide exchange in a A_4-GAPDH homotetramer and the binding of oxidized CP12, forming a GAPDH-CP12 binary complex. Unlike in *A. thaliana*, both oxidized and reduced forms of the PRK dimer can incorporate into the binary complex in *C. reinhardtii* and form the ternary PRK/CP12/GAPDH supramolecular complex. The dissociation constants (K_d) of interactions between the complex components are also indicated.

I.3.7. CP12 and its Intrinsically Disordered Protein Properties

The Calvin Cycle Protein 12 (CP12) is a small, nuclear-encoded chloroplast protein of about 80 amino acids in length. It is universally distributed in oxygenic photosynthetic organisms from cyanobacteria, mosses, algae to angiosperms; it was even found encoded in the genome of cyanophages infecting marine cyanobacteria, *Synechococcus* and *Prochlorococcus*, in which NADPH accumulation caused by the viral CP12-induced suppression of the Calvin cycle might favour nucleotide biosynthesis needed for the phage replication (Thompson et al., 2011).

Furthermore, CP12 is a conditional intrinsically disordered protein (IDP; Dyson & Wright, 2005). Protein structure studies of CP12 from *Synechococcus elongatus*, *C. reinhardtii*, and *A. thaliana*

have demonstrated that the protein is poorly structured under reducing conditions (Graciet et al., 2003a; Gardebien et al., 2006; Marri et al., 2010; Matsumura et al., 2011; Fermani et al., 2012; Launay et al., 2018). Even though formation of intramolecular disulphide bridges under oxidizing conditions promotes folding of α-helices that confer some sort of order to the protein, the structure remains highly flexible (Figure 6).

The oxidized form of CP12 from *A. thaliana* has a highly heterogeneous conformation and its C-terminus binds to a GAPDH tetramer via conformational selection by the target (Fermani et al., 2012). Oxidized CP12 can only reach its final conformation through induced folding upon its binding to the GAPDH protein (Fermani et al., 2012). Conversely, the oxidized CP12 protein of *C. reinhardtii* has its C-terminus forming a stable α-helix structure while the N-terminal region is highly dynamic, oscillating between helical turns and random coils (Figure 6; Launay et al., 2018). The stable C-terminal structure of *C. reinhardtii* CP12 makes its binding to the GAPDH fit better the "lock and key" model and thus reduce the cost of entropy. Further, upon binding of the C-terminus to the GAPDH tetramer, the N-terminus moiety undergoes an induced unfolding process (Launay et al., 2018). This phenomenon is called cryptic disorder which further decreases the entropy cost for the binary complex formation and contributes to the unusual high binding affinity between CP12 and GAPDH in *C. reinhardtii* (Graciet et al., 2003a; Launay et al., 2018).

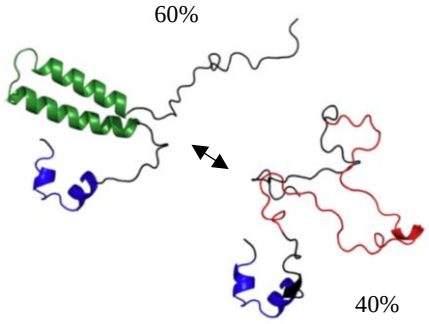

Figure 6. 3D-model illustrating conformational changes of the oxidized CP12 protein from *C. reinhardtii*. The models are modified from works published in Launay et al. (2018). The N-terminal region is highly dynamic oscillating between a random coil state (red) and a hairpin of two helices (green). It is connected by a disordered region (black) to the C-terminus which forms stable α-helix domain (blue).

IDPs constitute a significant fraction of the eukaryote proteome and play an important role as scaffold proteins (Cortese et al., 2008; Tompa & Fuxreiter, 2008; Zhang et al., 2018). Conformational diversity of the IDP suggests its binding to multiple partners, termed as binding promiscuity (Uversky, 2002; Tompa & Fuxreiter, 2008). This binding promiscuity has also been observed in CP12. For instances, CP12 has been reported binding aldolase (Erales et al., 2008) and *CP12* knockout in tobacco affected malate dehydrogenase activity (Howard et al., 2011a), suggesting CP12 can interact with other proteins apart from PRK and GAPDH. Additionally, CP12 is also known to chelate metal ions such as copper and calcium ions (Erales et al., 2009a; Rocha & Vothknecht, 2013). To summarize, the IDP properties especially the binding promiscuity of CP12 suggests that the protein can have a variety of functions which remain to be explored.

I.3.8. Physiological Roles of CP12

So far, there are only four *in vivo* studies published indicating the physiological roles and the significance of CP12. All of them were performed in different model organisms, namely *Synechococcus sp.* PCC 7942, *N. tabacum*, *A. thaliana* and the tropical legume *Stylosanthes guianensis* (Tamoi et al., 2005; Howard et al., 2011a; López-Calcagno et al., 2014; López-Calcagno et al., 2017; Li et al., 2018).

CP12 knockout has been demonstrated to affect cyanobacterial growths under the diurnal cycle due to the incomplete suppression of the Calvin cycle in the dark (Tamoi et al., 2005). Suppression of the Calvin cycle is needed for the activation of the OPPP in the dark. This is because there is a shared intermediate product between the Calvin cycle and the OPPP – ribulose-5-phosphate (Ru5P, compare Figure 1). Ru5P molecules can have two different fates: 1) it is converted by the PRK enzyme into RuBP which replenishes the Calvin cycle, 2) it turns into ribose-5-phosphate (R5P) and xylulose-5-phosphate (Xu5P) via the pentose phosphate pathway. Hence, to ensure Ru5P flow into the OPPP in the dark, strict inhibition of the PRK activity is required (Dennis and Blakeley, 2000; Taiz & Zeiger, 1998).

Why is the OPPP so important in the dark? This is because the OPPP is the only known pathway generating NADPH in the dark when the photosynthetic electron transport chain is inoperative (Kaiser & Bassham, 1979). Moreover, the Calvin cycle also has to be suppressed in the dark to avoid futility in the generation of reducing power since the Calvin cycle consumes NADPH. Not only in the light, but NADPH is also required in the dark for redox-homeostasis and reductive metabolism such as fatty acid biosynthesis (Kaiser & Bassham, 1979). Furthermore, sugar intermediates produced by the pentose phosphate pathway are also important materials for anabolic metabolism. For example, R5P and erythrose-4-phosphate (E4P) are precursors for nucleotide and aromatic amino acid biosynthesis, respectively (Zrenner et al., 2006; Maeda & Dudareva, 2012). Therefore, it is important to suppress the Calvin cycle to ensure operation of the OPPP in the dark. This carbon partition is regulated by CP12 in cyanobacteria.

There are three homologs of *CP12* found in the genomes of *A. thaliana* (Marri et al., 2005; López-Calcagno et al., 2014). They are differentially expressed: CP12-1 has a board coverage and is found in photosynthetic tissues, root tips, flowers, and seeds, while CP12-2 is abundant in photosynthetic tissues; lastly, CP12-3 mainly locates in roots, anthers and stigma (Singh et al., 2008). Worth to notify, *CP12-2* has also been found being co-ordinately expressed with *GapA, GapB, PRK* under different conditions in leaves (Marri et al., 2005). Furthermore, CP12-3 is comparatively diverse from the other two isoforms, CP12-1 and CP12-2 which are highly homologous. Hence, it is not surprising to notice that CP12-1 and CP12-2 show a functional redundancy (López-Calcagno et al., 2017). Evidence was provided by the detection of decreased photosynthetic performance, growth, and seed yield only upon the suppression of both *CP12-1* and *CP12-2* transcript levels using T-DNA and

RNAi approaches, while single gene manipulation showed no clear phenotype (López-Calcagno et al., 2017). On the other hand, CP12-3 showed no clear effect in the study (López-Calcagno et al., 2017).

The same study also demonstrated that depletions of *CP12-1* and *CP12-2* resulted in a decrease in the PRK protein level; once the depletion of PRK protein reached 80 % or more, the CO_2 assimilation rate reduced as well. This indicated that apart from inhibitory effects exerted via complex oligomerization, CP12 also affects *in vivo* PRK protein accumulation in *A. thaliana*. The authors suggested that this is probably due to the post-translational protection of the enzyme by CP12 or the PRK/CP12/GAPDH complex which has been evidenced by a couple of *in vitro* findings. First, *C. reinhardtii* CP12 has been reported to act as a chaperone for GAPDH, protecting it from thermal induced aggregation and inactivation (Erales et al., 2009b). Second, PRK and GAPDH of *A. thaliana* and *C. reinhardtii* were found less vulnerable to oxidative damages induced by glutathione disulphide (GSSG), S-nitrosoglutathione (GSNO) or hydrogen peroxide (H_2O_2), when they were present in a preformed PRK/CP12/GAPDH complex (Marri et al., 2014). To sum up, these studies demonstrated CP12, though known to be inhibitory to the enzyme activities via complex formation, simultaneously protect the enzymes from degradation. Hence, instead of an expected elevation of the enzyme activities, the reverse was observed in *A. thaliana CP12* loss-of-function mutations.

Similar findings were reported in the legume *S. guianensis*, *CP12* overexpression lines exhibited inclines in the PRK and GAPDH activities as well as the CO_2 assimilation rate as compared to the wild type, whereas *CP12* antisense plants showed the reverse (Li et al., 2018). Besides, *CP12* transcript was also found upregulated in *S. guianensis* under cold stress, and this increase was even more robust in the cold-tolerant lines (Li et al., 2018). In conjunction, the transgenic overexpression lines of *CP12* also displayed increased tolerance to chilling with higher survival rate at low temperature (6°C), while the antisense suppression of *CP12* led to the opposite phenotype (Li et al., 2018). These findings revealed the importance of CP12 in cold acclimation, suggesting a new role of CP12 beyond the adaptation to light intensity.

Another land plant which has been investigated is *N. tabacum*. Antisense suppression of *CP12* though was found impacting on NAD(H)-induced complex formation of PRK/CP12/GAPDH, had no effect on enzyme activities (Howard et al., 2011a). Regardless of this, the *CP12* antisense tobacco plants displayed a range of aberrant growth and development phenotypes including altered leaf morphology, decreased apical dominance, and lowered fertility (Howard et al., 2011a). Interestingly, the *CP12* antisense plants also exhibited lower malate dehydrogenase (MDH) activities, in conjunction with a mobility shift of the enzyme on Blue Native-PAGE gels, as compared to the wild type (Howard et al., 2011a). Changes in pyridine nucleotide content were also evident (Howard et al., 2011a). Together, these data imply CP12 to be involved in a change in the redox status or post-translational modifications of the MDH enzyme which in turn led to a reduction in the activity of the malate valve (Howard et al.,

2011a). Even though the mechanisms of action of CP12 on MDH remains elusive, the study suggested a new function of CP12 other than the complex formation of PRK/CP12/GAPDH. Another example of this is aldolase which has been reported to interact with CP12 in *C. reinhardtii* (Erales et al., 2008).

In summary, *CP12* knockout in cyanobacteria resulted in incomplete suppression of the Calvin cycle in the dark (Tamoi et al., 2005), consistent with the inhibitory effect of CP12 on the PRK and GAPDH enzymes via complex formation which has been well established by *in vitro* studies (Scheibe et al., 2002; Graciet et al., 2003a; Graciet et al., 2003b; Marri et al., 2009). Conversely, *in vivo* study in *A. thaliana* showed that the removal of CP12 led to reductions in photosynthetic CO_2 fixation instead, probably due to degradations of the enzymes, supporting the *in vitro* findings of enzyme protections by CP12 and the complex (Erales et al., 2009b; Marri et al., 2014; López-Calcagno et al., 2017; Li et al., 2018). Nonetheless, heterogeneity was observed in another higher plant, tobacco wherein CP12 gene deletion caused no significant changes in the PRK and GAPDH activities, but reduced the MDH activity instead (Howard et al., 2011a). Finally, Li's study demonstrated that CP12 also plays a role in cold acclimation besides responding to the light intensity like most of the redox-regulated Calvin cycle proteins (Li et al., 2018).

I.4 Cold Acclimation

Plants and other phototrophs in temperate climate zones experience both annual and diurnal temperature fluctuation. Low temperature is one of the most prominent abiotic stresses impeding growth and survival of these organisms, and thus a major concern in agriculture (Sanghera et al., 2011; Cruz et al., 2013; Chen et al., 2014). Low temperature in general decreases enzyme kinetics and denatures proteins, resulting in unwanted changes in metabolic and physiological activities to the organisms. Chilling also reduces membranes fluidity, imposing physical damages to structural membranes (Wang et al., 2006). Plants and algae cope with these chilling syndromes by adopting numerous adaptive mechanisms called cold acclimation (Thomashow, 1999).

Cold stress poses an impact on many aspects of photosynthesis in both land plants and green algae (Huner et al., 1998; Ensminger et al., 2006; Valledor et al., 2013; Miguez et al., 2017b; Hajihashemi et al., 2018; Zhu et al., 2018; Zheng et al., 2020). Light energy absorbed by photosystems is consumed by biochemical reactions mainly the Calvin cycle in which enzyme kinetics are highly temperature sensitive (Huner et al., 1993; Hutchison et al., 2000; Falkowski & Chen, 2003). The balance between the energy source and the energy sink is termed as photostasis (Melis, 1998; Huner et al., 2003). Disparity occurs when the light energy absorption exceeds the metabolic utilization, resulting in over-reduction of photosystems, mainly PSII (Aro et al., 1993; Long et al., 1994; Vasilikiotis & Melis, 1994). Overreduction of PSII causes not only reversible photoinhibition but also reactive oxygen species (ROS) generation via the Mehler reaction when photosynthetic electrons are accepted by

oxygen molecules instead of $NADP^+$ (Mehler, 1951; Savitch et al., 2000; Hashida & Kawai-Yamada, 2019b). It has been reported that chloroplast ROS content increases in the cold, causing oxidative damage to the cell (O'Kane et al., 1996). In fact, the ROS elevation is among the few early intracellular changes at low temperature and perceived by the cell as a signal to trigger a series of cold responsive mechanisms (Ensminger et al., 2006; Puyaubert & Baudouin, 2014; Zalutskaya et al., 2019; Bittner et al., 2020).

Moreover, PSII is the most sensitive component of the photosynthetic ETC, though PSI is also susceptible to photo-oxidative damage (Ivanov et al., 1998; Terashima et al., 1998; Sonoike, 2011). When the damage rate of PSII exceeds its repair cycle in the cold, it causes also chronic photoinhibition which is irreversible (Huner et al., 1993; Baroli & Melis, 1996). This is partly due to the slower rate of *de novo* synthesis of D1 proteins at low temperature which are required to replace the damaged ones in the PSII reaction centres (Huner et al., 1993; Murata et al., 2007).

Depending on the time length of cold exposure and the developmental state of a leaf or organism, photostasis can be re-established by several mechanisms (Huner et al., 1993). Firstly, a transient increase in NPQ dissipates the excess light energy as heat to protect the PSII reaction centres from overreduction (Miguez et al., 2017a; Kosuge et al., 2018; Li et al., 2020; Zheng et al., 2020). Secondly, upregulation of the Calvin cycle activities has also been observed in cold acclimated plants and is thought to increase the electron sink, avoiding electron leakage from the photosynthetic ETC (Åström et al., 1998; Strand et al., 1999; Stitt & Hurry, 2002; Calzadilla et al., 2019). Thirdly, enhanced abundances of numerous proteins involved in photosynthesis and thylakoid membrane organization have also been reported in both cold-acclimated plants and algae indicating recovery of the photosynthetic machinery (Valledor et al., 2013; Janmohammadi et al., 2015; Du et al., 2018; Szyszka-Mroz et al., 2019).

Further, lipid composition alteration such as increase in fatty acid desaturation helps to avoid cold-induced membrane rigidification (Steponkus, 1984; Vaultier et al., 2006; Upchurch, 2008; Valledor et al., 2013). Moreover, remodelling of starch metabolism has been reported in both cold adapted plants and microalgae and is thought to be related to its dissolved sugars, meaning in particular sucrose which serves as an important cryoprotectant in maintaining cellular osmolality (Valledor et al., 2013; Thalmann & Santelia, 2017). However, while sucrose and other organic cryoprotectants such as trehalose, glycerine, glycine betaine, proline, putrescine, and polyamines were found increased in cold acclimated plants (Hare et al., 1998; Livingston & Henson, 1998 ; Longo et al 2018), only mild changes were detected in *C. reinhardtii* (Lapina et al., 2013; Valledor et al., 2013). Therefore, the significance of these organic osmolytes in this green microalga requires further investigation.

Protein homeostasis is also unneglectable in cold acclimation. Rapid accumulation of heat-shock proteins (HSPs) which act as chaperones for denatured protein’s refolding has been reported in

cold-treated plants and algae (Renaut et al., 2006; Timperio et al., 2008; Maikova et al., 2016). Further, ubiquitination-directed degradation of misfolded proteins also elevates as a cold adaptation response of plants and algae (Heidarvand & Maali-Amiri, 2013; Valledor et al., 2013; Kazemi-Shahandashti & Maali-Amiri, 2018; Li et al., 2020).

In addition, over-accumulated ROS molecules from the photosynthetic ETC are scavenged by antioxidant enzymes such as ascorbate peroxidase (APX), catalase (CAT), and glutathione peroxidase (GPX) which have been found critical in cold-treated plants and algae (Suzuki & Mittler, 2006; Zalutskaya et al., 2019). Nonetheless, organic antioxidants such as ascorbic acid and glutathione was reported not involved in *C. reinhardtii* acclimation to cold stress (Valledor et al., 2013). Again, this puts a question on the role of organic cryoprotectants, including antioxidants and osmolytes mentioned above, in microalgae. Additionally, anthocyanin, an antioxidant pigment which elevates in cold-stressed land plants is absent in cyanobacteria and algae (Campanella et al., 2014; Schulz et al., 2016).

In summary, despite some of the mechanisms behind are not fully understood especially in microalgae wherein relatively fewer studies have been conducted as compared to land plants, cold acclimation generally involves maintenance of membrane fluidity and cellular osmolality, protein homeostasis and the re-establishment of photostasis (Morgan-Kiss et al., 2006; Ermilova, 2020).

I.5. Model Organisms in the Study

I.5.1 *Chlamydomonas reinhardtii*

C. reinhardtii is a small unicellular, biflagellate green alga of around 10 µm in size, found in freshwater and soil throughout the world (Figure 7). It is one of the most well studied photosynthetic eukaryotes and there are several reasons that make it an ideal model organism (Nickelsen & Kück, 2000; Salomé & Merchant, 2019).

Firstly, there are cultivation advantages in *C. reinhardtii*. As a microorganism, *C. reinhardtii* culture can be done on agar plates or in flasks with liquid media, with minimal space required. Furthermore, besides photoautotrophic growth, it can also grow heterotrophically when acetate is supplied as an external organic carbon source. This allows prolonged cultivation in the dark which is not possible in higher plant models. Additionally, it also has a relatively short asexual doubling time under favourable conditions. For instance, it takes about 12 hours for duplication when it is cultured in TAP medium, under 30 µE/s/m^2 light, at room temperature (23°C).

Secondly, some of the intrinsic characters of *C. reinhardtii* make it comparatively easier for genetic modification. The dominant phase of its life cycle is the haploid (gametophyte) stage which facilitates genome editing. Moreover, instead of having multiple plastids like higher plants do, it contains only one chloroplast with a unique cup-shaped form (Figure 7). This eases artificial

mutagenesis on chloroplast-encoded genes (Harris, 1989). In addition, sexual recombination of genetic materials from different mating types (mt+ and mt-) is inducible by nitrogen starvation which is doable in the laboratory (Ferris & Goodenough, 1994; Jiang & Stern, 2009). This allows the crossing of two different mutant strains and gives rise to another layer of genetic manipulation.

Thirdly, advantages also come from accumulated knowledges about this organism. The nuclear, chloroplastic and mitochondrial genomes of *C. reinhardtii* have been fully sequenced (Gray & Boer, 1988; Maul et al., 2002; Merchant et al., 2007) and the respective genetic transformation techniques have also been established (Kindle, 1990; Fischer et al., 1996; Shimogawara et al., 1998; Yamano et al., 2013). Briefly, the nuclear genome contains a haploid set of 17 chromosomes. This nuclear genome of approximately 110 Mb, together with a 203 kb chloroplast genome and a 16 kb mitochondrial genome carry a total of 14,000 protein-coding genes (Merchant et al., 2007). The Chlamydomonas Library Project (CLiP) has established a mapped collection of nearly 60,000 insertion mutant strains available for the research community (Zhang et al., 2014; Li et al., 2016; Li et al., 2019). Further, the disadvantage of extremely low frequency of homologous recombination incident in *C. reinhardtii* which hinder site-specific gene editing, has also recently been overcome by the CRISPR/Cas9 technique (Greiner et al., 2017).

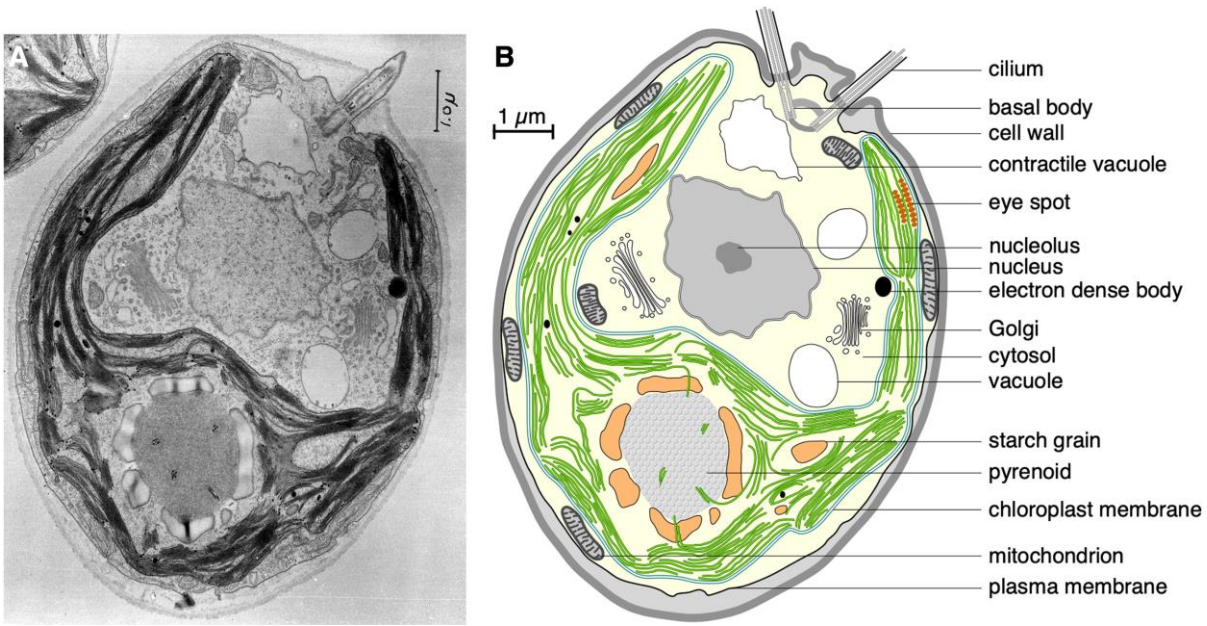

Figure 7: Anatomy of *Chlamydomonas reinhardtii*. A, Transmission electron micrograph (TEM) of a *C. reinhardtii* cell originally retrieved from Ohad et al. (1967) by Salome and Merchant and represented it in (B). **B,** a schematic drawing showing subcellular organelles of the unicellular microalga. Both the TEM image and the drawing are retrieved from Salomé & Merchant (2019).

Lastly, although the microalgal chloroplast shows a high similarity to that of land plants, it adopted a different evolutionary path to adapt to the aquatic habitat. The pyrenoid provides a brilliant example to

illustrate this. Pyrenoids are non-membrane bound micro-compartments found in chloroplasts of many microalgae (Figure 7). With high accumulations of Rubisco and other related proteins, the pyrenoid confers a CO_2-concentrating mechanism (CCM) distinct from that of C_4 land plants (Itakura et al., 2019; Wunder et al., 2019). Hence, findings in higher plants might not simply reflect the situation in microalgae which should be studied individually. Last but not least, aquatic photosynthetic microorganisms contribute to roughly 50 % of global photosynthetic CO_2 fixation (Field et al., 1998). Hence, it is very crucial to understand their physiology and metabolism, especially with the alarming global warming issues nowadays. *C. reinhardtii* serves as a good research model for this.

I.5.2 *Arabidopsis thaliana*

A. thaliana is a widely used flowering plant model (reviewed in Koornneef & Meinke, 2010). It has a short life cycle of 6-8 weeks besides its small size of about 20 cm, which both ease the cultivation. As compared to other angiosperms, the plant has a relatively small genome which has been fully sequenced. It harbours approximately 27,000 genes encoding for around 35,000 proteins (The Arabidopsis Genome Initiative, 2000). Moreover, a large number of T-DNA mutant lines is available in the Nottingham Arabidopsis Stock Center (NASC), facilitating functional characterization of genes of interest.

I.6. Aims of the Study

NTRC has been extensively studied in *A. thaliana* and *O. sativa* but almost nothing is known in algae. Moreover, cold tolerance conferred by NTRC has been attributed to its chaperone function (Moon et al., 2015), whilst the contribution from the well-characterized redox regulatory function remains undetermined. Therefore, the major goal of this thesis was the characterization of the molecular function of the NTRC in *C. reinhardtii* during cold acclimation.

In order to dissect the contradictory molecular mechanisms described for NTRC-mediated cold acclimation, *NTRC* knockout and redox-active cysteine mutations were performed to generate mutant strains for the study of NTRC's oxidoreductase function. Further, by using co-immunoprecipitation assay combined with mass spectrometry, it was intended to identify the downstream redox target(s) of NTRC which are responsible for cold tolerance. Interactions between the potential candidates and NTRC were then further scrutinized using biochemistry techniques. Site-directed knockout mutants of the potential candidates were also generated via CRISPR/Cas9 techniques for phenotypical and molecular analyses, to strengthen the evidence for a niche in cold-tolerance.

To obtain indications on the evolutionary conservation of NTRC's role in cold acclimation, it was also intended to extend key studies to the higher plant *A. thaliana.*

II. MATERIALS AND METHODS

II.1. Materials

II.1.1. Chemicals, kits, and enzymes

All chemicals, kits and enzymes used in this study were purchased from companies stated in Supplemental Table S1. The catalogue number of a material and the name of the company which supplied the material can be found individually in the corresponding method description in section II.2.

II.1.2. Antibodies

All antibodies used in this work are listed in Table 1, with the titres of working solutions included.

Table 1. Antibodies used in this study.

Antibody	Titre	Biological source	Source/ Reference
anti-ATPβ	1:4000	Chicken	Agrisera, #AS03-030-10
anti-CP47	1:1000	Rabbit	Agrisera, #AS04-038
anti-CP12	1:1000	Rabbit	Generated in this work
anti-D2	1:1000	Rabbit	Biogenes, #6441
anti-GapA	1:1000	Rabbit	Provided by Prof. R. Scheibe (University of Osnabrueck; Scheibe et al., 1996)
anti-HA	1:1000	Rabbit	Sigma Aldrich, #H6908
anti-NTRC	1:1000	Rabbit	Generated in this work
anti-PRK	1:1000	Rabbit	Provided by Prof. R. Scheibe (University of Osnabrueck; Scheibe et al., 1996)
anti-RbcL	1:1000	Rabbit	Provided by Prof. G.F. Wilder (Ruhr University of Bochum)
anti-Chicken	1:5000	Rabbit	Sigma Aldrich, #A9046
anti-Rabbit	1:5000	Chicken	Sigma Aldrich, #A9169

II.1.3. Oligonucleotides

All oligonucleotides were ordered from Sigma-Aldrich. Sequences of the oligonucleotides used in this study can be found in Supplemental Table S2.

II.1.4. Plasmids

All plasmids used in this research work are listed with short descriptions in Supplemental Table S3.

II.1.5. *Escherichia coli* strains

DH5α and XL1-Blue strains (Stratagene) were used in molecular cloning and plasmid amplification while BL21-DE3 (Stratagene) and M15 (Qiagen) strains were used in recombinant protein production.

II.1.6. *Chlamydomonas reinhardtii* strains

C. reinhardtii strains used in the study are compiled in Table 2.

Table 2. List of *C. reinhardtii* strains used in this work

Strains	Description	Source/ Reference
CC-4051	*nit1*, *nit2*, *137c*, mt+	Purchased from Chlamydomonas Resource Centre
ntrc	Insertion mutant, knockout of *NTRC* gene in CC-4051 background	Provided by Prof. Kris Niyogi
ntrc:NTRC	*ntrc* mutant complemented with plasmid encoding a C-terminal HA-tagged wild-type NTRC	Generated in this work
C455S	*ntrc* mutant complemented with plasmid encoding a C-terminal HA-tagged NTRC with C455S mutation	Generated in this work
C455S/C458S	*ntrc* mutant complemented with plasmid encoding a C-terminal HA-tagged NTRC with C455S and C458S mutations	Generated in this work
CC-406	*cw15,* mt-	Purchased from Chlamydomonas Resource Centre
cp12 #1	Insertion mutant, knockout of *CP12* gene in CC-406 background	Generated in this work
cp12 #2	Insertion mutant, knockout of *CP12* gene in CC-406 background	Generated in this work
neet	Insertion mutant, knockout of *NEET* gene in CC-406 background	Generated in this work
CC-4533	*cw15,* mt-	Purchased from Chlamydomonas Resource Centre

II.1.7. Software and online tools

Software and online tools used in the study are listed in Table 3.

Table 3. Compilation of software and online tools used in this research project

Software/ Online tool	Manufacturer/ Website	Reference	Application
Affinity Designer	Serif Europe		Diagram drawing
CLC Main Workbench	Qiagen		*in silico* cloning and sequence analysis
CRISPR-P v2.0	http://crispr.hzau.edu.cn/cgi-bin/CRISPR2/CRISPR	Lei et al. (2014)	gRNA design for CRISPR/Cas9 method
Cyanobase	http://genome.microbedb.jp/cyanobase/		Retrieval of gene and peptide sequences
MaxQuant	Max Planck Institute	Cox & Mann (2008)	Mass spectrometry quantitative analysis
Microsoft office	Microsoft Corporation		Data analysis and figure making
Perseus v1.6.2.3	Max Planck Institute	Tyanova et al. (2016)	Mass spectrometry statistical analysis
Phytozome	https://phytozome.jgi.doe.gov/pz/portal.html		Retrieval of gene and peptide sequences
PredAlgo	http://lobosphaera.ibpc.fr/cgi-bin/predalgodb2.perl?page=main	Tardif et al. (2012)	Prediction of protein subcellular localization
UniProt	https://www.uniprot.org/		Proteome database reference for Mass spectrometry analysis

II.2. Methods

II.2.1. *Chlamydomonas reinhardtii* Strains and Culture Conditions

C. reinhardtii algal strains were grown in Tris-acetate-phosphate (TAP) liquid medium under constant light of 30 µE/m^2/s at 23 °C, unless otherwise specified. Growth temperature was changed to 15 °C for cold studies; light intensity was switched between 0 µE/m^2/s and 30 µE/m^2/s every 12 hours for the light-dark rhythm. TAPS medium – TAP supplemented with 1 % sorbitol (w/v) – was used instead for culturing cell wall deficient (*cw15*) strains. *ntrc* knockout, complementation, and cysteine-substituted strains were generated from CC-4051 strain which has intact cell wall, whereas *cp12* knockout strains were of CC-406 (*cw15*) background.

II.2.2. Growth Studies in Liquid Medium and on Solid Agar

For growth studies in liquid medium, *C. reinhardtii* microalgae were inoculated in 50 ml conical flasks containing 25 ml of TAP or TAPS medium each. The initial optical density at 750 nm (OD_{750}) was 0.015. The cultures were shaken at 120 rpm under specified growth conditions. Culture densities were accessed by measuring OD_{750} every day or every second day. Growth curves were plotted using GraphPad Prism software (GraphPad Software). Doubling time was calculated at exponential growth phase.

For growth studies on solid agar, *C. reinhardtii* cultures were first resuspended in TAP or TAPS medium to a density of 2 x 10^7 cells/ml. This stock cell suspensions were then undergone 10-fold serial dilution to generate 5 more suspensions of different cell concentrations. 20 µl of each suspension was then spotted onto solid TAP agar, resulting in initial seeding number of 4 x 10^5, 4 x 10^4, 4 x 10^3, 400, 40 and 4 microalgae per spot, respectively. The agar plates were then incubated under 30 µE/m^2/s light, at 23 °C or 15 °C. Photos were taken after 8, 10 and 12 days.

II.2.3. Generation of pBC1-NTRC Constructs

To generate a plasmid construct for complementation as well as the expression of NTRC proteins with cysteine-to-serine mutation(s) in the CGPC motif and a C-terminal HA-tag, a two-step molecular cloning was performed: 1) generation of a wild-type, full length *NTRC* cDNA with a HA-tag coding sequence at its 3'-end; 2) introducing point mutations in the *NTRC* cDNA corresponding to cysteine-to-serine exchanges in the protein's CGPC motif via designed primers. Nonetheless, gene expression of *C. reinhardtii* empirically works better with a native promoter; genes under the control of non-native promoters were found usually lower expressed than expected. This also happened in *NTRC* expression from cDNA under control of the *PsaD* promoter. Hence, a chimeric *NTRC* genomic DNA (gDNA) was generated, preserving the 5'-UTR and introns but have its 3'-fragment (begins from *Csi*I cutting site or

position +4365 onwards, including part of the second last exon, the last exon and 3'UTR) replaced by that of cDNA encoding a C-terminal HA-tag and a wild-type CGPC motif or that with cysteine-to-serine mutation(s) (Supplemental Figure S1).

Firstly, total RNA was extracted from wild-type *C. reinhardtii* CC-4533 strain using the conventional phenol/chloroform/isoamyl alcohol method (Carl Roth, #A156.1). Total cDNA was then synthesized with oligo-dT primer using SuperScript™ III reverse transcriptase (Invitrogen, #18080093) according to the manufacturer's instructions. This total cDNA was used as a template in the following PCR reaction. The full sequence of *NTRC* cDNA was amplified by PCR using primer pair (NTRC cDNA forward (P-2227) and reverse (P-2228) primers) which introduced an HA-tag coding sequence to the 3'-end of the gene right before its stop codon. The PCR product was then inserted into the pBC1 vector (Neupert et al., 2009) via primer-introduced *Nde*I and *EcoR*I restriction sites and this generated pBC1: NTRC cDNA-HA construct.

Secondly, a C455S mutation was introduced by C455S primer (P-2237). The primer was paired with the NTRC cDNA forward primer (P-2227) for a PCR reaction using the pBC1: NTRC cDNA-HA construct as template. The resulting PCR products were then purified and used to replace the 3'-fragment of *NTRC* cDNA of the pBC1: NTRC cDNA-HA construct located between *Bsp120*I and *Nde*I restriction sites. This generated pBC1: NTRC cDNA (C455S)-HA. Similar procedures were repeated using C458S primer (P-2240) and NTRC cDNA reverse primer (P-2228) to introduce the second point-mutation into the pBC1: NTRC cDNA (C455S)-HA via *Bsp120*I and *EcoR*I restriction sites. This resulted in the pBC1: NTRC cDNA (C455S/C458S)-HA construct.

Thirdly, clone PTQ7836 from Bacterial Artificial Chromosome (BAC) library of *C. reinhardtii* generated by Clemson University Genetics Institute (CUGI) carries the *NTRC* gDNA in the pBeloBAC11 vector. It was amplified and extracted for DNA which was then digested by the *Sal*I restriction enzyme. The resulting fragment with a size of 7.3 kb was isolated and cloned into pBC1 vector at the *Xho*I restriction site which has compatible restriction overhangs with *SaI*I. This resulted in pBC1: NTRC gDNA construct.

Lastly, 3'-fragment of *NTRC* cDNA locates between *Nhe*I and *Csi*I restriction sites from pBC1: NTRC cDNA-HA, pBC1: NTRC cDNA (C455S)-HA, and pBC1: NTRC cDNA (C455S/C458S)-HA were cut out to replace fragment flanked by the same restriction sites in pBC1-NTRC gDNA. This fragment contained exon-9 and exon-10 of *NTRC* as well as an HA-tag. The CGPC motif of the NTRC protein is encoded by exon-9. This generated pBC1: NTRC gDNA-HA, pBC1: NTRC gDNA (C455S)-HA and pBC1: NTRC gDNA (C455S/C458S)-HA constructs which were further amplified in DH5α strain of *Escherichia coli* and purified using NucleoBond® Xtra midi-prep kit (Machery-Nagel, #740410). All restriction enzymes used were purchased from Thermo Fisher Scientific. Sequences of primers used can be found in Supplemental Table S2 in section VI.

II.2.4. Generation of *NTRC* Complementation and Cysteine-to-Serine Mutant Strains

C. reinhardtii strain with *NTRC* knockout denoted as *ntrc* was given by Professor Niyogi (UC Berkeley; Dent et al., 2005); it was generated from the CC-4051 background strain via insertional mutagenesis. This mutant strain was complemented with 1) *NTRC* gDNA carried by the pBC1 plasmid vector to generate the strain *ntrc:NTRC*; 2) *NTRC* gDNA with cysteine-to-serine mutation(s) at C455 or both C455 and C458 to generate *C455S* and *C455S/ C458S* mutant strains, respectively. All constructs fuse an HA-tag to the *NTRC* C-terminus.

For transformation, the *ntrc* strain was first cultured to approximately 1 x 10^6 cells/ml, at which *C. reinhardtii* was in its proliferation active phase. The culture was harvested and concentrated to a density of 1 x 10^8 cells/ml in TAP medium by centrifugation and resuspension. 250 µl of this cell suspension was then mixed with 50 µg of denatured salmon sperm and 5 µg of corresponding pre-linearized (by *Sca*I) plasmid DNA, in an electroporation cuvette with 4 mm gap width (Biozym Scientific, #748040). Subsequently, the cuvettes were incubated in 16 °C ice-water bath for 20 minutes followed by electroporation pulse shock using Gene Pulser II (Bio-Rad Laboratories). Electroporation settings used were number of pulses: 1; voltage: 1.1 kV; resistance: high range; capacity: 10 µF. After that, the cuvettes were incubated in 16 °C ice-water bath for 20 minutes before transferring the cells into flasks with 10 ml of TAP medium each, supplemented with 100 µg/ml Ampicillin for recovery overnight. The cultures were then harvested and spread onto TAP agar with 10 µg/ml paromomycin for selection for 10–14 days. Further screening for positive colonies were done by immunoblotting analysis using antiserum against NTRC.

II.2.5. Pulse-Amplitude-Modulation (PAM) Fluorometry

C. reinhardtii cultures were prepared on TAP agar plates as described above with an initial seeding number of 4 x 10^5 cells per spot and incubated at 30 µE/m^2/s light, at 23 °C for 1 week. Then, the maximum PSII quantum efficiency (F_v/F_m) and non-photochemical quenching (NPQ) of 5 minutes-dark-adapted cultures were determined using FluorCam 800MF chlorophyll fluorometer (Photon Systems Instruments). The protocol started by giving a measuring light to acquire minimum fluorescence (F_o) of the cultures. Then, the maximum fluorescence in the dark-adapted state (F_m) was measured under a short stimulation of 800 ms with saturating light pulse which reduce the reaction centres. The viable fluorescence (F_v) was derived by subtracting F_o from F_m. Subsequently, after a 30 s of dark relaxation, Kautsky effect was induced by actinic light (20 %) exposure of 10 minutes followed by a dark relaxation period of 10 minutes. During this 20 minutes, 10 saturating light pulses were irradiated every 2 minutes to probe the maximum fluorescence in light-adapted steady state (F_{m_Lss}). NPQ in light-adapted steady state was then calculated as $(F_m - F_{m\_Lss}) / F_{m\_Lss}$. For more details about the PAM measurement, refer to Oxborough & Baker (1997).

II.2.6. Stepwise Protein Extraction

C. reinhardtii cells were harvested from a 200 ml culture by centrifugation at 1000 g for 5 minutes. The cell pellet was then resuspended in 300 µl ice-cold IP lysis buffer (150 mM NaCl, 5 % glycerol (v/v), 1 mM EDTA, 20 mM Tris-HCl pH 7.8) modified from recipe of Pierce® IP lysis buffer of Thermo Fisher Scientific and supplemented with cOmplete™ protease inhibitor cocktail (Roche, #04693116001). Then, the cell suspension was vortexed with 0.5 mm glass beads by BeadBug™ microtube homogenizer (5 x 40 seconds, 4000 rpm; Biozym Scientific), followed by centrifugation at 20,000 g, 4 °C for 10 minutes. The supernatant which is also the soluble protein fraction was collected. The pellet was then washed with 300 µl IP lysis buffer before being resuspended in 300 µl ice-cold IP buffer with protease inhibitors and additional 1 M NaCl. The cell suspension was then vortexed for 40 seconds, at 4000 rpm followed by centrifugation at 20,000, 4 °C for 10 minutes. Hydrophilic peripheral membrane proteins were obtained in the supernatant. The pellet was collected and underwent two sequential rounds of the same procedures but with the buffer supplemented 8 M urea and 1 % Triton X-100 to fractionate hydrophilic peripheral membrane proteins and transmembrane proteins respectively. These protein fractions were then analysed by immunoblot assay (see section II.2.8) to determine the localization of NTRC.

II.2.7. Total Protein and Soluble Protein Extractions

Algal total protein extraction was performed using ice-cold RIPA buffer (150 mM NaCl, 20 mM Tris-HCl pH 7.8, 1 mM EDTA, 1 % (w/v) Triton X-100, 0.5 % (w/v) sodium deoxycholate, 0.1 % (w/v) SDS, and 5 mM β-mercaptoethanol) supplemented with 8 M Urea and cOmplete™ protease inhibitor cocktail (Roche #04693116001). The recipe was modified from the RIPA buffer recipe of the Cell Signalling Technology company. Lysates were homogenized (3 x 5 seconds, 10 % amplitude) on ice using Sonopuls HD2070 sonicator (Bandelin Electronics) followed by debris removal by centrifugation at 20,000g, 4 °C for 10 minutes. Protein concentrations were then determined using Pierce® BCA Protein Assay Kit (Thermo Fisher Scientific, #23225). Extracts were then used for immunoblotting analysis (see section II.2.8).

Soluble protein extracts were prepared for co-IP, SEC, and enzyme activity measurements (see sections II.2.9, II.2.12 and II.2.13 respectively) Algal cells were first resuspended in ice-cold IP lysis buffer (150 mM NaCl, 5 % glycerol (v/v), 1 mM EDTA, 20 mM Tris-HCl pH 7.8) modified from recipe of Pierce® IP lysis buffer of Thermo Fisher Scientific and supplemented with cOmplete™ protease inhibitor cocktail (Roche, #04693116001). Cell wall breakage was carried out with the help of 0.5 mm glass beads and BeadBug™ microtube homogenizer (5 x 40 seconds, 4000 rpm; Biozym Scientific), followed by centrifugation at 20,000 g, 4 °C for 20 minutes to remove unbroken cells and debris. Protein concentrations were then determined using ROTI® Quant Bradford assay (Carl Roth, #K015).

II.2.8. SDS-PAGE and Immunoblotting Analysis

Sodium dodecyl sulphate- polyacrylamide gel electrophoresis (SDS-PAGE) was performed to separate proteins using Mighty Small™ II mini-vertical electrophoresis system (SERVA Electrophoresis). The samples were first denatured with ROTI®Load1 reducing loading dye (Carl Roth, #K929) at 37 °C for 30 minutes, unless otherwise specified, before loading into a 14 % polyacrylamide gel. For each well, sample equivalent to 30 µg of total protein extract was loaded. For SEC fractions and co-IP elutes, 40 µl sample was loaded into each well instead. BlueStar pre-stained protein marker (NIPPON Genetics) was also loaded for as a reference of protein sizes. Proteins were separated in the gel with running buffer (25 mM Tris, 192 mM glycine, 1.5 % SDS) at a constant voltage of 120 V.

Subsequently, proteins were transferred from the gels onto nitrocellulose membranes (pore size 0.45 µm, AppliChem) with transfer buffer (40 mM glycine, 50 mM Tris, 20 % (v/v) methanol) at 0.8 mA/cm^2 for 150 minutes using a semi-dry electrotransfer apparatus (VWR). Subsequently, membranes were blocked with 5 % non-fat milk in TBS-T buffer (150 mM NaCl, 10 mM Tris/HCl pH 7.5, 0.1 % (v/v) Tween-20) for 1 hour at room temperature and then incubated with primary antibodies at 4 °C overnight. All primary antibodies except anti-ATPβ were extracted from rabbit sera and used at 1:1000 dilution in 5 % non-fat milk in TBS-T buffer. The anti-ATPβ antibody was produced by chicken and used at 1:4000 dilution. Antibodies against GapA and PRK were generously provided by Prof. R. Scheibe (University of Osnabrueck; Scheibe et al., 1996) while anti-RbcL antibody was a kind gift from Prof. G. F. Wildner (Ruhr University of Bochum). Antibodies against NTRC and CP12 were generated in course of this study as described in section II.2.18. Primary antibodies against HA (Sigma Aldrich, #H6908), ATPβ (Agrisera, #AS03-030-10), CP47 (Agrisera, #AS04-038) and D2 (Biogenes, #6441) were purchased from the respective companies.

On the next day, membranes were washed 4 times with TBS-T for 5 minutes before and after blotting and after incubation with the primary and with horseradish peroxidase (HRP) conjugated anti-rabbit (1:5000 dilution; Sigma Aldrich, #A9169) or anti-chicken (1:5000 dilution; Sigma Aldrich, #A9046) secondary antibodies at room temperature for 1 hour. Finally, enhanced chemiluminescence (ECL) solution (10 mM Tris/pH 8.5, 0.4 mM p-coumaric acid, 2.5 mM luminol, 0.7 % (v/v) DMSO, 0.01 % (v/v) H_2O_2) were applied onto the membrane for protein bands visualization using ImageQuant™ LAS 500 machine (GE Healthcare).

II.2.9. Co-Immunoprecipitation (co-IP)

The pull-down experiments were performed using Pierce® Anti-HA magnetic beads (Thermo Fisher Scientific, #88837) as per the manufacturer's manual. For each sample, 2 mg algal soluble proteins (in 500 µl) extracted as described in section II.2.7 was incubated with 50 µl of magnetic beads at 4 °C overnight. The beads were then collected with SureBeads™ magnetic rack (Bio-Rad Laboratories) and

washed 3 times with 500 µl IP lysis buffer. Then, acidic elution was performed at room temperature for 10 minutes using 50 µl of 0.1 M glycine, pH 2.0, followed by neutralization with 50 µl of 0.1 mM ammonium bicarbonate. Eluates were then either subjected to SDS-PAGE followed by silver staining (see section II.2.10) or sent for mass spectrometry analysis (see section II.2.11).

II.2.10. Silver Staining

Polyacrylamide gels were first fixed with fixing buffer (50 % (v/v) ethanol, 12 % (v/v) acetic acid, 0.05 % (v/v) formaldehyde) for 1 hour or overnight. Gels were then washed 3 times for 30 minutes with 50 % (v/v) ethanol, followed by 60 seconds sensitization with pre-staining buffer [0.2 mg/ml sodium thiosulphate (Sigma-Aldrich, #217263)]. Gels were then rinsed with distilled water 3 times of 30 seconds and stained with silver staining buffer [0.2 % (w/v) silver nitrate (Sigma-Aldrich, #209139), 0.075 % (v/v) formaldehyde] for 30 minutes in the dark. After that, gels were rinsed with distilled water again for 3 times, 30 seconds each. Gels were then developed in developing buffer [sodium bicarbonate (w/v; Sigma-Aldrich, S8875), 0.05 % formaldehyde (v/v), 4 µg/ml sodium thiosulphate (Sigma-Aldrich, #217263)] until protein bands were visible. The reaction was then stopped immediately by pouring in stop buffer (50 % (v/v) ethanol, 12 % (v/v) acetic acid). Gel images were then scanned and recorded.

II.2.11. Liquid Chromatography-tandem Mass Spectrometry

Neutralized co-IP eluates (see section II.2.9) were first alkylated with 5 mM iodoacetamide for 30 minutes at room temperature in the dark. Subsequently, the samples were digested overnight at 37 °C with 1.5 µg trypsin (Pierce® Trypsin Protease, MS Grade), the resulting peptides were desalted with home-made C18 stage tips (Rappsilber et al., 2003) and vacuum dried to near dryness before storing at -80 °C.

Liquid chromatography-tandem mass spectrometry (LC-MS/MS) was performed on an Ultimate 3000 nano-LC system (Thermo Fisher Scientific) coupled to an Impact II high-resolution Q-TOF (Bruker Daltonics). Peptides were loaded on 2 cm nano-trap column (Acclaim Pepmap, C18, 100 Å, 100 µm inner diameter; Thermo Fisher Scientific) and separated on a 50 cm analytical column (Acclaim Pepmap RSLC, C18, 100 Å, 75 µm inner diameter; Thermo Fisher Scientific). Chromatographic separation was carried out in a 50 °C column oven at a flow rate of 250 nl per minute using a two-step gradient, from 5 to 30 % Solution-B (acetonitrile, 0.1 % formic acid) over 60 minutes, followed by 15 minutes from 30 to 45 % Solution-B (acetonitrile, 0.1 % formic acid). MS1 spectra were acquired at 3 Hz with a mass range m/z 200–2000, and with the 18 most intense peaks being selected for fragmentation.

MS raw files were processed using MaxQuant software (version 1.6.2.10 and 1.6.3.4; Cox & Mann, 2008) and peak lists were searched against the UniProt *C. reinhardtii* reference proteome

database (downloaded on January 2019) using the built-in Andromeda search engine (Cox et al., 2011) with the default settings. The label-free quantification (LFQ) algorithm (Cox et al., 2014) with default settings was used to quantified proteins across samples. Downstream bioinformatic and statistical analysis were performed in Perseus (version 1.6.2.3; Tyanova et al., 2016). Potential contaminants, reverse hits, and proteins identified only by site modification were excluded; protein groups were retained if they had been quantified in at least 3 replicates in one genotype. Protein LFQ intensities were log2-transformed and missing values imputed from a normal distribution. Significantly enriched proteins were determined by t-test statistics and p-values adjusted for multiple comparisons according to the Benjamini-Hochberg approach (Benjamini & Hochberg, 1995). The mass spectrometry proteomics data have been deposited to the ProteomeXchange Consortium via the PRIDE (Vizcaino et al., 2016) partner repository with the dataset identifier PXD0277111 and can be accessed at www.ebi.ac.uk/pride/ with the following username: reviewer_pxd027711@ebi.ac.uk and password: UJHfdDQl.

II.2.12. Size Exclusion Chromatography (SEC)

The gel filtration experiments were carried out using a ÄKTA purifier 10 HPLC system (GE Healthcare). For each *C. reinhardtii* or *A. thaliana* sample, 5 mg soluble protein extract (in 500 µl) prepared as described in section II.2.7 was loaded onto Superdex®200 Increase 10/300GL column (GE Healthcare). Elution by IP lysis buffer was performed at flow rate of 0.5 ml/min, 4 °C, with fractionation volume of 1ml. After that, 30 µl of each fraction was mixed with 10 µl ROTI®Load1 (4 x) reducing loading dye (Carl Roth, #K929) before loading for SDS-PAGE and immunoblotting analysis (see section II.2.8).

For *in vitro* NADPH induced PRK/CP12/GAPDH dissociation studies, 5 mg soluble algal protein extract was pre-treated with 12 mM NADPH (Carl Roth, #AE14), 2 mg recombinant CrNTRC protein or both for 2 hours at 4 °C, before loading onto the column. On the other hand, DTT induced PRK/CP12/GAPDH dissociation was performed by pre-incubation of the soluble algal protein extract with 20 mM reduced DTT (AppliChem, #A2948) at 30 °C for 1 hour.

II.2.13. GAPDH, PRK and MDH Enzyme Activity Assays

Enzyme activity of GAPDH consumes NADPH which can be measured with its maximal absorbance at 340 nm. 10 µg of algal soluble protein extract was added into a reaction mixture containing 100 mM HEPES pH 8.0, 10 mM $MgCl_2$, 1 mM EDTA, 5 mM ATP (Sigma Aldrich, #A7699), 0.2 mM NADPH (Carl Roth, #AE14) and 10 U/ml phosphoglucokinase (PGK; Sigma Aldrich, #P7634) enzyme to make a final volume of 200 µl. The reaction was initiated by the addition of 0.3 mM glycerate 3-phosphate (3PG; Sigma Aldrich, #P8877) into each reaction mixture.

PRK enzyme activity was accessed by coupling the resulted ADP formation to the oxidation of NADH via pyruvate kinase (PK) and lactate dehydrogenase (LDH) enzymes. This allowed the PRK activity to be monitored at 340 nm. 5µg of soluble algal protein extract was added into a reaction mixture consists of 100 mM HEPES pH 8.0, 10 mM $MgCl_2$, 1 mM EDTA, 40 mM KCl, 1 mM ATP (Sigma Aldrich, #A7699), 0.5 mM NADH (Sigma Aldrich, 1mM phosphoenolpyruvate (PEP; Sigma Aldrich, #P7252), 2 U/ml PK (Roche, #10128103001) and 2 U/ml LDH (Roche, #10127884001) to make a final volume of 200 µl. 0.5 mM ribulose 5-phosphate (Ru5P; Sigma Aldrich, #83899) was added into the reaction mixture to initiate the reaction.

MDH activity was also assayed by its NADPH turnover rate. 10 µg soluble algal protein extract was added into a total reaction volume of 200 µl comprising 100 mM HEPES pH 8.0, 10 mM $MgCl_2$, 1mM EDTA, 5 mM ATP (Sigma Aldrich, #A7699), 0.2 mM NADPH (Carl Roth, #AE14). MDH reaction was started by adding of 2 mM oxaloacetate into the reaction mixture. All enzyme reactions including GAPDH, PRK and MDH were set up in 96 well plates (Sarstedt, #83.3924500) and took place at 30 °C. The absorbance at 340 nm was measured using FilterMax® F5 multi-mode microplate reader (Molecular Devices).

II.2.14. Recombinant Protein Expression and Purification

C. reinhardtii total cDNA prepared as described above (see section II.2.3), was used as template for PCR amplifications of *C. reinhardtii NTRC*, *CP12*, and *PRX1* cDNAs. For *CrNTRC* cDNA amplification, primer pair used were P-2885 and P-2884 while for *CrCP12* cDNA, primer pair used were P-2888 and P-2843. *CrPRX1* cDNA was amplified using P-2887 and P-2933 primer pair. *A. thaliana CP12-2* cDNA was synthesized directly by Integrated DNA Technologies (IDT), and further amplified using primer pair, P-2932 and P-2854. These full length cDNAs were then cloned into the pET-28b-Sumo vector (Bepperling et al., 2012) via primer-introduced *Nde*I and *Xho*I restriction sites. This resulted in pET-28b: CrNTRC-His and pET-28b: CrCP12-His, and pET-28b: AtCP12-2-His constructs. The pET-28b-Sumo vector introduced His-tags to the N-terminal of the expressed proteins which facilitated the later protein purification. All primer sequences can be retrieved in Supplemental Table S2.

These pET-28b plasmid constructs and pQE-30: OsNTRC (a gift from Professor Cejudo; Serrato et al., 2004) were introduced into *E. coli* BL21-DE3 (Stratagene) and M15 (Qiagen) strains, respectively, following standard heat shock transformation procedures. Recombinant protein syntheses by these *E. coli* transformant strains were induced by 1 mM isopropyl-β-D-thiogalactopyranosid (IPTG) when the cultures reached OD_{600} of 0.6 and grown in Luria-Bertani (LB) broth at 37 °C overnight. For each recombinant protein, 1 L bacterial culture was harvested the next day and lysed in 30 ml IP lysis buffer (see section II.2.7) using high shear cell disruptor (Microfluidics) with 12.5 kPa pressure. Cell

debris was first removed by centrifugation at 15000 g, 4 °C for 20 minutes. Lysate was then filtered using CLEARLine® syringe filter with 0.45 µm pore size (Biosigma, #146561); resulted filtrate was incubated with 250 µl Protino® Ni-NTA agarose beads (Macherey-Nagel, #745400) overnight at 4 °C. The beads were collected and washed with 30 ml IP lysis buffer followed by elution with 5 ml elution buffer (150 mM NaCl, 400 mM Imidazole, 50 mM Tris-HCl pH 8.0). Each eluate was then buffer-exchanged and concentrated with the aid of Amicon® Ultra-10 kDa centrifugal filter (Merck Millipore, # UFC901024) to a final volume of around 200 µl in IP lysis buffer with cOmplete™ protease inhibitor (Roche, #04693116001).

II.2.15. *In vitro* Redox Activity Assays

CrNTRC, OsNTRC, CrCP12 and AtCP12 recombinant proteins used in this assay were prepared as described in section II.2.14, while reaction buffer used was IP lysis buffer. 100 µg CP12 proteins were mixed with 150 µg NTRC proteins, 30 mM NADPH (Carl Roth, #AE14) or both. For untreated, positive, and negative controls, 100 µg CP12 or PRX1 proteins were treated with blank IP lysis buffer, 5 mM reduced DTT (AppliChem, #A2948) or oxidized DTT (Sigma Aldrich, #D3511), respectively. All reactions were equalized to a final volume of 20 µl in PCR tubes and incubated at 37 °C for 1.5 hours. Subsequently, each reaction was stopped by adding 7 µl of ROTI®Load2 (4 x) non-reducing loading dye (Carl Roth, #K930). The proteins were then separated by SDS-PAGE (see section II.2.8) and stained with Coomassie Brilliant Blue G250 (Carl Roth #9598).

II.2.16. Production of Antisera against NTRC and CP12

NTRC amino acid sequences from *C. reinhardtii, A. thaliana, Physcomitrella patens* and *Synechocystis sp.* PCC 6803 were aligned (Supplemental Figure S2). A highly conversed peptide fragment flanking the amino acid number 93 to 190 (98 amino acids in length) of CrNTRC was selected and the corresponding DNA sequence was amplified from total cDNA using P-1798 and P-1799 primer pairs. The amplified DNA fragment was then cloned into the pMal-c5x expression vector (GE Healthcare) via the primer-introduced restriction sites *BamH*I and *EcoR*I (Thermo Fisher Scientific). This produced pMal: CrNTRC (98 aa) construct which was then amplified in XL1-blue *E. coli* strain (Stratagene) and purified using NucleoBond® Xtra midi-prep kit (Machery-Nagel, #740410).

CrNTRC (98aa) peptide overexpression was carried out with BL21-D3E strain (Stratagene) and protein purification was performed according to the protocol described in section II.15 but with some modifications as stated in the following. Instead of nickel beads, 1ml of 80 % amylose resin (New England Biolabs (NEB), #E8021L) was used for binding MBP-fused CrNTRC peptide from the bacterial lysate. Further, MBP-lysis buffer (30 mM Tris pH7.5, 450 mM NaCl, 1 mM DTT) instead of

IP lysis buffer, was used for cell lysis and bead washing. Elution was also done by using MBP-elution buffer (MBP lysis buffer supplemented with 15 mM Maltose).

To produce polyclonal antisera against CrNTRC and CrCP12 proteins, 1 mg of each purified MBP-fused CrNTRC (98 aa) peptide and His-tagged CrCP12 (full length) recombinant proteins were sent as antigen to immunize a rabbit (Pineda Antikörper-Service). Immunoblotting analyses were carried out to test the produced antisera for specificity and sensitivity of CrCP12 antiserum (Supplemental Figure S3). CrNTRC antiserum was generated and tested by Dr. Daniel Neusius during his Master thesis study (Neusius, 2015).

II.2.17. Generation of *cp12* and *neet* Knockout Mutants via CRISPR/Cas9

CP12 knockout was carried out on *C. reinhardtii* CC-406 (*cw15*) strain using CRISPR/Cas9 technique following the protocol established by Greiner et al. (2017). First, CRISPR-P v2.0 online tool (http://crispr.hzau.edu.cn/cgi-bin/CRISPR2/CRISPR) was used to design two *CP12* crRNA sequences, namely *CP12* crRNA #1: 5'-AGCAGCGCUGAGCUCCUCAACGG-3' and *CP12* crRNA #2: 5'-AGCAGCGCUGAGCUCCUCAACGG-3' which later gave rise to *cp12* #1 and *cp12* #2 mutant strains, respectively. Next, annealing of the *CP12* crRNA (10 µM; Integrated DNA Technologies) with tracrRNA (10 µM; Integrated DNA Technologies, #1072533) was performed in DUPLEX buffer (Integrated DNA Technologies) to generate non-coding guide RNA (gRNA) which led the Cas9 endonuclease specifically to the target site – *CP12* exon-2. Further, a double stranded DNA mutation oligonucleotide was annealed from the primer pair – Flag-3xStop-EMX1 forward (P-2366) and reverse (P-2367) primers. This mutation oligonucleotide encoded *EMX1*, flanked by a pair of frameshift tolerant stop codons sequences and a reverse complementary pair of FLAG-tag sequences. *EMX1* is a well characterized, validated CRISPR site derived from human homeobox protein gene (Ran et al., 2015) and can serve as an additional targeting site for further genetic manipulation in future. The frameshift tolerant stop codons were designed to increase knockout efficiency while the FLAG-tag sequence was to facilitate colony screening via PCR. The annealing reactions for both gRNA and mutation oligonucleotide were carried out by heating at 95 °C for 2 minutes followed by a gradient temperature decrease of 0.1 °C/second to 20 °C. Next, the gRNA (3 µM) was then assembled with SpCas9 enzyme (3 µM) from *Streptococcus pyogenes* (Integrated DNA Technologies, #1081058) in 1 x Buffer O (Thermo Fisher Scientific, #BO5) at 37 °C for 15 minutes.

C. reinhardtii suspension with a density of 1 x 10^8 cells/ml in Max Efficiency® transformation buffer (Invitrogen, #A24229) supplemented with 40 µM sucrose was prepared. This algal suspension was pre-activated by warming at 40 °C plus 350 rpm slow shaking for 30 minutes followed by a recovery period of 30 minutes at room temperature. Subsequently, 0.3 µM SpCas9:gRNA complex, 0.5 µM mutation oligonucleotide, and 0.3 µg of pBC1 empty plasmid vector carrying a paromomycin

resistance cassette were added to 40 µl of the pre-activated algal suspension in an electroporation cuvette with 2 mm gap width (Nepa Gene, #EC-002S). Electroporation was then conducted using NEPA21 electroporator (Nepa Gene) with 2 pulses of 200 V (pulse length: 8 ms; interval between pulses: 50 ms; pulse decay rate: 40 %; pulse polarity: +) following by 5 pulses of 20 V (pulse length: 50 ms, interval between pulses: 50 ms; pulse decay rate: 40 %; pulse polarity: +/–). The observed optimal resistance fell around 300 Ω to 600 Ω. The electroporated algae were allowed for recovery in TAPS liquid medium under 30 µE/m^2/s light at 23 °C overnight. The algae were then spread on TAP agar with 10 µg/ml paromomycin for selection for around 10–14 days under 30 µE/m^2/s light at 23 °C.

After that, colony candidates were picked and screened by two rounds of colony PCR with the help of Phire™ Plant Direct PCR kit (Thermo Fisher Scientific, #F130WH) for the insertion of the mutation oligonucleotides into the *CP12* exon-2. The first round was with CP12 short locus primer pair (P-2892 and P-2893). The second round was using FLAG forward primer (P-2891) and CP12 long locus reverse primer (P-2895). Potential knockout candidates were then sequenced for their genomic *CP12* regions using CP12 long locus primer pair (P-2894 and P-2895). Immunoblot analysis with CP12 antibody was also performed as a confirmation test.

For generation of a *neet* knockout strain, similar procedures as above were performed with *NEET* crRNA sequence: 5'-UCUGCGCUCCGUUUCCUCCGCGG-3' target exon-1 of *NEET* gene. Two rounds of colony screenings via PCR were performed with NEET short locus primer pair (P-2898 and P-2897), followed by FLAG forward primer (P-2891) paired with NEET long locus reverse primer (P-2896). Putative positive colonies were then validated by sequencing using NEET long locus reverse primer (P-2897) and NEET short locus forward primer (P-2898). All primer sequences can be found in Supplemental Table S2.

II.2.18. Accession Numbers

DNA and amino acid sequences for genes of interest were retrieved from Phytozome v12.1 [Joint Genome Institute (JGI); https://phytozome.jgi.doe.gov/pz/portal.html] under the following loci identifiers: Cre01.g054150 (*CrNTRC*), Cre08.g380250 (*CrCP12*), Cre01.g050550 (*CrNEET*), Cre06.g257601 (*CrPRX1*), AT2G41680 (*AtNTRC*), AT3G62410 (*AtCP12-2*) and Pp3c20_5530 (*PpNTRC*). For *SyNTRC*, sequence was retrieved from CyanoBase (http://genome.microbedb.jp/cyanobase/) under gene identifier Slr0600.

III. RESULTS

III.1. *ntrc* Mutant Displays a Redox-dependent Cold Phenotype

Characterizations of NTRC have been done primarily in *A. thaliana* and *O. sativa*, but not much is known in lower photoautotrophs such as microalgae. To investigate the role of NTRC in *C. reinhardtii*, a *ntrc* knockout mutant obtained from the Niyogi Lab (UC Berkeley, California) was used for complementation studies with various versions of the *NTRC* gene. The *ntrc* strain was generated via random insertional mutagenesis using a linearized pMS188 plasmid (Dent et al., 2005). A fragment of around 10.8 kb covering the *NTRC* gene was found spontaneously deleted after the pMS188 insertion at the first intron of the *NTRC* gene (Figure 8; Dent et al., 2005). Detailed mapping of the pMS188 insertion region was carried out by Dr. Daniel Neusius during his Master study (Neusius, 2015). He found the deleted fragment covers a major part of the *NTRC* gene, a nuclear genome locus Cre01.g054200, as well as the 3'UTR and 34 bp of the last exons of the *Cytochrome P450* gene (Figure 8). Other the other hand, Cre01.g054200 is unannotated of functional domains and function. It is not found in other photoautotrophs except *Volvox carteri*, another member of the Chlamydomonadales order.

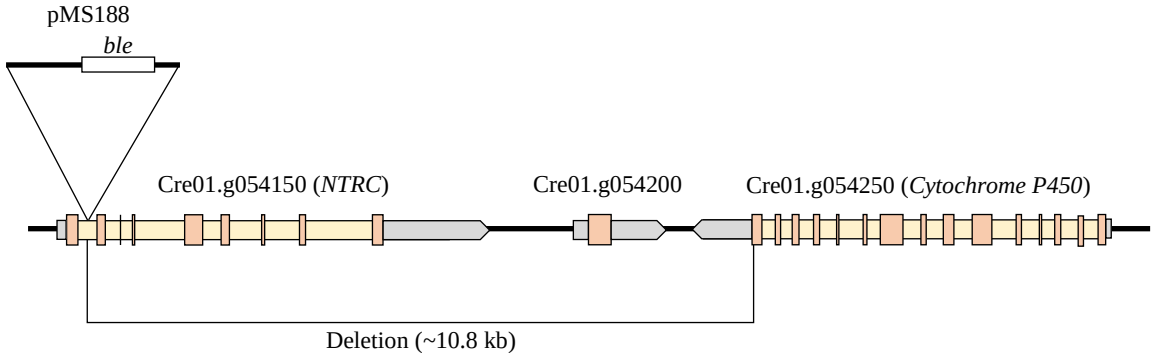

Figure 8. Schematic map showing deletion of the genomic region upon pMS188 vector insertion on chromosome-1 in the *C. reinhardtii ntrc* knockout strain. Linearized pMS188 plasmid was inserted into the first intron of *NTRC* gene. The vector has a size of 4.7 kb, carrying a zeocin antibiotic resistance cassette (*ble*). Promoters and replication origin of the plasmid are not shown. Orange- and light-orange-coloured bars represent exons and introns of a gene, respectively. Grey blunt and pointed bars denote 5'UTR and 3'UTR, respectively. A 10.8 kb DNA fragment downstream of the pMS188 insertion site, was spontaneously deleted. The deleted fragment contains a major part of the *NTRC* gene, the entire Cre01.g054150 locus, as well as the 3'UTR and exactly 34 bp of the last exon of the *Cytochrome P450* gene.

The absence of the NTRC protein in this strain was first confirmed by Western blot analysis shown in Figure 9A. Complementation of the mutant with plasmid construct carrying the *NTRC* gene under control of the native *NTRC* 5'UTR (see Supplemental Figure S1 for a plasmid map) restored the accumulation of the protein in the transformants (*ntrc:NTRC*). However, likely due to epigenetic effects

caused by the random nuclear insertion of the re-introduced *NTRC* gene, the complemented strains revealed different levels of the NTRC protein. To exclude any dosage effects, one transformant accumulating wild-type-like level of the NTRC protein was chosen for all further experiments (Figure 9A).

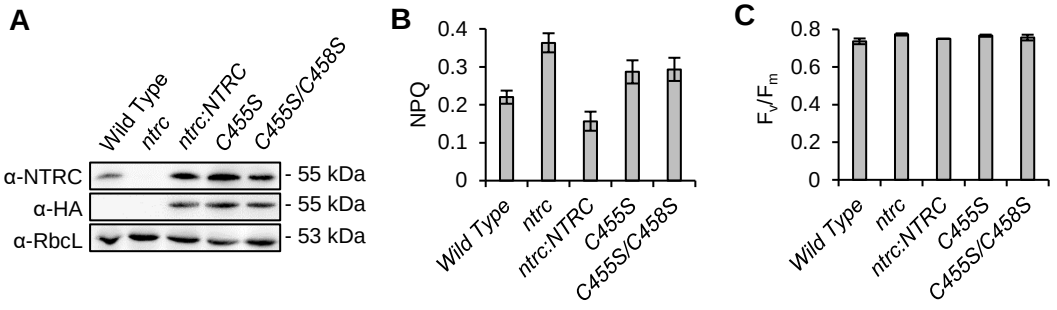

Figure 9. Immunoblot and PAM fluorometry analyses characterising *C. reinhardtii* strains with different genetic statuses of *NTRC*. *ntrc* denotes *NTRC* knockout, *ntrc:NTRC* represents the *ntrc* strain complemented with the *NTRC* gene while *C455S* and *C455S/C458S* were generated from the *ntrc* strain complemented with *NTRC* carrying point mutations leading to single or double cysteine to serine exchanges at the thioredoxin domain CGPC motif active site, respectively. **A,** Western blot analysis of NTRC protein levels is shown; Applied antibodies are indicated on the left, molecular weights in kDa at the right of each panel. RbcL served as a loading control. **B – C,** NPQ (B) and F_v/F_m magnitudes (C) of the *ntrc* knockout strain, its background wild type strain CC-4051 as well as the three complemented strains *ntrc:NTRC*, *C455S*, and *C455/C458S*, respectively. Data presented are means and standard deviations derived from three independent *C. reinhardtii* culture spots on TAP agar, grown at 23 °C, 30 µE/m^2/s.

To obtain further indications if the observed cold-specific phenotype of the *ntrc* mutant points to an oxidoreductase activity of the NTRC protein (compare section I.2.2), the complementation study was expanded to strains expressing mutated NTRC proteins. More precisely, cysteines located at the CGPC motif of NTRC's thioredoxin domain, namely C455 and C458, were exchanged to serine. These cysteine residues are known to form disulphide bridges, critical for the redox interactions between NTRC and its downstream targets (compare section I.2.2; Holmgren & Bjornstedt, 1995). Instead of using a wild-type *NTRC* gene, the *ntrc* strain was complemented with a plasmid vector encoding a NTRC with either single or double cysteine mutation(s), resulting in *C455S* and *C455S/C458S* mutant strains, respectively (see Supplemental Figure S1 for a plasmid map). Also, for these strains expressing mutated NTRC proteins, transformants with wild-type like NTRC protein levels were chosen for further analysis (Figure 9A). To facilitate the detection and purification of the NTRC proteins expressed by all complemented strains in later experiments the proteins were C-terminally fused with a hemagglutinin (HA) tag and could additionally be detected by an HA-specific antiserum (Figure 9A).

Next, an initial functional test on the generated strains was performed using pulse amplitude modulation (PAM) fluorometry. This is because the loss of NTRC function in *A. thaliana* mutants has been reported to cause an elevation in NPQ which can be estimated by PAM measurement (Carrillo et

al., 2016; Naranjo et al., 2016). NPQ is a photoprotective strategy by which excess light energy absorbed is dissipated as heat to protect the photosystems from damage (reviewed in Müller et al., 2001). Consistent with reported data from *Arabidopsis thaliana*, *ntrc*, *C455S* and *C455S/C458S* strains showed higher magnitudes of NPQ than the wild-type and *ntrc:NTRC* strains (Figure 9B), validating genetic modifications of the microalgal strains have been functionally translated. F_v/F_m values on the other hand, which indicate PSII activity were unaltered in *ntrc* and all three complemented strains as compared to the wild type (Figure 9C).

Subsequently, a series of growth studies of the generated strains was conducted under different culturing conditions (Figure 10, Supplemental Tables S4 and S5). All analysed strains showed similar doubling times of around 11 hours in TAP liquid medium, at 23 °C (Figure 10, A and C). Nevertheless, clear differences were observed at 15 °C. The *ntrc* mutant grew slower than the wild type, having a longer doubling time of about 33 hours, as compared to that of 21.5 hours of wild-type (Figure 10, B and D). This suggests a cold tolerance coffered by NTRC. In contrast, the *ntrc:NTRC* strain at 15 °C exhibited a doubling time comparable to that of the wild type, verifying the observed growth phenotype in the cold to be *NTRC*-specific (Figure 10, B and D). Additionally, a strain with complementation of both *NTRC* and Cre01.g054200 gDNA into the *ntrc* mutant was also generated. This strain showed neither different from *ntrc:NTRC* nor the wild-type in growth at 15 °C (and 23 °C), indicating the additionally deleted gene in the *ntrc* mutant has no influence on cold-tolerance (data not shown).

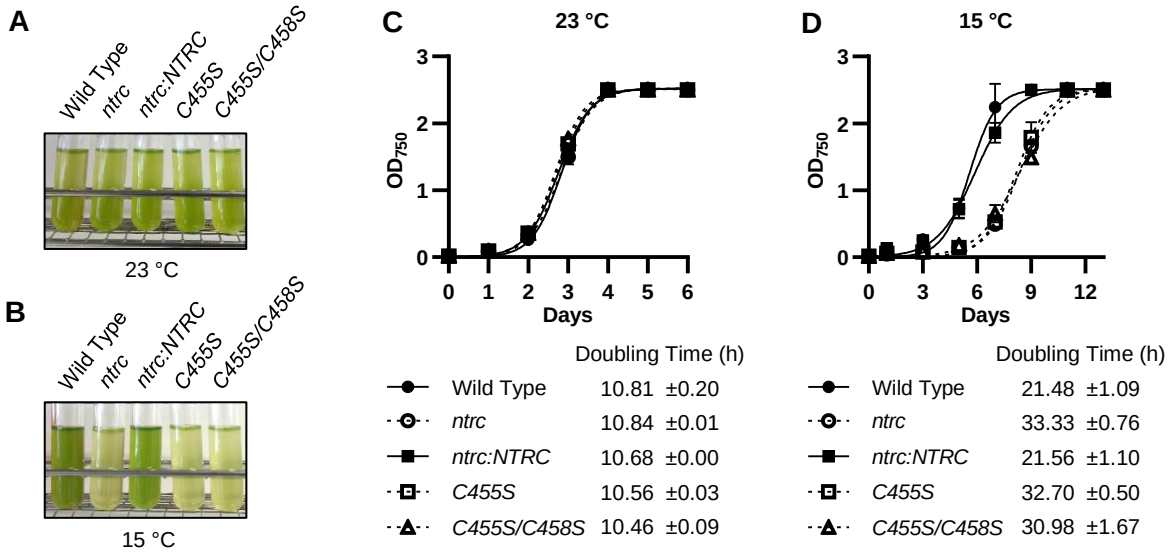

Figure 10. Mutations in the *NTRC* gene affect the growth behaviour of *C. reinhardtii* under cold conditions. Growth studies of microalgal strains with different *NTRC* genotypes in TAP liquid medium at 23 °C or 15 °C. The liquid cultures with initial optical density (OD_{750}) of 0.015 were grown in flasks with 25 ml TAP medium, and culture densities were accessed every 2 days at OD_{750}. **A – B,** Photographs of the cultures grown at 23 °C (A) and 15 °C (B) were taken at day 10. 5 ml culture of each strain was then placed into a glass tube for image capturing. **C – D,** Growth curves compiling data from three

independent cultures were then plotted using GraphPad Prism v8 software. Error bars denote standard deviations (SD). Doubling times in hours are shown underneath the graphs, with the corresponding SD values shown after '±' signs.

When the *C455S* and *C455S/C458S* strains were cultured at 23 °C, they both grew at the wild-type rate, with an 11-hour doubling time (Figure 10, A and C). However, when the microalgal cultures were incubated at 15 °C, the cold phenotype appeared again; both *C455S* and *C455S/C458S* strains behaved like the *ntrc* strain, growing slower than the wild type (Figure 10, B and D). The growth experiment was also repeated on solid media, and similar growth patterns were observed (Figure 11). There was no difference in the algal density among all the five analysed strains at 23 °C after 8- or 12-day growth on the agar (Figure 11). On the contrary, at 15 °C, the *ntrc* knockout and cysteine-substituted strains grew much slower than the wild-type and *ntrc:NTRC* as indicated by densities of the algal spots on the agar (Figure 11). Taken together, both of the growth studies in liquid and on solid media provide strong evidence for the redox dependency of NTRC-mediated cold acclimation in *C. reinhardtii* which is likely conveyed by at least one reducible downstream target of the NTRC protein.

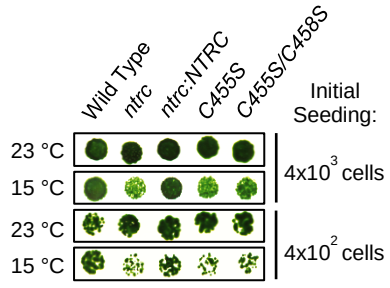

Figure 11. Growth studies of *C. reinhardtii* strains with different *NTRC* genotypes on solid agars. *C. reinhardtii* strains were grown on TAP agar at different initial densities and incubated at different temperatures as indicated. Photographs for 23 °C and 15 °C were taken on day 8 and day 12, respectively, when their wild-type CC-4051 controls reached comparable densities to each other. Only growth with initial seeding numbers of 4000 or 400 cells per spot are presented here. The experiment was repeated two times with similar results.

III.2. NTRC Interacts with CP12 in the Cold

This finding of redox-dependency of NTRC-mediated cold tolerance is startling because the only report describing the cold acclimation role of NTRC, published in 2015 by Moon and co-workers, attributed the phenotype to NTRC's cryoprotective chaperone binding activities to nucleic acids and proteins (compare section I.2.4). In order to identify NTRC's downstream redox target(s) which is(are) responsible for cold acclimation, it was intended to perform co-immunoprecipitations of the HA-tagged NTRC protein using the complemented strain *ntrc:NTRC*. Therefore, the subcellular localisation of the NTRC protein was determined first by a cell fractionation study (Figure 12). Proteins were extracted stepwise as described in Figure 12A. The obtained soluble protein fraction as well as fractions containing hydrophilic peripheral membrane proteins, hydrophobic peripheral membrane proteins or integral membrane proteins were immunologically analysed (Figure 12B). NTRC proteins were present almost exclusively in the soluble fraction while only minor amounts of the protein could be detected in the peripheral membrane protein fractions.

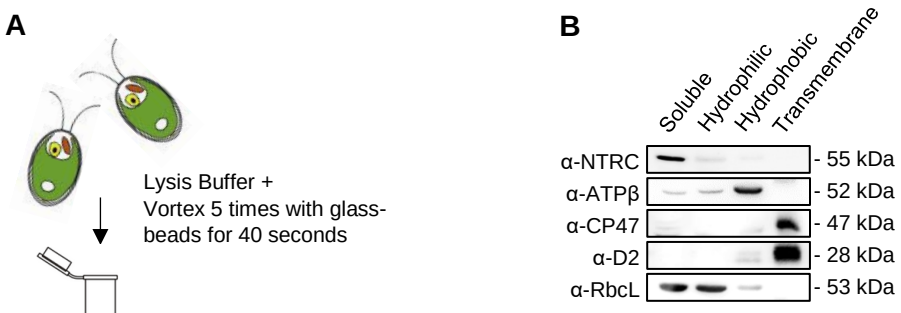

Figure 12. NTRC is a soluble protein. **A,** Diagram illustrating the protein extraction protocol. Algal proteins from wild-type CC-4051 were released step by step using mechanical force, high concentration NaCl salt solution, chaotropic urea, and detergent (Triton-X100). **B,** Immunoblot analysis of protein fractions obtained via the protein fractionation method described in (A). While RbcL served as marker protein for the soluble chloroplast stroma, the β-subunit of the chloroplast ATP synthase (ATPβ) is peripherally attached to the thylakoid membrane. CP47 and D2 represent integral membrane proteins.

According to the determined subcellular localisation of the NTRC, for the co-immunoprecipitation (co-IP), only the soluble protein fraction was used to reduce the number of contaminating proteins and improve the signal-to-noise ratio. Proteins were pulled down from the *ntrc:NTRC* strain with the assistance of the HA-epitope tag and precipitates were analysed by silver staining after separation in an SDS PAGE gel (Figure 13A). Two sharp bands with protein sizes corresponding to NTRC and PRX1, the already known and well-characterized redox target of NTRC (compare section I.2.3), appeared in the protein precipitate from the *ntrc:NTRC* strain but not from the wild type, indicating the success of the pull-down assay (Figure 13A).

Mass spectrometry analysis of the co-IP output was then conducted, and a number of putative NTRC binding protein candidates was identified and shortlisted based on several criteria including the presence of cysteine residues and/or chloroplast localization (Supplemental Table S6). These candidates are from various functional categories including proteins involved in carbon fixation as well as in protein and lipid metabolisms (Supplemental Table S6). There are also four proteins of unknown function identified; their respective Uniport identity codes are given in Supplemental Table S6. Further, several proteins showed temperature-dependent precipitation such as CP12, protein disulphide

isomerase 4 (PDI4), acetyl-CoA carboxylase subunit-C (AccC), the PSII stability/assembly factor High Chlorophyll Fluorescence 136 (HCF136), the stromal Heat Shock Protein 70B (HSP70B), as well as three of the uncharacterized proteins (Supplemental Table S6). These proteins demonstrated a detectable binding to NTRC only under cold conditions. However, among them, only three proteins showed a redox-dependent precipitation, evidenced by the reduced or non-detectable binding enrichments from the *C455S/C458S* strain in which the disulphide-forming C455 and C458 residues of NTRC were mutated. They are CP12, PDI4 and one of the uncharacterized proteins – A8HND3 (Supplemental Table S6). According to the Uniprot database, A8HND3 with a zinc-finger CDGSH domain is predicted to be a homolog of the *A. thaliana* iron metabolism-related protein NEET (Nechushtai et al., 2012; Zandalinas et al., 2020), but has not been investigated in algae. Both proteins, CP12 and the NEET protein are predicted to localise to chloroplasts based on PredAlgo algorithm (Tardif et al., 2012), while PDI4 is not found to have a chloroplast transit sequence and was therefore excluded from further analyses.

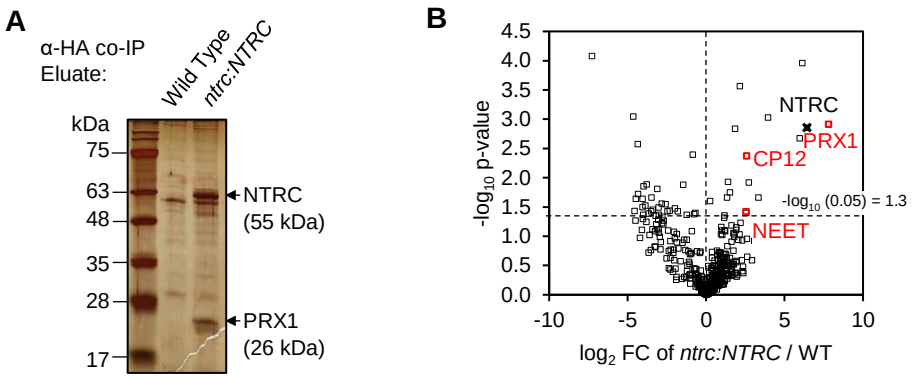

C

Phytozome Accession #	Protein Candidates	Binding Enrichment (log_2 FC compared to WT)			
		23 °C		15 °C	
		ntrc:NTRC	*C455S/C458S*	*ntrc:NTRC*	*C455S/C458S*
Cre01.g054150	NTRC	14.90	16.34	6.41	7.27
Cre06.g257601	PRX1	5.72	2.45	7.80	3.67
Cre08.g380250	CP12	-	-	2.56	-
Cre01.g050550	NEET	-	-	2.53	-

Figure 13. Co-immunoprecipitation (co-IP) analysis of HA-tagged NTRC. Anti-HA antibodies were used in the pull-down experiments; co-IP eluates from *C. reinhardtii ntrc:NTRC* strain expressing HA-tagged NTRC proteins, was compared to those from the wild-type CC-4051 strain which served as a negative control. The *C455S/C458S* strain served as an additional control to access the redox dependency of protein interactions. **A,** Silver-stained SDS-PAGE gel separating the co-IP eluates derived from wild-type and *ntrc:NTRC* strains which had been grown at 15 °C for 48 hours. **B – C,** Mass spectrometry analysis of eluates derived from HA-tagged NTRC co-IP. All data were derived from four biological replicates. **B,** Scatter plot demonstrating binding of CP12 to NTRC in *ntrc:NTRC* strain which had been inoculated at 15 °C for 48 hours. log_2 fold change (FC) represents binding enrichment, while -log p-value larger than 1.3 indicates statistical significance with a p-value smaller than 0.05. Protein candidates of interest are labelled in red. **C,** Table showing binding enrichments of potential protein

candidates to NTRC at different growth temperatures and different CGPC motif status. '–' sign denotes non-detectable binding. Data presented are with p-value <0.05.

Hence, in particular, CP12 and NEET stood out among the candidates (Figure 13B). As just mentioned above, both of them exhibited non-perceivable binding enrichments from the *C455S/C458S* strain (Figure 13C). Similar binding behaviour was also observed for PRX1 which showed decreased binding affinity to the mutated NTRC (Figure 13C). These data imply that CP12 and NEET, like PRX1, are downstream redox targets of NTRC. Besides, CP12 also fulfils the basic criteria as a known chloroplast protein with four redox-sensitive cysteine residues (Pohlmeyer et al., 1996; Wedel et al., 1997), while NEET exhibits three cysteine residues. More importantly, the binding of CP12 and NEET to NTRC were only detectable when the algae were cultivated at 15 °C but not at 23 °C as summarized in Figure 13C, suggesting their binding is cold-related. Nonetheless, the study of NEET in *C. reinhardtii* is still at a preliminary stage, and CP12 is on the main focus of this thesis.

III.3. NTRC Reduces CP12 *in vitro*

In vitro redox activity assays were performed to verify if the physical interaction between NTRC and CP12 also involves a redox exchange between their disulphides, in other words, to find out if CP12 is indeed a redox target of NTRC. To this end, recombinant *C. reinhardtii* (Cr) NTRC, CP12 and PRX1 proteins were expressed and purified from *E. coli*. The redox capacity of the purified recombinant CrNTRC protein was first tested on recombinant CrPRX1 (Supplemental Figure S4A). Under untreated and oxidized conditions, CrPRX1 appeared as around 50 kDa in size on a non-reducing SDS-PAGE gel due to the dimer formation via intermolecular disulphide bridges (Supplemental Figure S4A). Conversely, under reducing conditions generated by reduced DTT or a combined treatment with CrNTRC and NADPH, PRX1 was present in the monomeric form of 26 kDa (Supplemental Figure S4A). Nonetheless, single treatment with CrNTRC or NADPH alone failed to reduce the disulphide bridges of PRX1 dimers, demonstrating the NTRC-catalysed reduction reaction requires NADPH from which the enzyme derives its reducing power (Supplemental Figure S4A). Together, these results indicate that the recombinant CrNTRC prepared is active and could be used for the study of CP12.

Consistent with what has been reported (Oesterhelt et al., 2007), the DTT-reduced recombinant CrCP12 exhibited an upward shift in non-reducing SDS-PAGE gels, having a size of about 20 kDa as compared to that of 17 kDa in the untreated and oxidized controls (Figure 14). This suggests the existence of intramolecular disulphide bridges which compress the protein confirmation. On the other hand, similar to CrPRX1, neither NADPH nor recombinant CrNTRC alone could sufficiently reduce CrCP12 (Figure 14). However, an upward shift was again detected when CrCP12 was treated with NADPH and CrNTRC combinedly, suggesting CrNTRC, deriving its reducing potential from NADPH,

reduces CrCP12 (Figure 14). Furthermore, cross-species reactivity was observed in CP12 reduction by NTRC; an algal NTRC can reduce a plant CP12, and vice versa (Figure 14). CrNTRC with NADPH can reduce recombinant CP12 isoform-2 of *A. thaliana* (At; Figure 14). Besides, *OsNTRC* gene has been known 72.4% identical to *AtNTRC* gene (Serrato et al., 2004). With the kind gift of pQE-30: OsNTRC plasmid from Prof. Cejudo, recombinant NTRC of *O. sativa* (Os) was expressed, purified, and used for the study of plant NTRC's redox activity on CP12. The recombinant OsNTRC was first tested catalytically active on CrPRX1 (Supplemental Figure S4B). And then, when incubated with recombinant CP12s, OsNTRC supplemented with NADPH not only can reduce AtCP12-2 but also CrCP12 (Figure 14). These *in vitro* data reveal that the reduction of CP12 by NTRC is phylogenetically conserved across oxygenic photosynthetic eukaryotes.

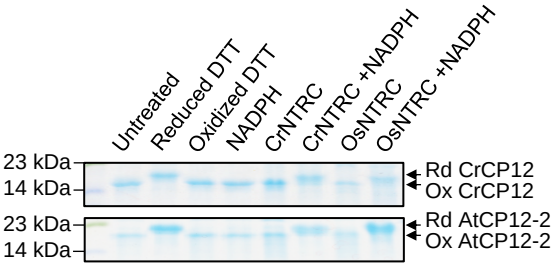

Figure 14. *In vitro* redox activity assays accessing reducing reactivity of recombinant NTRC on CP12. Recombinant NTRC and CP12 proteins of *C. reinhardtii* and *A. thaliana* were used in this assay. NTRC of *O. sativa* was used as a plant reductase in the assay. In general, 100 µg CP12 proteins were either treated with 30 mM of NADPH, 150 µg NTRC proteins or a combination of both. Plain buffer solution was used as the untreated control, while treatment with 5 mM of either reduced or oxidized DTT served as positive and negative controls, respectively. The reaction mixes were then incubated for 1.5 hours at 37 °C before proceeding to non-reducing SDS-PAGE followed by Coomassie blue staining. Pictures are from a representative experiment which had been repeated at least two times with similar results.

III.4. *Chlamydomonas* NTRC Dissociates the PRK/CP12/GAPDH Complex *in vitro*

CP12 is known to functions as a linker protein for GAPDH and PRK across phototrophs, to form an autoinhibitory supracomplex ranging from 460 to 640 kDa in size, comprising two GAPDH tetramers, two PRK dimers and four CP12 monomers (Avilan et al., 1997; Wedel et al., 1997; Wedel & Soll, 1998; Scheibe et al., 2002; Graciet et al., 2004; Marri et al., 2005; Marri et al., 2008). The complex integrity has also been suggested depending on CP12 redox status (Wedel et al., 1997; Lebreton et al., 2006; Marri et al., 2008). Hence, it is vital to question if NTRC as a reductase for CP12 has an impact on the complex assembly.

First, the native PRK/CP12/GAPDH complex status of proteins extracts from the wild-type and *ntrc* mutant of *C. reinhardtii* was analysed using size exclusion chromatography (SEC). The complex status was followed by PRK, GAPDH subunit-A, and CP12 protein detection using their corresponding antibodies. In the wild-type algal protein extract (untreated), all the three proteins were detected at around 440 kDa, with overlapping peaks of elution in fractions 10 and 11 which were estimated to contain protein complexes of ~ 350 to ~ 550 kDa (Figure 15A, left panel). These high molecular weight

complexes likely represent the PRK/CP12/GAPDH complex of *C. reinhardtii* which has a reported size of 460 kDa (Avilan et al., 1997; Graciet et al., 2004). Worth noting, PRK and GapA protein were mostly detected in these complexes and there existed only faint bands at about 152 kDa and 90 kDa which are the calculated sizes of GAPDH tetramers and PRK dimers, respectively (Figure 15A, left panel; Avilan et al., 1997). On the other hand, in addition to the high molecular weight elution fractions, CP12 was also detected predominantly in the range of about 29 to 43 kDa which are probably the free CP12 monomers (Figure 15A, left panel). Although CP12 is predicted to be 14 kDa in size based on its amino acid composition, possibly due to its intrinsically disorder properties (compare section I.3.7), it has also been detected in the range of 29 to 35 kDa in SEC assays conducted by Marri et al. (2005).

NADPH binding to GAPDH enzyme has been demonstrated to favour the dissociation of the PRK/CP12/GAPDH complex (compared sections I.3.5 and I.3.6; Wedel et al., 1997; Wedel & Soll, 1998; Tamoi et al., 2005; Trost et al., 2006). Likewise, when the soluble protein extract from the wild-type *C. reinhardtii* was treated with NADPH, there were pronounced shifts in PRK, GapA, and CP12 protein distributions, towards the direction of lower molecular weight (Figure 15A, left panel). PRK was found to have peaks of elution corresponding to ~ 80 to 158 kDa (fractions 13 and 14), likely reflecting the accumulation of free PRK dimers which have a size of roughly 90 kDa (Figure 15A, left panel). Concomitantly, GapA's elution peaks were detected in the range of ~ 80 to 232 kDa (fractions 12 to 14), consistent with the size of an A_4-GAPDH tetramer (152 kDa), while CP12 appeared solely at approximately 35 kDa (fraction 16) which denotes the free monomer (Figure 15A, left panel). Although very mere GapA signals were also found at about 440 kDa, in the elution fractions 10 and 11, PRK and CP12 were no longer detectable in these fractions upon NADPH treatment (Figure 15A, left panel). Together, these observations clearly demonstrate a radical dissociation of the PRK/CP12/GAPDH complex in the NADPH-treated wild-type algal extract (Figure 15A, left panel).

Apart from that, when the protein extract was untreated, the *ntrc* knockout mutant displayed highly similar PRK/CP12/GAPDH complex elution profile as that of the wild type. However, contrary from the wild type, the complex dissociated only partially when a protein extract from the *ntrc* strain was treated with NADPH (Figure 15A, right panel). This was evidenced by the observation that although GapA tetramer identification in the range of ~ 80 to 232 kDa increased significantly as compared to the untreated control, prominent bands representing the complex still appeared at around 440 kDa when detected with all the three antibodies, (Figure 15A, right panel).

Interestingly, a complete complex dissociation in the *ntrc* algal protein extract can be achieved with prolonged NADPH incubation (data not shown) or by simply adding recombinant CrNTRC (Figure 15A, right panel). Upon NADPH combined CrNTRC treatment, PRK, GapA, and CP12 proteins accumulated only in the low molecular weight range, peaking at ~ 80 to 158 kDa, ~ 80 to 232 kDa, and ~ 35 kDa, respectively (Figure 15A, right panel). These results reveal that the accumulation of the free

enzymes upon NADPH-induced complex dissociation, can be accelerated *in vitro* by recombinant CrNTRC, especially in the *ntrc* algal protein extract wherein native NTRC proteins are absent. In contrast, the NADPH/CrNTRC-treated wild-type algal protein extract exhibited a highly similar PRK/CP12/GAPDH protein distribution profile to that with NAPDH-treatment, indicating with the presence of native NTRC, addition of recombinant CrNTRC add no further effect in catalysing the complex dissociation (Figure 15A, left panel). Aside from that, applying recombinant CrNTRC protein alone was found insufficient to cause any effect on the complex status in both wild-type and *ntrc* algal protein extracts, indicating that there was a need of reducing potential derived from NADPH for NTRC to deliver the complex dissociating effect (Figure 15A). Taken together, these *in vitro* results together provide evidence supporting that NTRC as a redox regulator for CP12, can subsequently promote the PRK/CP12/GAPDH complex dissociation.

Furthermore, to validate if the PRK/CP12/GAPDH complex assembly is indeed catalytically inhibitory to PRK and GAPDH enzyme activities, elution fractions 10 and 13 of SEC-separated wild-type algal protein extract were compared for their enzyme activities (Figure 15B). The PRK and GAPDH enzyme activities were accessed by photometrical assays measuring the consumption rate of NADPH and NADH, respectively. While NAPDH is a direct substrate of GAPDH, the photometrical assay for PRK activity was facilitated by the coupling of ADP formation by the PRK catalytic reaction to the oxidation of NADH via PK and LDH enzymes. The elution fractions 10 and 13 likely contained the PRK/CP12/GAPDH complex and free enzymes, respectively. To have a complete complex dissociation so as to enhance the free enzymes collection in fraction 13, an algal protein extract was also treated with NADPH and included in the comparison (Figure 15B).

As indicated by the SEC analysis, both PRK and GapA protein detections peaked at approximately 440 kDa (fractions 10 and 11), demonstrating the integrity and predominance of the PRK/CP12/GAPDH complex in the wild-type strain (Figure 15B, upper panel). There existed no difference in both PRK and GAPDH enzyme activities between elution fractions 10 and 13 of the untreated protein extract, regardless of their differences in enzyme accumulation (Figure 15B, lower panel). On the contrary, the NADPH-treated algal protein extract experienced a drastic complex dissociation as indicated by the rightward shift in PRK and GapA protein distribution in the SEC analysis (Figure 15B, upper panel). PRK and GapA proteins accumulated in fractions 12 to 14 (Figure 15B, upper panel). Concomitantly, there was a dramatic increase of both PRK and GAPDH enzyme activities in fraction 13 as compared to fraction 10 (Figure 15B, lower panel). It is difficult to conclude from here that the difference in enzyme activities was either a result of the complex status change or the variation in protein amounts. Nonetheless, when comparing the complex-containing fraction 10 of the untreated control and the free enzyme-containing fraction 13 of the NADPH-treated algal protein extract, it is clear that the PRK/CP12/GAPDH complex showed relatively lower enzyme activities as compared to the free enzymes (Figure 15B, lower panel).

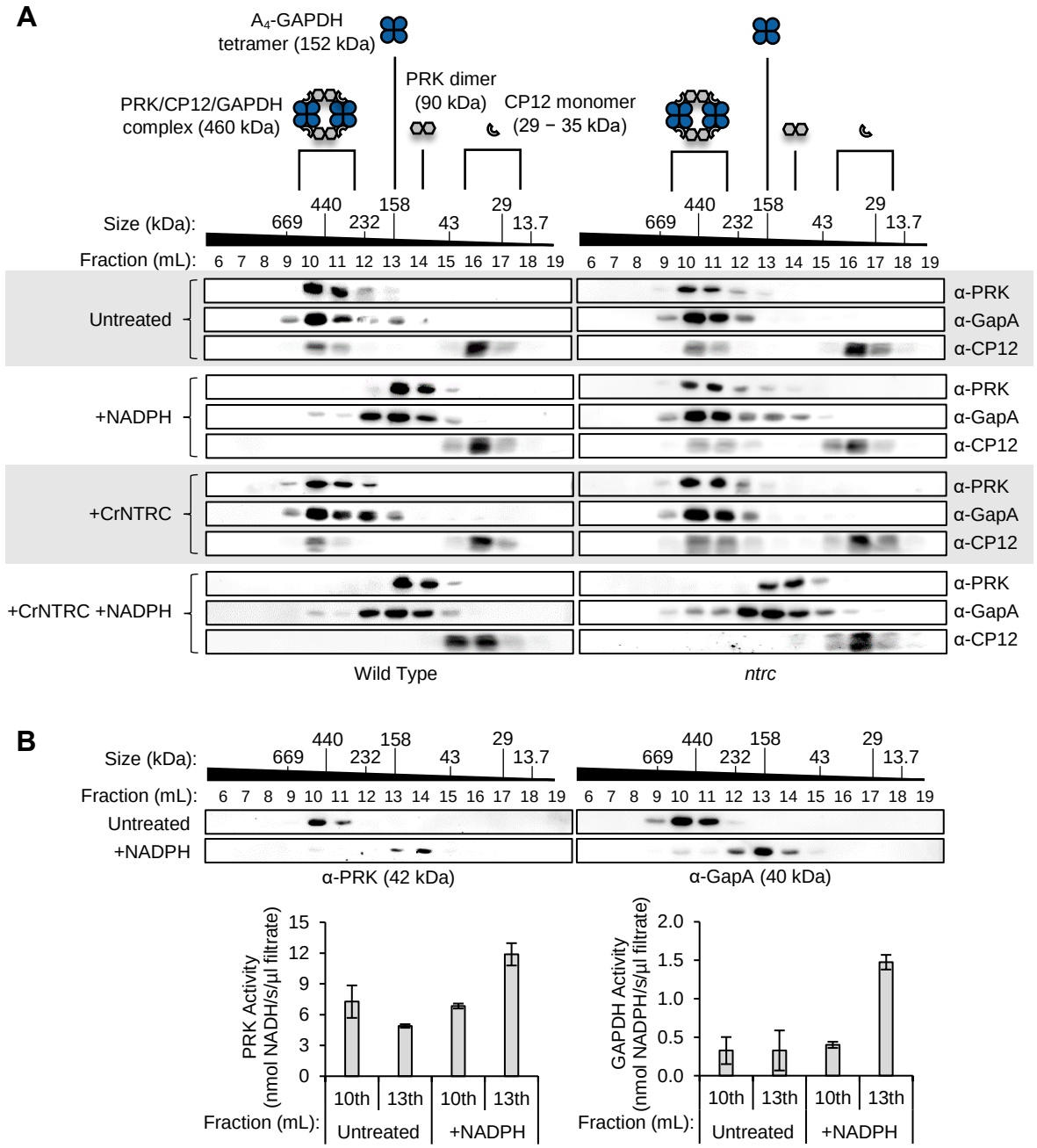

Figure 15. *In vitro* PRK/CP12/GAPDH complex dissociation studies. 5 mg soluble proteins extracted from wild-type CC-4051 or *ntrc* strains of *C. reinhardtii* were treated with 2 mg recombinant CrNTRC proteins, 12 mM NADPH or both for two hours on ice, before proceeding to SEC. **A,** SEC-immunoblotting analysis comparing responses of the native PRK/CP12/GAPDH complex extracted from wild-type and *ntrc* strains to different combinations of recombinant CrNTRC and NADPH treatments. Results presented are from single experiment which have been repeated at least two times with similar results. Expected sizes of PRK/CP12/GAPDH complexes, A_4-GAPDH tetramers, PRK dimers and CP12 monomers were labelled above the molecular weight scale. **B,** PRK and GAPDH enzyme activity assays comparing the PRK/CP12/GAPDH complex and NADPH-induced dissociated free enzymes derived from the wild-type *C. reinhardtii* soluble protein extracts. Upper panel, SEC-immunoblotting data showing the complex status with and without NADPH treatment. Lower panel, PRK and GAPDH enzyme activities of fractions 10^{th} ml and 13^{th} ml obtained from the SEC assay are presented in the graphs. Data shown in the graph are means and standard deviations of three technical replicates. All experiments were repeated twice with similar results.

Moreover, the PRK/CP12/GAPDH complex status and enzyme activities of *C. reinhardtii* were also accessed under the treatment of another reducing agent – reduced DTT (Figure 16A). This experiment serves as an additional test to consolidate the positive correlation between the complex dissociation and the enzyme activities observed in Figure 15. It was found in the SEC analysis that DTT triggered PRK, GAPDH and CP12 proteins to shift towards the lower molecular weight range, indicating the dissociation of PRK/CP12/GAPDH complex (Figure 16A). Consistently, the DTT-treated algal protein extract also showed drastic increases in the enzyme activities of PRK and GAPDH (Figure 16, B and C). This discernibly demonstrates the complex dissociation is accompanied with enzyme activation of PRK and GAPDH. Taken together, these data are consistent with previous *in vitro* findings in *C. reinhardtii* (Lebreton et al., 1997; Lebreton & Gontero, 1999; Graciet et al., 2003a; Graciet et al., 2003b; Lebreton et al., 2003), demonstrating the native PRK/CP12/GAPDH complex exerts an auto-inhibitory effect on its PRK and GAPDH enzyme activities, and the inhibition is relieved upon complex dissociation.

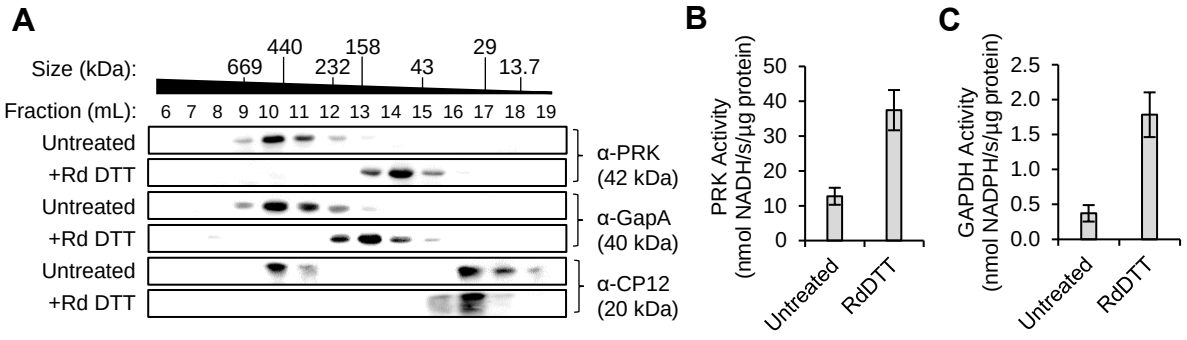

Figure 16. DTT-induced PRK/CP12/GAPDH complex dissociation. *C. reinhardtii* soluble protein extract was incubated with 20 mM reduced DTT or distilled water (negative control) at 30 °C for 1 hour, followed by SEC and enzyme activity assays. **A,** SEC-immunoblotting analysis showing dissociation of the PRK/CP12/GAPDH complex upon DTT treatments. **B – C,** PRK and GAPDH enzyme activity assays comparing DTT-treated sample to the control. Graphs presenting averages and standard deviations of three technical measurements.

III.5. *NTRC* Knockout Suppresses the *in vivo* PRK/CP12/GAPDH Complex Dissociation in *Arabidopsis* but not in *Chlamydomonas*

Next, the SEC study was extended to the *in vivo* complex integrity in different genetic statuses of *NTRC* as well as of organisms grown at different temperatures. First, the *C. reinhardtii* PRK/CP12/GAPDH complex status was again followed by the detection of PRK protein or subunit-A of the GAPDH enzyme (Figure 17A). In wild-type, *ntrc*, and *ntrc:NTRC* strains grown at room temperature, the PRK-containing complex was detected at around 440 kDa, with peaks of elution in fractions 10 and 11 which likely contain ~ 350 to ~ 550 kDa protein complexes by estimation (Figure 17A, left panel). Similarly, in all the three algal strains analysed, GAPDH-containing complexes had an overlapping size with that

of PRK, also appeared at about 440 kDa (fractions 10 and 11; Figure 15A, right panel). As described in the previous section, these complexes represent probably the PRK/CP12/GAPDH complexes of *C. reinhardtii* which have a reported molecular weight of 460 kDa (Avilan et al., 1997; Graciet et al., 2004). Conversely, PRK and GAPDH were hardly detectable at about 152 kDa and 90 kDa which mark the sizes of the free and active GAPDH tetramers and PRK dimers, respectively (Figure 17A). These low molecular weight forms of PRK and GAPDH enzymes were not detectable in any of the examined *C. reinhardtii* strains (Figure 17A).

The same PRK and GAPDH distribution pattern was observed at 15 °C, with all analysed algal strains exhibited SEC-elution peaks of both enzymes at about 440 kDa (fractions 10 and 11), indicating neither temperature nor NTRC influences the complex integrity *in vivo* (Figure 17A). In spite of the promising *in vitro* data demonstrating NTRC accelerates the dissociation of PRK/CP12/GADPH complex (compare Figure 15A), *NTRC* deletion in *C. reinhardtii* exerted no observable effect on the *in vivo* complex status.

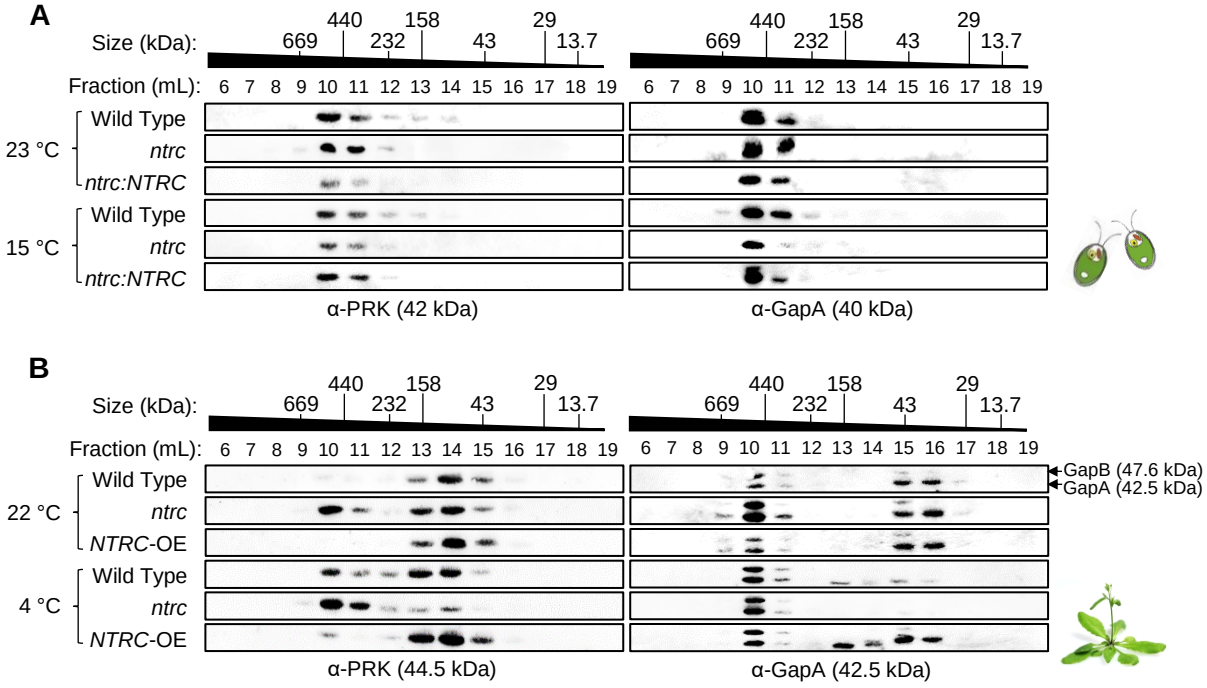

Figure 17. SEC studies of the *in vivo* complex status of PRK/CP12/GAPDH. A, SEC-immunoblotting analysis comparing the PRK/CP12/GAPDH complex status in wild-type CC-4051, *ntrc*, and *ntrc:NTRC* strains of *C. reinhardtii* cultured at 15 °C or 23 °C for 48 hours. The experiment was repeated more than two times, and similar results were obtained. **B,** SEC assay profiling the PRK/CP12/GAPDH complex status in different *A. thaliana* lines at different growth temperatures. *ntrc* indicates *NTRC* knockout, whereas *NTRC*-OE denotes *NTRC* overexpression. Four weeks old plants were grown under 100 µE/m^2/s light at 4 °C or 22 °C for 2 days before leaf soluble proteins were extracted for SEC analysis followed by Western blot detection of PRK and GapA proteins. Arrows pointing GapA (42.5kDa) and nonspecific GapB (47.6kDa) signals respectively. The complex SEC-profiles presented are from single experiment out of biological triplicates with similar results.

Nonetheless, very different results were obtained for *A. thaliana*. Despite no difference appeared among the *C. reinhardtii* strains, the PRK/CP12/GAPDH complex status in *A. thaliana* was surprisingly, strongly affected by the protein level of NTRC (Figure 17B). Wild-type, *ntrc* knockout and *NTRC* overexpression lines of *A. thaliana* were used in the SEC experiment (Figure 17B). Prior to that, they were verified by Western blot analysis, showing a complete NTRC depletion in the *ntrc* line and a five-fold increment of the protein in the *NTRC*-OE line as compared to the wild-type (unpublished data, personal communication with Verena Leitz from AG Geigenberger).

The complex status of these plants was followed by detection of PRK and GAPDH proteins in SEC analyses. At room temperature, PRK was detected in both wild-type and *NTRC*-OE lines of *A. thaliana*, peaking in the range of about 43 to 158 kDa (fractions 13 to 15; Figure 17B, left panel). This low-molecular weight PRK complex likely represent PRK dimers which has been reported to have an apparent size of about 110 kDa in the SEC analysis of *A. thaliana* (Marri et al., 2005). On the contrary, there were dual elution peaks of PRK in the *ntrc* knockout plant; PRK proteins in the *ntrc* line were almost equally distributed at around 440 kDa (fractions 10 and 11) and 43 to 158 kDa rough range (fractions 12 to 14; Figure 17B, left panel). The former PRK-containing assemblies were probably the PRK/CP121/GAPDH complex which have a reported size of approximately 500 kDa, while the latter marked the free PRK dimers (Marri et al., 2005; Marri et al., 2008; Marri et al., 2009).

Likewise, the complex status of the plants was studied by examining the GAPDH protein distribution (Figure 17B, right panel). Unlike *C. reinhardtii*, *A. thaliana* possesses an additional subunit of GAPDH in the chloroplast, namely GapB. Apparently, the GAPDH detection using anti-GapA antiserum was accompanied with a non-specific detection of this GapB subunit in *A. thaliana* (Figure 17B, right panel). All the three *A. thaliana* lines showed two distinct peaks of about 440 kDa (fractions 10 and 11) and 43 kDa (fractions 15 and 16) which are compatible to the expected size of the PRK/CP12/GAPDH complex and GAPDH monomer, respectively. However, the *ntrc* lines stood out among the three lines by displaying a relatively higher accumulation of the high molecular weight GAPDH-containing complex as compared to the wild-type and *NTRC*-OE plants (Figure 17B, right panel). Altogether, the *ntrc* line obviously had a different PRK and GAPDH distribution pattern as compared to the wild-type and *NTRC*-OE plants. These results strongly suggest that the absence of NTRC impedes dissociations of PRK/CP12/GAPDH complexes in *A. thaliana*.

The impact of NTRC on the complex was even more robust in cold-treated *A. thaliana* plants (Figure 17B). Nearly 90 % of PRK accumulated at roughly 440 kDa (fraction 10 and 11) in the *ntrc* mutant plant, whereas wild-type *A. thaliana* plants exhibited a more even distribution of PRK, with two distinct SEC-elution peaks of around 440 kDa (fractions 10 and 11) and ~ 80 to 158 kDa range (fractions 13 and 14; Figure 17B, left panel). On the other hand, in the *NTRC*-OE line, PRK was detected prevalently in the range of about 43 to 158 kDa (fractions 13 to 15), and the 440 kDa PRK-containing

complex (fraction 10 and 11) was barely perceptible (Figure 17B, left panel). These results demonstrate a positive correlation between NTRC protein levels and the accumulation of low molecular weight PRK-containing complexes or simply, PRK dimers.

Similarly, GAPDH was exclusively detected at 440 kDa (fraction 10 and 11) in the *ntrc* plant (Figure 17B, right panel). Conversely, the wild-type and *NTRC*-OE plants showed GAPDH distribution at both around 440 kDa (fraction 10 and 11) and ~35 to 158 kDa (fractions 13 to 16), with the *NTRC*-OE had a more skewed GAPDH distribution toward the smaller molecular weight (Figure 17B, right panel). The 440 kDa GAPDH-containing complex denotes the PRK/CP12/GAPDH complex, while the ~35 to 158 kDa fractions probably contained both GAPDH monomers and tetramers which has been reported to have an apparent size of about 120 kDa in the SEC analysis of *A. thaliana* (Marri et al., 2005). These results illustrate a dose-dependent effect of NTRC proteins on dissociating the PRK/CP12/GAPDH complex. To sum up, the *in vivo* SEC study of *A. thaliana* convincingly suggests that the complex status is affected by NTRC, and the effect seems to be enhanced under cold conditions.

In addition, the PRK and GAPDH proteins in *A. thaliana* did not always show consistent distribution ratio between the high molecular weight complex and the lighter dissociated forms. For instance, the wild-type plant PRK proteins at room temperature, existed dominantly in the range of 43 to 158 kDa while its GAPDH proteins inconsistently appeared as 440 kDa complexes in addition to the 43 kDa monomers (Figure 17B). This is probably because in parallel to the PRK/CP12/GAPDH complex, *A. thaliana* GAPDH can also aggregate autonomously to form a $(A_2B_2)_4$-GAPDH complex (compare section I.3.4). Even though this $(A_2B_2)_4$-GAPDH complex constitutes only a marginal portion of GAPDH aggregate pool in *A. thaliana* (Howard et al., 2011b), it has a size of about 550 kDa, very close to that of the PRK/CP12/GAPDH complex (Pupillo & Piccari, 1973; Cerff, 1982).

III.6. Loss of NTRC's Redox Function in *Chlamydomonas* Impairs Cold-induced Elevation of GAPDH Enzyme Activity

Next, it is crucial to find out if NTRC affects PRK and GAPDH enzyme activities. Therefore, enzyme activities in *ntrc* knockout and cysteine-substituted mutant strains of *C. reinhardtii* were examined. The PRK activity did not change by either temperature or *NTRC* mutations (Figure 18A). All the examined strains showed indifferentiable PRK activity (close to 1-fold) between the two growth temperatures – 23 °C and 15 °C. In contrast, a general increase in GAPDH enzyme activities was detected when the cultures were shifted from 23 °C to 15 °C for incubation (Figure 18B). This increase was partially impaired in the *ntrc* and *C455S/C458S* mutant strains; there were only around 4-fold increments in the mutants as compared to that of roughly 7-fold in wild-type and *ntrc:NTRC* strains (Figure 18B). These results indicate that the loss of NTRC's oxidoreductase function in *C. reinhardtii* did affect the activity

of GAPDH, in spite of the non-detectable changes in the *in vivo* PRK/CP12/GAPDH complex status (compare Figure 17A).

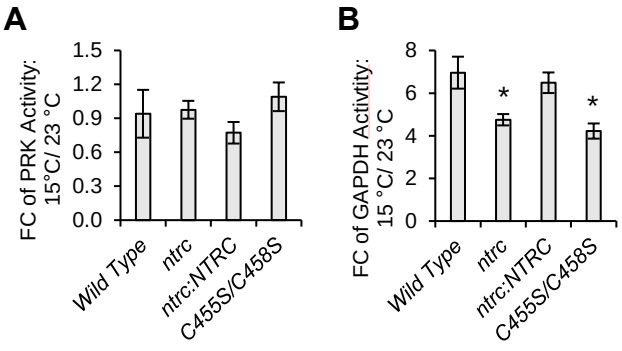

Figure 18. PRK and GAPDH enzyme activities of *C. reinhardtii* strains of various *NTRC* genotypes. Enzyme activities of soluble protein extracts of *C. reinhardtii* strains which had been grown for 48 hours at 15 °C and 23 °C were compared and presented in fold change (FC) as indicated in the graphs. Data show compilations of more than three biological repeats. Error bar denotes standard deviation. Asterisks (*) denote statistical significance as compared to the wild type, with p-values smaller than 0.05, evaluated by two-tailed student's t-tests.

III.7. *Chlamydomonas cp12* Knockout Mutants are Cold-sensitive

The identification of CP12 as a downstream redox target of NTRC (Figure 14) and their interaction at low temperature (Figure 13, B and C) suggested that the loss of CP12 function might also affect the growth of *C. reinhardtii* under cold stress. Such a demonstration would strengthen the evidence for the involvement of CP12 in the NTRC-mediated cold acclimation. To this end, *C. reinhardtii cp12* knockout mutants were generated via the CRISPR/Cas9 technique. Mutagenesis was conducted via site-directed insertion of a frameshift-tolerant stop codon sequence into the second exon of the *CP12* gene, which would eventually lead to a halt in protein translation (Figure 19). The site-specific DNA digestion by the Cas9 endonuclease followed by the insertion of the annealed mutation oligonucleotide was guided by two distinct gRNA targeting events on different sites of *CP12* exon-2 (Figure 19). The pBC1 plasmid vector carrying a paromomycin resistance cassette was co-transferred with the Cas9/gRNA conjugate into the microalgal cell as a selection marker. Antibiotic-resistant transformants were screened via colony-PCR, followed by DNA sequencing to confirm the introduction of stop codons into the nuclear *CP12* gene (see section II.2.17 for method details). Eventually, two *cp12* knockout mutant strains, namely *cp12* #1 and *cp12* #2 were obtained (Figure 20A).

The deletion of *CP12* in these strains was further verified by Western blot; both of them showed a complete erasure of CP12 protein (Figure 20A). Interestingly, PRK and GAPDH protein accumulations also decreased remarkably in *cp12* knockout mutants (Figure 20A). Similar observation has also been reported in *A. thaliana* wherein PRK protein level reduced in *cp12* knockout lines; and it was thought to be likely due to the loss of protein stabilizing effect exerted by CP12 in these mutants (compare section I.3.8; López-Calcagno et al., 2017). Besides, unlike in the wild-type, PRK and GapA proteins separated via SEC, were not detectable at about 440 kDa (fractions 10 and 11) in both knockout strains (Figure 20B). Instead, the proteins appeared in the range of around 43 to 232 kDa which

represent the dissociated forms of the enzymes (Figure 20B). The failure of the knockout strains in forming the PRK/CP12/GAPDH complex is clearly evidenced by these gel filtration results (Figure 20B). Further, there existed no obvious differences between wild-type and *cp12* mutant strains when they were grown at room temperature, with all of them having a doubling time of around 10 hours (Figure 20C). In contrast, both *cp12* #1 and *cp12* #2 strains demonstrated decreased growth rates as compared to that of the wild type when they were cultivated in cold conditions (Figure 20D). The *cp12* strains duplicated roughly every 43 hours while the wild-type strain had a shorter doubling time of about 35 hours. These differential growth rates at 15 °C suggest that CP12 is indeed, also involved in cold acclimation.

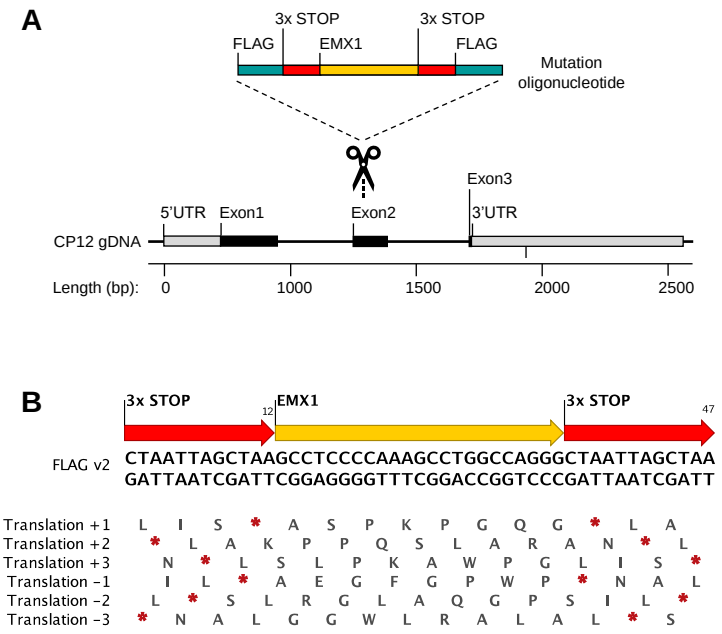

Figure 19. Generation of cp*12* knockout in *C. reinhardtii* using CRISPR/Cas9 method. **A,** Diagram showing experiment design for *CP12* knockout. Exon-2 of *CP12* was targeted for Cas9 digestion led by designed gRNA. The double-stranded mutation oligonucleotide encoding a FLAG-tag, the human *EMX1* gene and frameshift tolerant stop codons (denoted as 3x STOP) was inserted at the cutting site. **B,** Part of the DNA sequence of the annealed mutation oligonucleotide and its corresponding amino acid sequences translated in all possible reading frames are shown. The sequence of the mutation oligonucleotide was retrieved from the webpage of Hegemann laboratory, Humboldt University Berlin, https://box.hu-berlin.de/f/6a62c43789484c11b6a8/

Apart from that, it was noticed that *CP12* deletion in *C. reinhardtii* not only impaired the PRK/CP12/GAPDH complex assembly but also caused dramatic declines in PRK and GADPH protein accumulations (Figure 20A). This is partially consistent with the findings published by Lopez-Calcagno and his colleagues (2017) who reported that PRK protein level decreased substantially, but the GAPDH protein level remained unchanged in *cp12* knockout lines of *A. thaliana.* Further, the mRNA level of PRK did not change as well, suggesting a post-translational regulation of PRK accumulation by CP12 (compare section I.3.8; López-Calcagno et al., 2017). These findings demonstrate that besides assembling PRK dimers and GAPDH tetramers, CP12 also affects PRK and GAPDH protein accumulations. Additionally, *NTRC* loss-of-function mutations in *C. reinhardtii* did not cause any significant changes to the protein levels of PRK and GAPDH, suggesting that the change in redox status of CP12 by NTRC is inadequate to cause such an effect (Supplemental Figure S5).

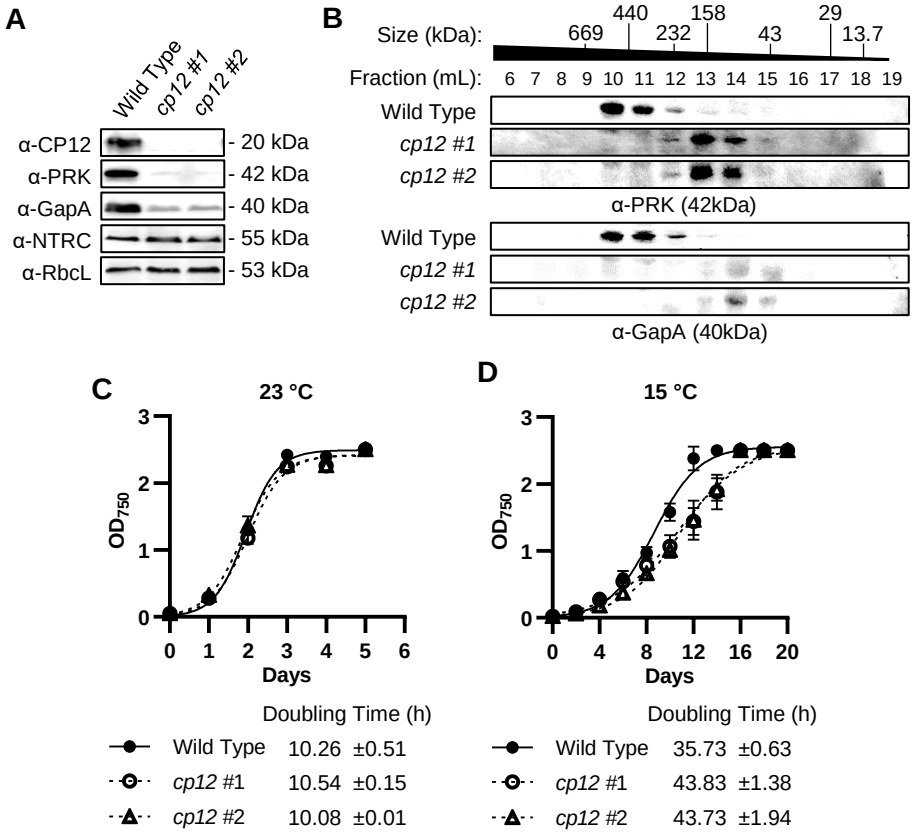

Figure 20. Characterization of *C. reinhardtii cp12* knockout mutants under cold condition. The *cp12* knockout mutants were generated with aid of CRISPR-Cas9. Two knockout mutant strains were obtained namely, *cp12* #1 and *cp12* #2. **A,** Immunoblotting analysis comparing CP12, PRK, GapA and NTRC protein accumulations in wild-type CC-406 and *cp12* mutant strains; RbcL served as a loading control. Blots shown are representative from three biological replicates with similar results. **B,** SEC profiles of GAPA-CP12-PRK complex in *cp12* mutant strains as compared to that of the wild type. The cultures were grown in TAPS liquid medium at 23 °C. of PRK and GapA signals of *cp12* mutants has been adjusted for better visualization. **C – D,** Growth studies of *cp12* strains and the wild type in TAPS liquid medium at 23 °C and 15 °C respectively. OD_{750} of the cultures as read every two days. Data was derived from three separate cultures, and growth curves were drawn using GraphPad Prism v8 software. Error bars represent standard deviations (SD). Values below the curves are doubling times (hours) and their respective SD.

III.8. Changes of PRK and GAPDH Enzyme Activities in *cp12* Knockout Strains

In order to better understand the role of CP12 in Calvin cycle regulation, PRK and GAPDH enzyme activities in *C. reinhardtii cp12* knockout mutants were also studied. The enzyme activity assays were conducted for both 23 °C and 15 °C of algal growth temperatures. Surprisingly, at room temperature, the mutants were found to possess higher GAPDH and PRK activities than the wild type (Figure 21, A and B), regardless of their drastically declined protein levels (Figure 21C). This implies that the drawback of protein depletions on PRK and GAPDH activities has been overcome by the enzyme activating effect from PRK/CP12/GAPDH complex dissociation in *cp12* knockout mutants.

When the algal cultures were cold treated for 48 hours, the wild type exhibited an unaltered PRK activity (a fold change of nearly 1; Figure 12A) but an ~ 1.8-fold inclined GAPDH activity (Figure 21B). These observations were consistent with what has been found in another wild-type *C. reinhardtii* strain – CC-4051 (compare Figure 18), suggesting a cold-induced upregulation of GAPDH activity. On the other hand, in *cp12* knockout strains, chilling triggered the PRK activity to drop almost to the wild-type level (Figure 21A) but increased the GAPDH activity further from that of wild-type (Figure 21B). Without cross-comparison to the wild-type strain, cold-stressed *cp12* knockout strains had the PRK activity decreased to ~ 0.4 to 0.6-fold of their own original levels at room temperature (Figure 21A), whilst had an ~ 2.6 to 3.0-fold increment in the GAPDH activity (Figure 21B).

These cold-triggered enzyme activity changes in the knockout strains appear to be correlate with changes in PRK and GAPDH protein accumulations (Figure 21C). While *cp12* mutants had already been observed to have declined levels of PRK and GAPDH proteins at room temperature, chilling was found to exacerbate the depletion of PRK but partially recover GAPDH protein accumulation (Figure 21C). However, these low temperature-induced drastic changes of PRK and GAPDH protein accumulations were not evident in the wild type (Figure 21C). The wild-type microalga exhibited constant levels of PRK and GAPDH proteins regardless of the cultivation temperature (Figure 21C). This implies a higher protein turnover rates of PRK and GAPDH enzymes was taking place in the cold-treated *cp12* knockout strains as compared to the wild type. And, the fluctuation of PRK and GAPDH enzyme accumulations in the absence of CP12 in *cp12* knockout strains suggests a role of CP12 in maintaining a stable enzyme repertoire.

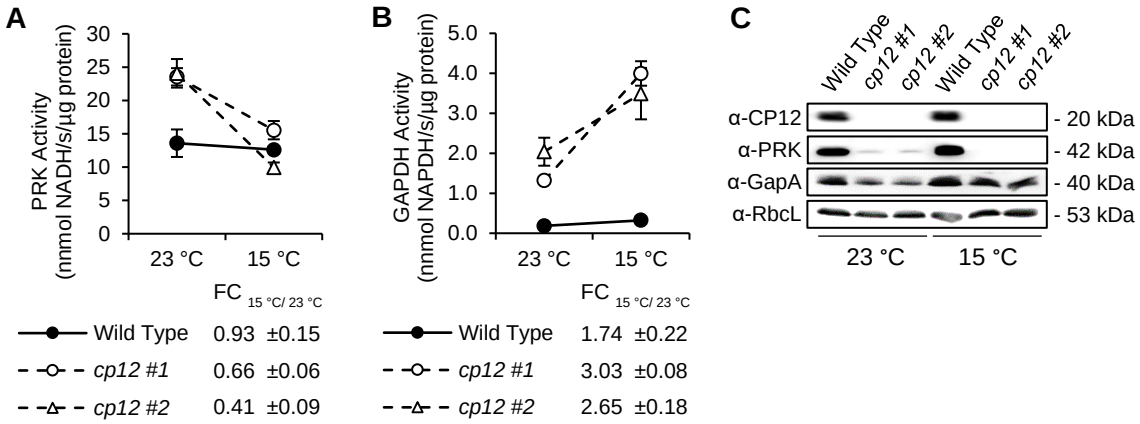

Figure 21. PRK and GAPDH enzyme activities of *C. reinhardtii cp12* knockout strains in comparison to the wild-type CC-406. The *C. reinhardtii* strains had been grown at 23 °C and 15 °C for 48 hours before harvested for the preparation of soluble proteins extracts for the following assays. **A – B,** Enzyme activities of PRK and GAPDH were measured. Means and standard deviations presented in the line graphs were derived from biological triplicates. Fold changes (FC) of enzyme activity of 15 °C relative to 23 °C are shown below the graphs, with the corresponding SD values shown after '±' signs. **C,** Western blot analysis showing changes of PRK and GAPDH protein levels in *cp12* knockout strains at 23°C and under cold treatment. RbcL served as loading control. Approximate sizes of proteins are indicated on the right.

III.9. CP12 in the Light-Dark Cycle

Past studies in cyanobacteria and pea plants have suggested that CP12 plays a role in regulating the PRK/CP12/GAPDH complex during the light-dark cycle (compare section I.3.8; Tamoi et al., 2005; Howard et al., 2008). In this context, the role of CP12 in the light-dark cycle of *C. reinhardtii* is of particular interest as comparing metabolic roles of CP12 in response to these two distinct but equally prominent abiotic factors – light intensity and temperature, could be helpful for a better understanding of CP12 functions.

Wild-type *C. reinhardtii* was grown in a 12-hour light (30 µE/m^2/s) – 12-hour dark cycle and the PRK/CP12/GAPDH complex status and enzyme activities between the light and dark phases were compared. Very similar to what had been observed in the SEC analyses for microalgal strains grown in cold conditions (compare Figure 17A), there appeared no changes in the PRK/CP12/GAPDH complex status when microalgae were shifted from the dark to the light phase (Figure 22A). PRK and GapA proteins were detected under both light regimes, only peaking at around 440 kDa (fractions 10 and 11) as shown in Figure 22A. The dissociated forms of PRK and GADPH could never be detected. On the other hand, CP12 though peaking twice at around 440 kDa and in 29 to 35 kDa range (fractions 16 and 17), respectively, intensities of the two peaks showed no difference between the light and dark phases (Figure 22A). These results illustrate that the complex status of PRK/CP12/GAPDH in *C. reinhardtii* does not response to light intensity.

Moreover, PRK activity of the wild-type *C. reinhardtii* also did not change between the two phases (Figure 22B). On the contrary, a significant drop was measured for the GAPDH activity when the algal culture was shifted from the light to the dark (Figure 22C). These data suggest that, highly similar to the observations in the cold-treated *ntrc* strain (compare Figure 18), the GAPDH catalytic activity is also uncoupled from the complex status and PRK enzyme activity during the light-dark cycle.

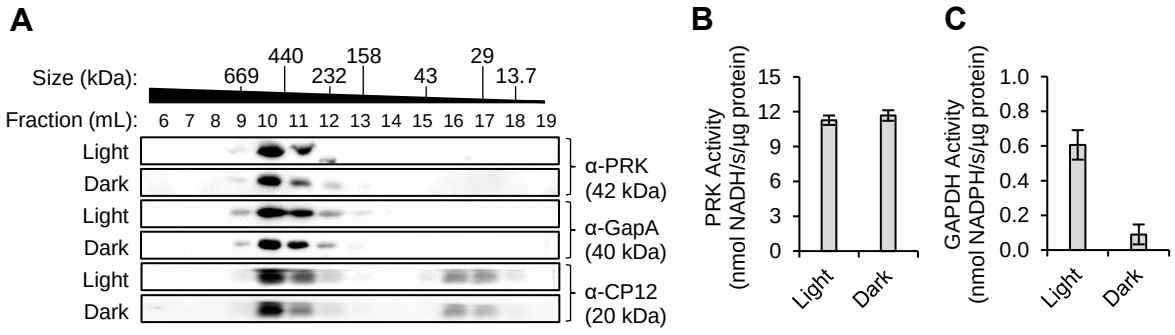

Figure 22. Profiling of the PRK/CP12/GAPDH complex under light-dark cycle. Wild-type *C. reinhardtii* (CC-4051 strain) cultured under 12-hour light (30 µE/m^2/s) – 12-hour dark rhythm. Cultures were grown under the light-dark cycle for 2 days and harvested in the late light or late dark phase (12 hours) for the following analyses. **A,** SEC analysis of the PRK/CP12/GAPDH complex status under the light-dark cycle. **B – C,** PRK and GAPDH enzyme activity assays comparing

soluble protein extracts harvested in the light and dark phases. Data presented are means derived from technical triplicates of a single set of experiment which has been repeated twice with similar results obtained. Error bars denote standard deviations.

In addition, to clarify the doubt that stronger stimuli might be needed to have a detectable complex dissociation, the complex integrity under high light and photoautotrophic conditions was examined. The culturing light intensity was changed from 30 µE/m^2/s of usual cases to 100 µE/m^2/s. Further, algal cultures were also inoculated in high salt minimal (HSM) medium instead of TAP medium. The TAP medium provides an additional organic carbon source – acetate – for alga, which is absent in HSM medium. Hence, in HSM photoautotrophic growth is mandatory and carbon assimilation via Calvin cycle enzymes activities is in greater demand. With these dual stimuli, a more obvious complex dissociation would be expected. Yet, the SEC analysis showed that both PRK and GapA detections were still peaking at roughly 440 kDa, and not found in the low molecular weight range where the PRK dimers (90 kDa) or GAPDH tetramers (152 kDa) would be expected (Figure 23). This result again demonstrates the PRK/CP12/GAPDH complex is the dominant form and free enzymes are undeniably hardly detectable *in vivo.*

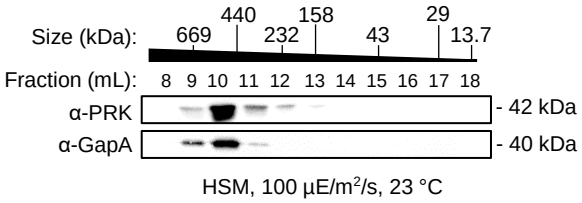

Figure 23. The PRK/CP12/GAPDH complex status of *C. reinhardtii* under high-light, photoautotrophic growth. Wild-type CC-4051 strain was cultured in HSM, at 23 °C under 100 µE/m^2/s light for 48 hours before the gel filtration assay. The experiment was repeated more than two times, and similar results were obtained.

Moreover, it was observed that both *cp12* #1 and *cp12* #2 strains grew slower than the wild type in the light-dark cycle (Figure 24, A and B) but not under continuous light conditions (compare Figure 20C), similar to what has been published for cyanobacterial *CP12* deletion (Tamoi et al., 2005). The *cp12* knockout mutants duplicated every 13 to 14 hours, while the wild type took only 9.5 hours to complete one division during the diurnal cycle (Figure 24 B).

The molecular mechanism behind this light-dark phenotype was then scrutinized; PRK and GAPDH enzyme activities were measured at early state (2 hours) and late state (12 hours) of both light and dark phases (Figure 24A). The *C. reinhardtii* wild-type was found to have a constant PRK activity but a significantly decreased GAPDH activity in the entire dark phase, consistent with what has been shown in Figure 22. On the other hand, the *cp12* knockout strains showed clearly upregulated PRK and GAPDH activities in the light phase and the early dark phase (Figure 24, D and E). Surprisingly, in the late dark phase, the PRK and GAPDH activities of both *cp12* #1 and *cp12* #2 were suppressed to wild-type levels (Figure 24, D and E). This implies that there exists other regulatory mechanism(s) which could bypass CP12 to suppress PRK and GAPDH enzyme activities, probably by modulating the protein

amounts as shown by the Western blot data (Figure 24C). PRK and GAPDH protein levels in both *cp12* knockout strains started to decline in the early dark phase and went to almost complete depletions in the late dark phase; protein accumulations took places again in the early light phase and reached the climax in the late light phase (Figure 24C). Although this cyclical protein accumulation-degradation mechanism could eventually lead to the same level of enzyme activity suppression in the dark, *CP12* deletion in *C. reinhardtii* imposed a delay in the response to changes in light intensity.

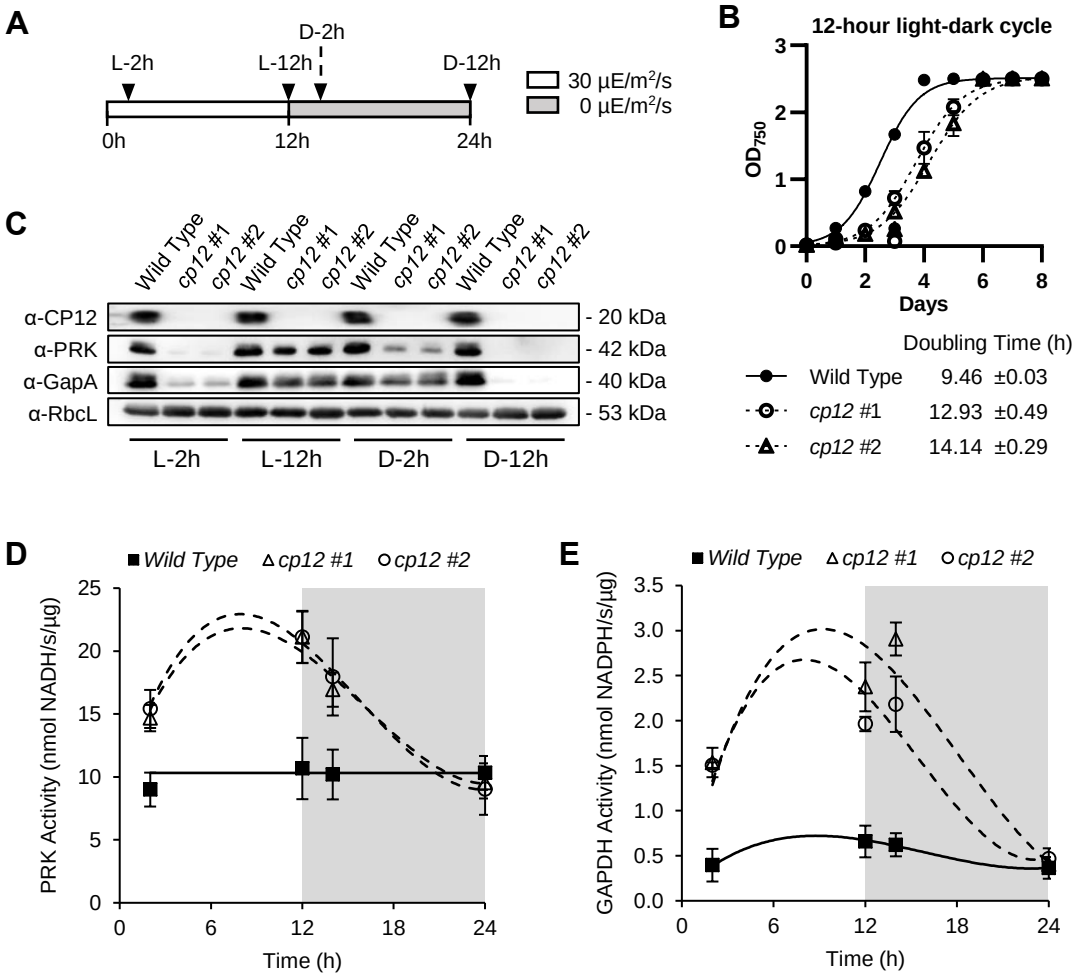

Figure 24. Characterization of *C. reinhardtii cp12* knockout mutants under the light-dark cycle. *C. reinhardtii* strains were first cultured under 12-hour light (30 µE/m²/s) – 12-hour dark rhythm for 2 days. On the 3rd day, the cultures were harvested for analysis at different time points namely 2 hours or 12 hours in the light or dark phase as indicated in diagram **A**. **B,** Growth curves comparing the *cp12* knockout mutants and the wild-type CC-406 strain in TAPS liquid medium, at 23 °C, under the light-dark rhythm. Data presented are means and standard deviations from biological triplicates. Doubling times in hours with corresponding standard deviations were indicated below the curves. **C,** Immunoblot analysis accessing PRK, GapA and CP12 protein amounts in wild-type and *cp12* knockout strains harvested at different time points during the light-dark cycle as indicated. Equal RbcL protein levels indicate even loadings. **D – E**, PRK and GAPDH enzyme activities of wild-type and *cp12* knockout strains of *C. reinhardtii* were compared at different time points during the light-dark cycle. The white and grey backgrounds represent hours in the light and dark phases, respectively. Data presented are means derived from technical triplicates of a single set of experiment which has been repeated twice with similar results obtained. Error bars denote standard deviation. Curves are 3rd order polynomial trendlines based on the enzyme catalytic rates at different time points.

Lastly, it comes to the question if NTRC is involved in the regulation of CP12 functions in the light-dark cycle. To this end, *ntrc* and cysteine-substituted mutant strains were grown in the light-dark rhythm instead of continuous light (compare Figure 20C). However, no difference in the growth rate of the mutants compared to wild-type and *NTRC* complementation strains could be observed (Figure 25). All strains showed a doubling time of around 12 hours (Figure 25). This indicates that NTRC plays no regulatory role via CP12 or other redox targets in the diurnal cycle.

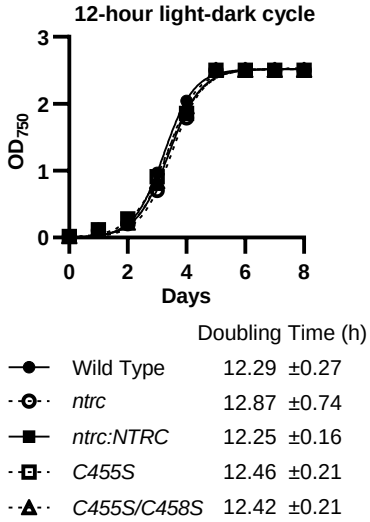

Figure 25. Growth curves of *C. reinhardtii* strains with different *NTRC* genotypes in the light-dark cycle. Microalgal strains presented were generated from a background strain of CC-4501. They were grown in TAP liquid medium and subjected to the light (30 µE/m^2/s)-dark switch every 12 hours. OD_{750} values of the cultures were read every two days. Data were compiled from three independent cultures, and growth curves were drawn using GraphPad Prism software. Error bars mark standard deviations (SD). Values below the curves are doubling times (hours) and their respective SD.

IV. DISCUSSION

The study of Moon and co-workers (2015) has suggested that NTRC plays a role in adaptation of *A. thaliana* to temperature changes. However, the attribution of the cold-sensitive phenotype of *ntrc* mutants to the chaperone functions of NTRC lacks the support of *in vivo* evidence (Moon et al., 2015). For instance, the study did not show the oligomeric status of NTRC which represents the holdase capacity upon cold or heat shock treatment (compare section I.2.4). This is necessary to strengthen the evidence for a causal relationship between NTRC chaperone functions and cold tolerance. Aside from the chaperone function of oligomeric NTRC, NTRC functions as an oxidoreductase enzyme in its dimeric form and the niche of this redox function in cold acclimation was not addressed by the authors (Moon et al., 2015). In other word, there remained a question if NTRC-conferred cold tolerance also involves its redox regulatory function. If that is the case, the precise redox regulatory mechanism behind also needs to be elucidated.

Within the framework of this thesis, the significance of the oxidoreductase function of NTRC in cold acclimation could be clearly demonstrated. Furthermore, during the course of scrutinizing the molecular mechanism behind, co-IP and *in vitro* redox activity assays have identified CP12 as a redox target of the NTRC in *C. reinhardtii.* As CP12 is required for the formation of a PRK/CP12/GAPDH supracomplex, complex composition under different growth conditions and its enzyme activities were investigated in *C. reinhardtii,* as well as *A. thaliana* for comparison. Several aspects of the complex formation have been spotted different between the two model organisms in this study and other published reports; the differences will be discussed in detail in the following sections. And finally, overviews of roles and the redox-dependent regulation of CP12 in cold acclimation and the light-dark adaptation are presented in a postulated model derived from findings in this study.

IV.1. NTRC-mediated Cold Acclimation via Redox Regulation of CP12

First of all, growth studies of cysteine-substituted strains of *C. reinhardtii* in Figures 10 and 11 indicate that NTRC's chaperon function suggested by Moon et al. (2015) should not be the only factor contributing to the NTRC-mediated cold tolerance. With the redox-active cysteine residues C455 and C458 being mutated, the thioredoxin domain of NTRC is not functionable and cannot reduce its downstream redox-targets (compare section I.2.2; Holmgren & Bjornstedt, 1995). The slower growth of the cysteine-substituted strains of *C. reinhardtii* at 15 °C in comparison to that of the wild type has unambiguously illustrated the significance of NTRC's oxidoreductase enzyme activity in cold acclimation (Figure 10 and 11).

Interestingly, the cysteine-mutated NTRC protein from the *C455S/C458S* strain also showed no detectable binding to CP12, despite their interaction was significantly perceived in the *ntrc:NTRC*

complemented strain by co-IP/MS assays, suggesting CP12 as a redox-target of NTRC (Figure 13, B and C). Moreover, the NTRC-CP12 interaction was also found to be cold-dependent which was only detected in microalgae grown at 15 °C but not 23 °C, implying that the interaction is cold-related (Figure 13, B and C). Furthermore, *in vitro* redox activity studies in Figure 14 clearly demonstrated NAPDH-dependent reduction reaction of NTRC on CP12 from both flowering plants and microalga, consolidating CP12 as a downstream redox-target of NTRC.

CP12 is known as a linker protein for PRK and GAPDH across photoautotrophic species (Avilan et al., 1997; Wedel et al., 1997; Wedel & Soll, 1998; Scheibe et al., 2002; Graciet et al., 2004; Marri et al., 2005; Marri et al., 2008). And indeed, NTRC was observed to regulate this protein scaffold function of CP12 in *C. reinhardtii*, affecting both oligomeric status and catalytic activities of the enzymes (Figures 15A and 16B). Recombinant NTRC, compensating the absence of native NTRC protein, was found able to catalyse NADPH-induced *in vitro* dissociation of PRK/CP12/GAPDH complex in the *ntrc* knockout strain (Figure 15A). Besides, loss of NTRC's redox function was found to suppress the elevation of algal GAPDH activity triggered by low temperature (Figure 16B). In addition, SEC analysis of the *in vivo* PRK/CP12/GAPDH complex status in *A. thaliana* also showed that *NTRC* deletion impeded complex dissociations, and this effect was even more robust in cold conditions (Figure 17B). This provides further evidence for the regulation of CP12's protein scaffold function by NTRC under cold stress.

In a nutshell, data presented in this thesis demonstrate that NTRC reduces CP12, leading to the dissociation of PRK/CP12/GAPDH complex which release the enzymes for catalytic activities (a model of regulatory mechanism is presented in Figure 26). This redox regulatory pathway appears to be crucial in *C. reinhardtii* and *A. thaliana* during cold acclimation.

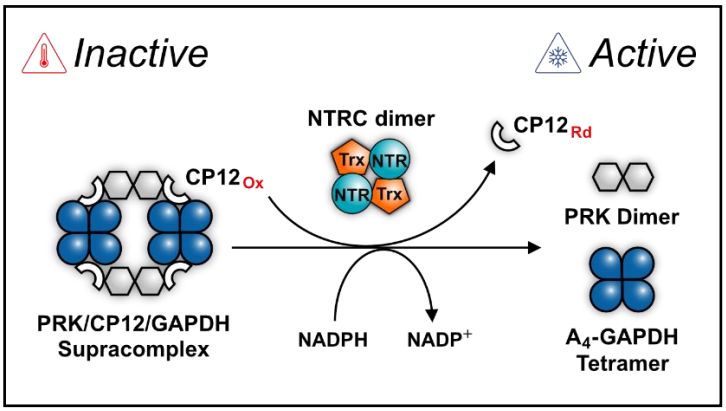

Figure 26. Redox regulation of CP12 by NTRC and its impact on PRK and GAPDH oligomeric status. NTRC dimer contains two antiparallelly orientated monomers with each consists of a $NADP^+$-thioredoxin reductase (NTR) domain (light blue sphere) and a thioredoxin domain (orange star). NTRC reduces CP12 by deriving the reducing potential from NAPDH. This in turn dissociate the PRK/CP12/GAPDH complex and release the free and active enzymes.

IV.2. Heterogeneity in the PRK/CP12/GAPDH Complex Stability and Predominance between *Chlamydomonas* and *Arabidopsis*

PRK/CP12/GAPDH complex dissociation under reducing conditions has been described in both algae and higher plants to increase the enzymatic activity of its components (Lebreton et al., 1997; Scheibe et al., 2002; Graciet et al., 2003b; Oesterhelt et al., 2007; Howard et al., 2008; Marri et al., 2009). In agreement with this, *in vitro* analysis of the PRK/CP12/GAPDH complex composition in *C. reinhardtii* represented here revealed that a complex dissociation induced by DTT or NADPH was constantly accompanied with increased enzyme activities of PRK and GADPH (Figures 15B and 16). However, it is puzzling as the *in vivo* data never turn out the same. The *in vivo* complex status did not correlate with the enzyme activities; the complex remained fully assembled in the cold-treated *ntrc* knockout mutant (Figure 17A) as well as throughout the light-dark cycle (Figure 22A), even though changes in the GAPDH activity were observed (Figures 18B and 22C). *In vivo* complex dissociation seems not to appear at all as free PRK dimers and GAPDH tetramers could never be detected in SEC without a trigger by artificial reductants. For these, a thorough survey on published literatures was carried out and it was found that in all reports of the PRK/CP12/GAPDH complex in *C. reinhardtii*, none have demonstrated a detection of native free PRK dimers or GAPDH tetramers *in vivo* (Avilan et al., 1997; Wedel & Soll, 1998).

We speculate that the dissociated forms might be present in very low amounts *in vivo* which hinder detection by common laboratory techniques. This speculation is supported by a couple of evidence obtained in this thesis. First, in the absence of CP12 in *cp12* knockout strains, the PRK/CP12/GAPDH complex was found disassembled (Figure 20B). This disassembly led to higher enzymatic activities of both PRK and GAPDH (Figure 21, A and B), regardless of their severely declined protein amounts which were also noticed upon *CP12* deletion (Figures 20A and 21C). This suggests that the free enzymes are highly active, and a relatively low number of free enzymes can give a substantial level of enzyme activities. Hence, a mild and undetectable dissociation could also give a significant elevation in the enzyme activity.

Second, the PRK/CP12/GAPDH complex stability of *C. reinhardtii* and *A. thaliana* has been found largely variable (Figure 5). The dissociation constant (K_d) of GAPDH-CP12 of *C. reinhardtii* (0.44 nM; Graciet et al., 2003a) has been described to be about 400-fold lower than that of *A. thaliana* (180 nM; Marri et al., 2008). The interaction between PRK and the GAPDH-CP12 binary complex of *C. reinhardtii* (K_d = 60 nM; Graciet et al., 2003a) though is not as robust as that between GAPDH and CP12, is also 3-fold stronger than that of *A. thaliana* (K_d = 0.17 µM; Marri et al., 2008). A higher dissociation constant means a more stable complex which requires a higher enthalpy for dissociation. Therefore, in equilibrium, without any extrinsic interference, a much lower proportion of free enzymes should be expected in *C. reinhardtii*. This is supported by SEC analyses of *in vivo* oligomeric status of

PRK and GAPDH enzymes which showed mainly assembled complexes in *C. reinhardtii*, whilst more variable complex sizes were detected in *A. thaliana* (Figure 17). In fact, contrary to *C. reinhardtii*, the complex was reported by other groups non-detectable in *A. thaliana* (and tobacco) without a pre-treatment with NAD^+ which promotes complex assembly (Howard et al., 2011a; Howard et al., 2011b). This is partially consistent with the SEC data; even though in a relatively low amount, the complex could be detected in *A. thaliana*, and the detection can be further improved by growing the plant in cold conditions (Figure 17B).

In conclusion, heterogeneity in the complex stability does exist between the two phototrophic eukaryotes, and this intrinsically determines the oligomeric status of PRK and GAPDH enzymes in the species. SEC and native-PAGE data presented here and by other groups have demonstrated the fully assembled complex is dominating in *C. reinhardtii* while the free enzymes are the predominant ones in *A. thaliana*, as summarized in Figure 27.

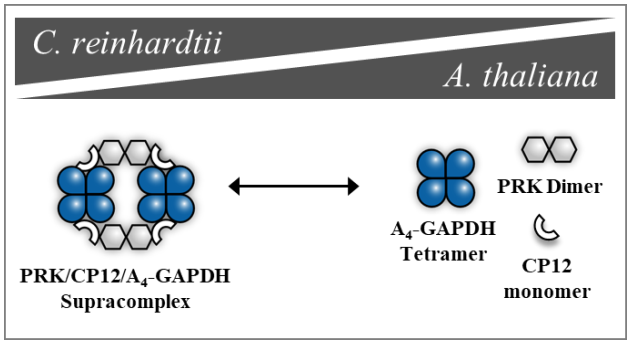

Figure 27. Variation in the oligomeric status of PRK and GAPDH enzymes between *C. reinhardtii* and *A. thaliana*. PRK and GAPDH can form a supracomplex with the aid of a scaffold protein – CP12, or exist as free dimers and tetramers, respectively. The *in vivo* amount of the enzymes in these two oligomeric states was symbolically presented by right triangles; the thicker end denotes the predominant form, while the pointed end marks the one presents in a less amount.

IV.3. Dual Impacts of CP12 on PRK and GAPDH Enzymes

The complex stability is not only a factor determining the assembly status of the PRK/CP12/GAPDH complex in the respective organism but may also have consequences on protein stability. A higher complex dissociation constant could also imply a stronger stabilizing effect of the complex over its enzyme members which confers protection against degradation.

In fact, in spite of the very well described suppression of PRK and GAPDH enzyme activities by PRK/CP12/GAPDH complex formation, CP12 and the complex have also been shown to stabilize and protect GAPDH and PRK proteins (compare section I.3.8). Two independent *in vitro* studies have demonstrated that CP12 works as a chaperone for GAPDH against heat-induced aggregation and deactivation (Erales et al., 2009b) and that the complex protects PRK and GAPDH proteins from oxidative damages (Marri et al., 2014). In conjunction, *cp12* knockout lines of *A. thaliana* displayed a declined PRK protein level while GAPDH protein accumulation was unaffected (López-Calcagno et al., 2017). Similarly, *CP12* deletion in *C. reinhardtii* was found to cause severe decreases not only in PRK but also GADPH protein amounts (Figures 20A and 21C) which might be related to its extremely

low CP12-GAPDH dissociation constant (Graciet et al., 2003a). These *in vivo* findings consolidate the evidence for a stabilizing effect of CP12 and the assembled complex on PRK and GAPDH proteins. Concomitantly, it was also evidently shown that PRK and GAPDH protein levels fluctuated in *cp12* mutants under cold stress and during the diurnal cycle, whereas wild-type algae had their enzyme amounts remained unaltered by these changes of incubation conditions (Figures 21C and 24C). A stable repertoire of enzymes did not seem to exist in the absence of CP12, revealing a role of CP12 in maintaining PRK and GAPDH protein homeostasis.

To sum up, CP12 and the PRK/CP12/GAPDH complex exerts both inhibitory and protective effects on PRK and GAPDH enzymes. In the first sense, these effects seem counteracting each other, resulting in futility. However, they are actually both important properties to prepare a repertoire of enzymes, enabling spontaneous responses to environmental changes. By protecting the enzymes from degradation, the cell can have a significant reserve of enzymes with the activities suppressed in normal condition but poised to rapid activation when the environment changes.

IV.4. Uncoupling of PRK and GAPDH Enzyme Activities in *Chlamydomonas*

The PRK dimer possesses redox-sensitive cysteine residues which form disulphide bridges, and reduction of the disulphide is needed for a full activation of the enzyme (Porter et al., 1988; Geck & Hartman, 2000). Past studies demonstrated that both reduced or oxidized PRK can incorporate into the complex of *C. reinhardtii* and pea plants (Lebreton et al., 2003; Howard et al., 2008) whereas only oxidized PRK can be inserted into the complex of *A. thaliana* (Figure 5; Marri et al., 2005). In fact, it has been demonstrated that the PRK/CP12/GAPDH complex in *C. reinhardtii* (and pea plants) can possess active PRK dimers and hence catalytic activity (Lebreton et al., 1997; Lebreton & Gontero, 1999; Graciet et al., 2003a; Graciet et al., 2003b). On the other hand, *C. reinhardtii* has only one type of plastid GAPDH subunits – GapA. The A_4-GAPDH homotetramer formed by GapA subunits is redox-insensitive, and thus the regulation of GAPDH activity in *C. reinhardtii* depends solely on the PRK/CP12/GAPDH complex status.

These could explain the uncoupled PRK and GAPDH activities in both an *NTRC* loss-of-function mutant and in the light-dark cycle. In the cold-treated *ntrc* mutant as well as in the dark phase, lower GAPDH activities than in their respective controls were detected, while the PRK activity remained constant (Figures 18A and 22B). Consistently, a substantial PRK activity in contrast to a minimal GAPDH activity was also perceived in the complex-containing SEC-elution fraction (Figure 15B), indicating the complex contains active PRK dimers. Nevertheless, the complex formation does inhibit the PRK activity but to a much lesser extent as compared to that of GAPDH, as shown in Figures 15B, 16B and 21A where the PRK activity elevated when a complete dissociation of the complex happened.

IV.5. Roles of CP12 in Cold Acclimation

Despite extensive studies of CP12 have been carried out, most of them were *in vitro* studies and the *in vivo* roles of CP12 remain inconclusive. This study demonstrates the role of CP12 in cold acclimation which has thus far only been reported in a tropical legume (Li et al., 2018).

First, it was found that low temperature triggered an elevation of GAPDH activity in *C. reinhardtii* wild type strains (Figures 18B and 21B). On the other hand, this elevation was not so pronounced in *ntrc* and *C455S/C458S* mutants as compared to the wild type (Figure 18B), and simultaneously a slower growth was also observed in these strains under cold stress (Figure 10, B and D). This suggests that the elevation of GAPDH activity can be beneficial for algal growths under cold stress as outlined in the following.

It has been reported that ROS production increases under cold stress (O'Kane et al., 1996; Ensminger et al., 2006; Puyaubert & Baudouin, 2014; Zalutskaya et al., 2019; Bittner et al., 2020). General reduction in enzyme kinetics especially those of the Calvin cycle at low temperature disrupts the balance of energy flow between the photochemical input and metabolic output, also known as photostasis in the chloroplast (compare section I.4; Aro et al., 1993; Long et al., 1994; Vasilikiotis & Melis, 1994). Excess electrons from photosynthetic ETC are accepted by O_2 molecules and this generates H_2O_2 in the Mehler reaction (Mehler, 1951; Savitch et al., 2000). The release of active enzymes from the PRK/CP12/GAPDH complex can contribute to $NADP^+$ regeneration which absorbs excess electrons from the thylakoid ETC, and hence minimizes the generation of oxidative toxic H_2O_2 molecules. A schematic synopsis of the importance of GAPDH activation in reducing ROS generation is shown below in Figure 28.

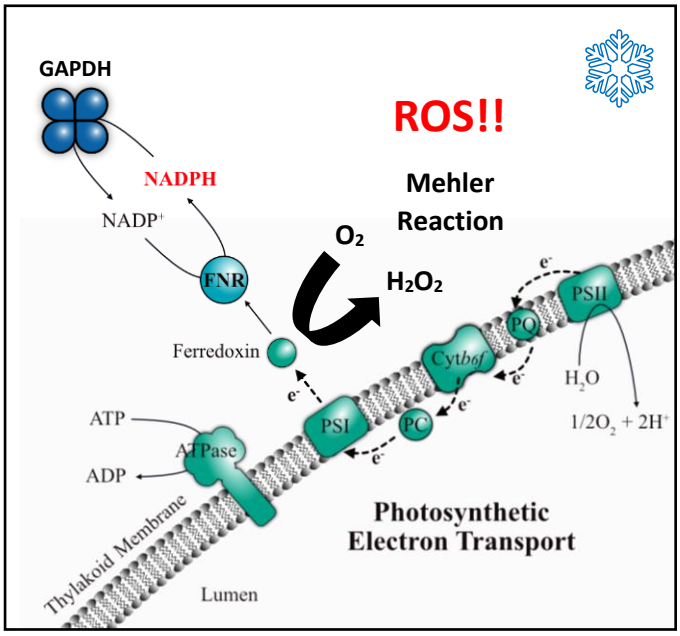

Figure 28. GAPDH activation prevents ROS generation via the Mehler reaction in the cold. Ferredoxins accept electrons from the ETC during photosynthesis and then reduce $NADP^+$ molecules via ferredoxin-$NADP^+$ reductase (FNR). The NAPDH generated are utilized in the Calvin cycle. However, at low temperature, reduction in enzyme catalytic activities disrupt this balance. Mehler reaction thus provides an alternative for the removal of excess electrons from the ETC. However, this generates H_2O_2 which is a reactive oxygen species (ROS), harmful to the cell. Hence, GAPDH activation is important to regenerate $NAPD^+$ so as to avoid the Mehler reaction and re-establish the photostasis in the chloroplast.

Nonetheless, with increased GAPDH activities (Figure 21B), *cp12* knockout strains did not proliferate faster than the wild type under cold stress (Figure 20D). An explanation for this comes from the drawback of PRK and GAPDH enzyme depletions in the *cp12* knockout mutants. Since CP12 and the PRK/CP12/GAPDH complex formation do not only inhibit the enzyme activities but also exert a stabilizing effect on the enzymes, the balance between the two these two effects seems to determine the phenotype of *cp12* knockout mutants. It appears that it is critical for the microalgal cell to maintain a sufficient number of both PRK and GAPDH enzymes so as to sustain the Calvin cycle activities under cold stress. However, protein homeostasis is difficult to be maintained in the cold due to increased rates of protein denaturation and damage but a slower rate of *de novo* protein synthesis. The situation is even worse in *cp12* mutants which have lost the enzyme repertoire formed by the PRK/CP12/GAPDH supracomplex as indicated by their dramatically reduced PRK and GAPDH protein amounts (Figure 20A). Hence, one could imagine more energy and resources have to be shifted away from biomass production for growth and division and spent by the mutant algae in maintaining protein homeostasis of PRK and GAPDH. Indeed, under cold stress, there were obvious changes in the protein levels of PRK and GAPDH enzymes in *cp12* knockout mutants but not the wild type, likely illustrating a higher PRK and GAPDH protein turnover rates in the mutants (Figure 21C).

The difficulty in maintaining the enzymes is particularly clear in the case of PRK. The protein level of PRK appears to be much more dependent on CP12 and the formation of the PRK/CP12/GAPDH complex as compared to the GAPDH enzyme. This is supported by the evidence that PRK depletion was always more severe than that of GAPDH in *C. reinhardtii cp12* knockout strains (Figure 20A and 21C). Also, only PRK but not GAPDH protein accumulation was found decreased in *A. thaliana CP12* knockout (López-Calcagno et al., 2017). Although it was observed that the PRK activity of wild-type microalgae did not change in the cold, suggesting a minimal role in cold acclimation, a severe depletion of PRK could turn the enzyme into a rate-determining factor for the Calvin cycle. *CP12* knockout though led to an increased PRK activity at room temperature, the enzyme activity diminished in the cold (Figure 21A). This is probably due to the failure in forming the PRK/CP12/GAPDH complex which has been reported to protect the enzymes from oxidative damages which prevail under cold stress (Marri et al., 2014). Indeed, there was a severe decline in PRK protein amount in *cp12* knockout mutants, and the decline exacerbated further under cold stress (Figure 21C).

Studies of CP12 and the PRK/CP12/GAPDH complex have been solely focused on their inhibitory functions on the enzyme activities (Lebreton et al., 1997; Scheibe et al., 2002; Graciet et al., 2003b; Tamoi et al., 2005; Oesterhelt et al., 2007; Howard et al., 2008; Marri et al., 2009), while this study demonstrates additionally that the protein protecting effect is equally important and should not be neglected. Formation of an enzyme repertoire by the PRK/CP12/GAPDH supracomplex reduces protein homeostasis burden, besides enabling the possibility of a rapid response to environmental changes. Nevertheless, further investigations are necessary to consolidate this postulation. For instance, direct

studies on protein translation and turnover rates of the enzymes can help us to understand the molecular mechanisms in more detail. In addition, besides seasonal changes, plants, algae, and other photoautotrophs also experience diurnal temperature variations. Hence, studying the impact of *CP12* knockout on growth and metabolism during a 12-hour warm-cold cycle will further expand the knowledge on its regulative role in these processes.

IV.6. Roles of CP12 in the Light-Dark Transition

Knockout studies in cyanobacteria have suggested that CP12 plays a role in carbon partition between the Calvin cycle and the OPPP which is especially important in the light-dark adaptation (compare section I.3.8; Tamoi et al., 2005). This regulatory function of CP12 on carbon flow has been attributed to its protein scaffold function which aggregates PRK and GAPDH enzymes into the autoinhibitory PRK/CP12/GAPDH supracomplex (Figure 29).

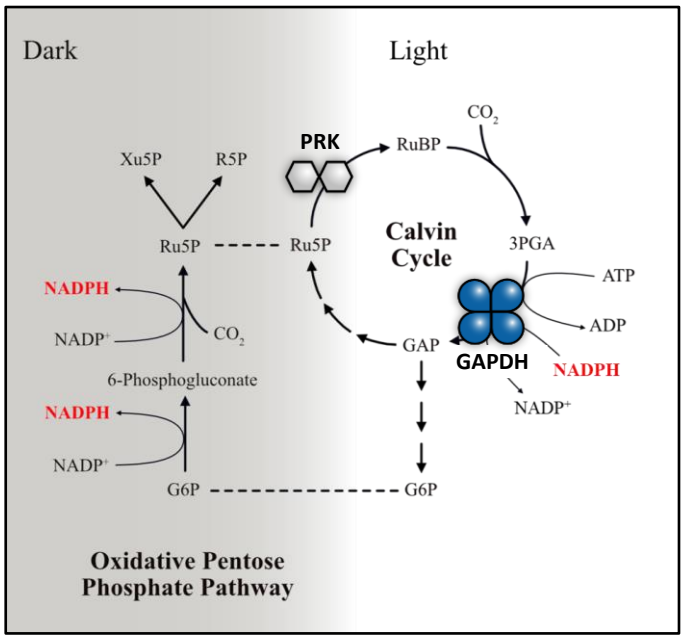

Figure 29. Carbon partition between the Calvin cycle and the OPPP during the diurnal cycle. Ribulose-5-phosphate **(**Ru5P) is an intermediate metabolite of both the Calvin cycle and the OPPP in the chloroplast. Hence, the inhibition of enzyme activities of the Calvin cycle including those of PRK and GAPDH is required in the dark to ensure sufficient carbon flow into the OPPP. Moreover, the Calvin cycle utilizes NAPDH while the OPPP generates NADPH. The partition is also important to avoid a futile cycle in NAPDH metabolism.

Since Ru5P is an intermediate product of both the Calvin cycle and the OPPP, PRK which converts Ru5P into RuBP has been described by Tamoi and colleagues (2005) as the key enzyme in determining the carbon flow destination. PRK activation in the light will lead Ru5P to the Calvin cycle while the inactivation of PRK will shift the substrate to the OPPP in the dark. Nonetheless, it was observed in *C. reinhardtii* that only a suppression of GAPDH activity but no significant changes in the PRK activity during the dark phase (Figure 22, B and C). This indicates that the Calvin cycle activity is regulated as a whole, the rate limiting step appears to be the GAPDH reaction in this case.

Further, instead of an incomplete suppression of the Calvin cycle as reported in cyanobacteria (Tamoi et al., 2005), the time-point enzyme activity study shown in Figure 24 D and E demonstrated

that *CP12* knockout leads to a lagged suppression of the Calvin cycle during the dark phase of *C. reinhardtii*. Full suppression of the enzyme activities can still be achieved as observed in the late dark phase (Figure 22, D and E). Drastic changes were observed in the protein levels of the PRK and GAPDH enzymes during the light-dark cycle in *cp12* knockout mutants but not in the wild type (Figure 24C). These changes are cyclical and strongly correlated with the enzyme activities of the mutants during the light-dark rhythm. This reveals the existence of another regulatory mechanism which is activated upon *CP12* knockout. It takes over the niche of CP12 to accomplish complete down-regulation of the Calvin cycle in the dark phase by controlling the enzyme accumulations.

To figure out possible alternative mechanisms modulating PRK and GAPDH enzyme accumulations in *cp12* mutants, both transcriptional and translational rates of the enzymes deserve a closer examination. They determine protein synthesis rates of the enzymes and could contribute to the waveform of enzyme accumulations in *cp12* mutants during the diurnal cycle (Figure 24C). As a matter of fact, circadian control of gene expression at transcriptional and translational levels has been well characterized in photoautotrophs (reviewed in Covington et al., 2008; Mittag, 2009).

However, unlike in algae and cyanobacteria, glucose-6-phosphate dehydrogenase (G6PDH) in higher plants can be reduced and inactivated by Trx-*f* (Wenderoth et al., 1997; Kruger & von Schaewen, 2003; Née et al., 2009; Tamoi & Shigeoka, 2015). G6PDH is the first enzyme of the OPPP, hence this mechanism could be adequate to avoid the futile cycle between the Calvin cycle and OPPP from happening, making absolute suppression of PRK and GAPDH in the dark unnecessary. Further, the PRK/CP12/GAPDH complex is not always detectable in darkened leaves of higher plants such as tobacco and *A. thaliana* (Howard et al., 2011a; Howard et al., 2011b). These raise questions about the importance of CP12 in light-responsive carbon flow control in higher plants. In conjunction, the study of *cp12* antisense tobacco plant found no reduction in PRK activity but a suppression of malate dehydrogenase activity, pointing the physiological role of CP12 to a new direction – malate valve control (Howard et al., 2011a). However, the regulatory mechanism of malate dehydrogenase by CP12 remains unknown.

Overall, data presented here further support findings of Tamoi et al. (2005) that CP12 is crucial in carbon flow regulation during the light-dark cycle in oxygenic photoautotrophic microorganisms, but the role in higher plants remains uncertain and needs further investigation.

IV.7. Comparing CP12 regulation by NTRC and Thioredoxin-*f/m*

As mentioned in section IV.1, NTRC-mediated redox regulation of CP12 is involved in cold acclimation, the situation in the diurnal rhythm does not appear to be the same. While deletion of the *CP12* gene in *C. reinhardtii* led to a reduced growth rate in the light-dark cycle (Figure 24B), it was observed that

ntrc and cysteine-substituted mutants grew at a rate comparable to that of the wild type (Figure 25). This eliminates NTRC from the possibility of playing a regulatory role in the CP12-mediated diurnal regulation of PRK and GAPDH enzymes (Figure 24). The redox-regulation of CP12 in the light-dark rhythm is probably executed by the ferredoxin-thioredoxin system. It has been shown *in vitro* that Trx-*f* dissociated the PRK/CP12/GAPDH complex of *Pisum sativum* (Howard et al, 2008). Further, Trx-*f* and Trx-m_1/m_2 have also been demonstrated to activate both PRK and GAPDH enzyme activities of reconstituted *A. thaliana* PRK/CP12/A_4-GAPDH complexes *in vitro* (Marri et al., 2009). Since the A_4-GAPDH tetramer lacks a thioredoxin-sensitive disulphide (Marri et al., 2005), the activation was suggested to be carried out by CP12 reduction which release the enzyme from the inhibitory complex (Marri et al., 2009). Besides, these versatile thioredoxins depends on ferredoxins for reducing powers and are therefore activated only in the light and inactive in the dark. The role of ferredoxin-thioredoxin system in regulating the Calvin cycle during the diurnal rhythm is well established since its discovery (Buchanan, 1980, 1991; Buchanan et al., 2002). Nonetheless, the regulatory role of Trx-*f/m* for CP12 in the cold remain unknown and should not be excluded as functional overlaps between the ferredoxin-thioredoxin system and the NTRC system have been reported (Thormählen et al., 2015; Nikkanen et al., 2016).

Moreover, PRK and GADPH (only the GapB subunit in higher plants) enzymes possess redox-sensitive disulphides allowing direct regulation by thioredoxins (Porter et al., 1988; Li & Anderson, 1997; Geck & Hartman, 2000; Sparla et al., 2002). Co-IP assays conducted by Nikkanen and colleagues (2016) have also identified PRK as interaction partner of NTRC in *A. thaliana*. Besides, the *in vivo* redox status of PRK, and GADPH have been shown dependent on NTRC in *A. thaliana* (Pérez-Ruiz et al., 2017; Ojeda et al., 2018). Further, *in vitro* study by Marri et al. (2005) has shown that only oxidized PRK can incorporate into the CP12-GAPDH binary complex, implying the redox status of PRK can be a determining factor for the complex status. Nevertheless, the influence of the GAPDH redox status on the complex integrity remains unclear as only the A_4-GAPDH tetramer but not the redox-sensitive A_2B_2-GAPDH tetramer has been used to reconstitute and study the PRK/CP12/GAPDH complex *in vitro* (Marri et al., 2005; Fermani et al., 2012). Taken together, one might therefore, question if the observed changes of the complex status in *A. thaliana* were also results of the direct redox regulation of the enzymes by NTRC (Figure 17B). Nonetheless, this possibility is ruled out in *C. reinhardtii* because the PRK/CP12/GAPDH complex formation-dissociation is so far the only known redox-regulatory mechanism for the algal GAPDH activity due to the absence of GapB subunit (Petersen et al., 2006).

In conclusion, the presented findings suggest NTRC as a redox regulator of CP12 during cold acclimation. NTRC-induced elevation of GAPDH activity in the cold could contribute to minimizing ROS generation by the Mehler reaction. On the other hand, the Trx-*f/m* regulates CP12 during the diurnal rhythm wherein NTRC does not seem to be involved. A schematic summary of these is provided in Figure 30.

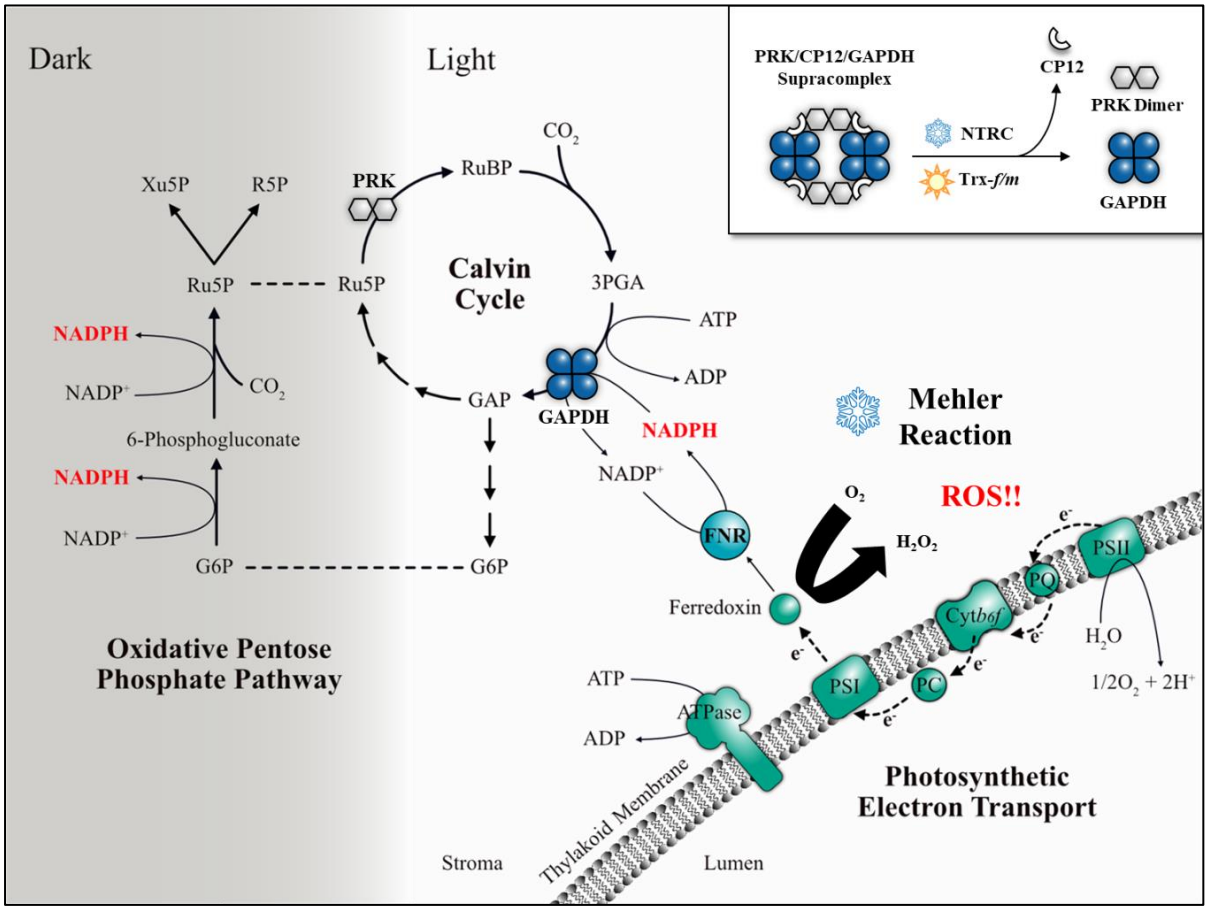

Figure 30. Schematic diagram proposing regulation of CP12 by NTRC and Trx-*f/m* in response to temperature and light intensity respectively. During photosynthesis, electrons from the photosynthetic electron transport chain are accepted by ferredoxins which in turn reduce $NADP^+$ molecule via ferredoxin-$NADP^+$ reductase (FNR). The generated NADPH was then utilized to drive the Calvin cycle. Regeneration of $NAPD^+$ is crucial especially in the cold condition to remove excess electrons from the ETC which could otherwise be accepted by O_2 and generate H_2O_2, a process termed Mehler reaction. This reactive oxygen species (ROS) can then impose oxidative damage to the cells. NTRC rescues the cell from this by reducing CP12 which rapidly releases active PRK and GAPDH enzymes from the supracomplex. In the dark, strict suppression of the Calvin cycle enzymes including PRK and GAPDH are required to shift carbon flow into the oxidative pentose phosphate pathway which sustains the NADPH pool and provides metabolic intermediates for anabolic biosynthesis processes. The light-dark switch of CP12 is postulated to be regulated by Trx-*f/m* which are ferredoxin- and light-dependent.

IV.8. Significance of the Study

This study identifies NTRC as a redox regulator of CP12 which was previously unreported. It also unravels the role of NTRC in the redox regulation of Calvin cycle during cold acclimation which was previously attributed to its chaperone functions. Besides, the *C. reinhardtii CP12* knockout studies also demonstrated *in vivo* roles of CP12 which have not been well examined and understood especially in cold acclimation. Last but not least, the PRK/CP12/GAPDH complex regulation by NTRC under cold stress was compared in *C. reinhardtii* and *A. thaliana* which represent the two major groups of photoautotrophic eukaryotes – aquatic algae and land plants respectively.

IV.9. Future Perspectives

The growth inhibitory effect of *CP12* knockout at 15 °C (Figure 20D) is not as robust as that of *NTRC* knockout (Figure 10D), implying other downstream redox targets of NTRC might also participate in the NTRC-mediated cold acclimation. First of all, the well-established NTRC's redox target, 2-Cys peroxiredoxin (Serrato et al., 2004), is a ROS scavenging enzyme and hence could also contribute to overcoming cold-induced oxidative stress. Another potential candidate is NEET which has been found to be critical in iron homeostasis in *A. thaliana* (Zandalinas et al., 2020). NEET exhibited cold- and redox-dependent bindings to NTRC, according to the co-IP-mass spectrometry data (Figure 13, B and C). Interestingly, bioinformatic data retrieved from Phytozome v12.1 (JGI) indicates that NEET is also co-expressed with CP12. In conjunction, preliminary growth studies of *neet* knockout strains also suggest that NEET plays a role in both cold acclimation and the light-dark adaptation (Supplemental Figure S6). Lastly, both CP12 and NEET are involved in metal ion homeostasis in the chloroplast; CP12 has been reported binding copper and calcium (Erales et al., 2009a; Rocha & Vothknecht, 2013), while NEET is an iron-sulphur protein (Nechushtai et al., 2012; Zandalinas et al., 2020). The strong correlation between NEET and CP12 in NTRC binding, gene expression, growth phenotypes and physiological functions have definitely drawn attention for further research.

Disproportional to the hardly detectable free PRK and GAPDH enzymes in the native *C. reinhardtii* lysate, a high amount of CP12 proteins in the low molecular weight elution fractions in the SEC studies was always noticed (Figures 15A, 16A and 22A). This again suggest that CP12, besides assembling PRK and GAPDH, does have other functions. Pulling down CP12 proteins from these low molecular weight fractions of SEC filtrates could help us to identify more interaction partners of CP12. In fact, apart from metal ion binding, CP12's binding promiscuity as an IDP has also been demonstrated in its interactions with aldose and MDH (Erales et al., 2008; Howard et al., 2011a). Nonetheless, unlike what has been reported in tobacco, neither mutations of *CP12* or *NTRC* nor cold treatment caused significant changes in the MDH activity of *C. reinhardtii* (Supplemental Figure S7).

Additionally, other post-translational regulations of CP12 do exist besides redox modulation. Recent phospho-proteomic studies have identified seven putative phosphorylation sites of CP12, suggesting additional post-translational modification of the protein in parallel with disulphide bond formation (Wang et al., 2014; McConnell et al., 2018). The effect of phosphorylation on CP12 is another topic requires further investigation.

To sum up, there are lots of remaining questions to be explored for CP12 such as its role in metal ion metabolism and the identification of further interaction partners. Scrutinizing molecular mechanisms of this protein will extend our understanding of chloroplast stress responses which can be beneficial in agricultural applications.

V. REFERENCES

Aro, E. M., Virgin, I., & Andersson, B. (1993). Photoinhibition of Photosystem II. Inactivation, protein damage and turnover. *Biochim Biophys Acta, 1143*(2), 113-134. doi:10.1016/0005-2728(93)90134-2

Åström, J., Savitch, L. V., Ivanov, A. G., Huner, N. P. A., Öquist, G., & Gardeström, P. (1998). Effects of low temperature stress and cold acclimation on photosynthesis in *Arabidopsis thaliana* Leaves. In G. Garab (Ed.), *Photosynthesis: Mechanisms and Effects.* Dordrecht: Springer.

Avilan, L., Gontero, B., Lebreton, S., & Ricard, J. (1997). Memory and imprinting effects in multienzyme complexes. *European Journal of Biochemistry, 246*(1), 78-84. doi:10.1111/j.1432-1033.1997.00078.x

Baalmann, E., Backhausen, J. E., Rak, C., Vetter, S., & Scheibe, R. (1995). Reductive modification and nonreductive activation of purified spinach chloroplast NADP-dependent glyceraldehyde-3-phosphate dehydrogenase. *Archives of Biochemistry and Biophysics, 324*(2), 201-208. doi:10.1006/abbi.1995.0031

Baalmann, E., Scheibe, R., Cerff, R., & Martin, W. (1996). Functional studies of chloroplast glyceraldehyde-3-phosphate dehydrogenase subunits A and B expressed in *Escherichia coli*: Formation of highly active A_4 and B_4 homotetramers and evidence that aggregation of the B_4 complex is mediated by the B subunit carboxy terminus. *Plant Molecular Biology, 32*(3), 505-513. doi:10.1007/BF00019102

Baroli, I., & Melis, A. (1996). Photoinhibition and repair in Dunaliella salina acclimated to different growth irradiances. *Planta, 198*(4), 640-646. doi:10.1007/BF00262653

Bassham, J. A., Benson, A. A., & Calvin, M. (1950). The path of carbon in photosynthesis. *Journal of Biological Chemistry, 185*(2), 781-787.

Benjamini, Y., & Hochberg, Y. (1995). Controlling the false siscovery rate: A practical and powerful approach to multiple testing. *Journal of the Royal Statistical Society: Series B (Methodological), 57*(1), 289-300. doi:10.1111/j.2517-6161.1995.tb02031.x

Bepperling, A., Alte, F., Kriehuber, T., Braun, N., Weinkauf, S., Groll, M., Haslbeck, M., & Buchner, J. (2012). Alternative bacterial two-component small heat shock protein systems. *Proceedings of the National Academy of Sciences, 109*(50), 20407. doi:10.1073/pnas.1209565109

Bernal-Bayard, P., Ojeda, V., Hervás, M., Cejudo, F. J., Navarro, J. A., Velázquez-Campoy, A., & Pérez-Ruiz, J. M. (2014). Molecular recognition in the interaction of chloroplast 2-Cys peroxiredoxin with NADPH-thioredoxin reductase C (NTRC) and thioredoxin x. *FEBS Letters, 588*(23), 4342-4347. doi:10.1016/j.febslet.2014.09.044

Bittner, A., van Buer, J., & Baier, M. (2020). Cold priming uncouples light- and cold-regulation of gene expression in *Arabidopsis thaliana*. *BMC Plant Biology, 20*(1), 281. doi:10.1186/s12870-020-02487-0

Buchanan, B. B. (1980). Role of light in the regulation of chloroplast enzymes. *Annual Review of Plant Physiology, 31*(1), 341-374. doi:10.1146/annurev.pp.31.060180.002013

Buchanan, B. B. (1991). Regulation of CO2 assimilation in oxygenic photosynthesis: The ferredoxin/thioredoxin system: Perspective on its discovery, present status, and future development. *Archives of Biochemistry and Biophysics, 288*(1), 1-9. doi:10.1016/0003-9861(91)90157-E

Buchanan, B. B. (2016). The carbon (formerly dark) reactions of photosynthesis. *Photosynthesis Research, 128*(2), 215-217. doi:10.1007/s11120-015-0212-z

Buchanan, B. B., & Balmer, Y. (2005). Redox regulation: a broadening horizon. *Annual Review of Plant Biology, 56*(1), 187-220. doi:10.1146/annurev.arplant.56.032604.144246

Buchanan, B. B., Schürmann, P., Wolosiuk, R. A., & Jacquot, J.-P. (2002). The ferredoxin/thioredoxin system: from discovery to molecular structures and beyond. *Photosynthesis Research, 73*(1), 215-222. doi:10.1023/A:1020407432008

Calzadilla, P. I., Vilas, J. M., Escaray, F. J., Unrein, F., Carrasco, P., & Ruiz, O. A. (2019). The increase of photosynthetic carbon assimilation as a mechanism of adaptation to low temperature in *Lotus japonicus*. *Scientific Reports, 9*(1), 863. doi:10.1038/s41598-018-37165-7

Campanella, J. J., Smalley, J. V., & Dempsey, M. E. (2014). A phylogenetic examination of the primary anthocyanin production pathway of the Plantae. *Botanical studies, 55*(1), 10-10. doi:10.1186/1999-3110-55-10

Carrillo, L. R., Froehlich, J. E., Cruz, J. A., Savage, L. J., & Kramer, D. M. (2016). Multi-level regulation of the chloroplast ATP synthase: the chloroplast NADPH thioredoxin reductase C (NTRC) is required for redox modulation specifically under low irradiance. *The Plant Journal, 87*(6), 654-663. doi:10.1111/tpj.13226

Cerff, R. (1979). Quaternary structure of higher plant glyceraldehyde-3-phosphate dehydrogenases. *European Journal of Biochemistry, 94*(1), 243-247. doi:10.1111/j.1432-1033.1979.tb12891.x

Cerff, R. (1982). Evolutionary divergence of chloroplast and cytosolic glyceraldehyde-3-phosphate dehydrogenases from angiosperms. *European Journal of Biochemistry, 126*(3), 513-515. doi:10.1111/j.1432-1033.1982.tb06810.x

Chae, H. B., Moon, J. C., Shin, M. R., Chi, Y. H., Jung, Y. J., Lee, S. Y., Nawkar, G. M., Jung, H. S., Hyun, J. K., Kim, W. Y., Kang, C. H., Yun, D. J., Lee, K. O., & Lee, S. Y. (2013). Thioredoxin reductase type C (NTRC) orchestrates enhanced thermotolerance to *Arabidopsis* by its redox-dependent holdase chaperone function. *Molecular Plant, 6*(2), 323-336. doi:10.1093/mp/sss105

Chen, L. J., Xiang, H. Z., Miao, Y., Zhang, L., Guo, Z. F., Zhao, X. H., Lin, J. W., & Li, T. L. (2014). An overview of cold resistance in plants. *Journal of Agronomy and Crop Science, 200*(4), 237-245. doi:doi.org/10.1111/jac.12082

Collet, J.-F., & Messens, J. (2010). Structure, function, and mechanism of thioredoxin proteins. *Antioxidants & Redox Signaling, 13*(8), 1205-1216. doi:10.1089/ars.2010.3114

Collin, V., Issakidis-Bourguet, E., Marchand, C., Hirasawa, M., Lancelin, J. M., Knaff, D. B., & Miginiac-Maslow, M. (2003). The *Arabidopsis* plastidial thioredoxins: new functions and new insights into specificity. *Journal of Biological Chemistry, 278*(26), 23747-23752. doi:10.1074/jbc.M302077200

Cortese, M. S., Uversky, V. N., & Dunker, A. K. (2008). Intrinsic disorder in scaffold proteins: getting more from less. *Progress in Biophysics and Molecular Biology, 98*(1), 85-106. doi:10.1016/j.pbiomolbio.2008.05.007

Covington, M. F., Maloof, J. N., Straume, M., Kay, S. A., & Harmer, S. L. (2008). Global transcriptome analysis reveals circadian regulation of key pathways in plant growth and development. *Genome Biology, 9*(8), R130. doi:10.1186/gb-2008-9-8-r130

Cox, J., Hein, M. Y., Luber, C. A., Paron, I., Nagaraj, N., & Mann, M. (2014). Accurate proteome-wide label-free quantification by delayed normalization and maximal peptide ratio extraction, termed MaxLFQ. *Molecular & Cellular Proteomics, 13*(9), 2513-2526. doi:10.1074/mcp.M113.031591

Cox, J., & Mann, M. (2008). MaxQuant enables high peptide identification rates, individualized p.p.b.-range mass accuracies and proteome-wide protein quantification. *Nature Biotechnology, 26*(12), 1367-1372. doi:10.1038/nbt.1511

Cox, J., Neuhauser, N., Michalski, A., Scheltema, R. A., Olsen, J. V., & Mann, M. (2011). Andromeda: A peptide search engine integrated into the MaxQuant environment. *Journal of Proteome Research, 10*(4), 1794-1805. doi:10.1021/pr101065j

Cruz, R. P. d., Sperotto, R. A., Cargnelutti, D., Adamski, J. M., de FreitasTerra, T., & Fett, J. P. (2013). Avoiding damage and achieving cold tolerance in rice plants. *Food and Energy Security, 2*(2), 96-119. doi:10.1002/fes3.25

Da, Q., Wang, P., Wang, M., Sun, T., Jin, H., Liu, B., Wang, J., Grimm, B., & Wang, H.-B. (2017). Thioredoxin and NADPH-dependent thioredoxin reductase C regulation of tetrapyrrole biosynthesis. *Plant Physiology, 175*(2), 652-666. doi:10.1104/pp.16.01500

Dent, R. M., Haglund, C. M., Chin, B. L., Kobayashi, M. C., & Niyogi, K. K. (2005). Functional genomics of eukaryotic photosynthesis using insertional mutagenesis of *Chlamydomonas reinhardtii*. *Plant Physiology, 137*(2), 545. doi:10.1104/pp.104.055244

Droux, M., Jacquot, J. P., Miginac-Maslow, M., Gadal, P., Huet, J. C., Crawford, N. A., Yee, B. C., & Buchanan, B. B. (1987). Ferredoxin-thioredoxin reductase, an iron-sulfur enzyme linking light to enzyme regulation in oxygenic photosynthesis: Purification and properties of the enzyme from C3, C4, and cyanobacterial species. *Archives of Biochemistry and Biophysics, 252*(2), 426-439. doi:10.1016/0003-9861(87)90049-X

Du, Z.-Y., Lucker, B. F., Zienkiewicz, K., Miller, T. E., Zienkiewicz, A., Sears, B. B., Kramer, D. M., & Benning, C. (2018). Galactoglycerolipid lipase PGD1 is involved in thylakoid membrane remodeling in response to adverse environmental conditions in *Chlamydomonas*. *The Plant Cell, 30*(2), 447-465. doi:10.1105/tpc.17.00446

Dyson, H. J., & Wright, P. E. (2005). Intrinsically unstructured proteins and their functions. *Nature Reviews Molecular Cell Biology, 6*(3), 197-208. doi:10.1038/nrm1589

Ensminger, I., Busch, F., & Huner, N. P. A. (2006). Photostasis and cold acclimation: sensing low temperature through photosynthesis. *Physiologia Plantarum, 126*(1), 28-44. doi:10.1111/j.1399-3054.2006.00627.x

Erales, J., Avilan, L., Lebreton, S., & Gontero, B. (2008). Exploring CP12 binding proteins revealed aldolase as a new partner for the phosphoribulokinase/glyceraldehyde 3-phosphate dehydrogenase/CP12 complex – purification and kinetic characterization of this enzyme from *Chlamydomonas reinhardtii*. *The FEBS Journal, 275*(6), 1248-1259. doi:10.1111/j.1742-4658.2008.06284.x

Erales, J., Gontero, B., Whitelegge, J., & Halgand, F. (2009a). Mapping of a copper-binding site on the small CP12 chloroplastic protein of *Chlamydomonas reinhardtii* using top-down mass spectrometry and site-directed mutagenesis. *Biochemical Journal, 419*(1), 75-86. doi:10.1042/BJ20082004

Erales, J., Lignon, S., & Gontero, B. (2009b). CP12 from *Chlamydomonas reinhardtii*, a permanent specific "chaperone-like" protein of glyceraldehyde-3-phosphate dehydrogenase. *The Journal of Biological Chemistry, 284*(19), 12735-12744. doi:10.1074/jbc.M808254200

Ermilova, E. (2020). Cold Stress Response: An Overview in *Chlamydomonas*. *Frontiers in Plant Science, 11*, 569437. doi:10.3389/fpls.2020.569437

Falkowski, P. G., & Chen, Y. (2003). Photoacclimation of light harvesting systems in eukaryotic algae. In B. R. Green & W. W. Parson (Eds.), *Light-Harvesting Antennas in Photosynthesis. Advances in Photosynthesis and Respiration* (Vol. 13). Dordrech: Springer.

Fermani, S., Sparla, F., Falini, G., Martelli, P. L., Casadio, R., Pupillo, P., Ripamonti, A., & Trost, P. (2007). Molecular mechanism of thioredoxin regulation in photosynthetic glyceraldehyde-3-phosphate

dehydrogenase. *Proceedings of the National Academy of Sciences, 104*(26), 11109. doi:10.1073/pnas.0611636104

Fermani, S., Trivelli, X., Sparla, F., Thumiger, A., Calvaresi, M., Marri, L., Falini, G., Zerbetto, F., & Trost, P. (2012). Conformational selection and folding-upon-binding of intrinsically disordered protein CP12 regulate photosynthetic enzymes assembly. *Journal of Biological Chemistry, 287*(25), 21372-21383. doi:10.1074/jbc.M112.350355

Ferris, P. J., & Goodenough, U. W. (1994). The mating-type locus of *Chlamydomonas reinhardtii* contains highly rearranged DNA sequences. *Cell, 76*(6), 1135-1145. doi:10.1016/0092-8674(94)90389-1

Field, C. B., Behrenfeld, M. J., Randerson, J. T., & Falkowski, P. (1998). Primary production of the biosphere: integrating terrestrial and oceanic components. *Science, 281*(5374), 237. doi:10.1126/science.281.5374.237

Figge, R. M., Schubert, M., Brinkmann, H., & Cerff, R. (1999). Glyceraldehyde-3-phosphate dehydrogenase gene diversity in eubacteria and eukaryotes: evidence for intra- and inter-kingdom gene transfer. *Molecular Biology and Evolution, 16*(4), 429-440. doi:10.1093/oxfordjournals.molbev.a026125

Fischer, N., Stampacchia, O., Redding, K., & Rochaix, J. D. (1996). Selectable marker recycling in the chloroplast. *Molecular and General Genetics MGG, 251*(3), 373-380. doi:10.1007/BF02172529

Florencio, F. J., Pérez-Pérez, M. E., López-Maury, L., Mata-Cabana, A., & Lindahl, M. (2006). The diversity and complexity of the cyanobacterial thioredoxin systems. *Photosynthesis Research, 89*(2), 157-171. doi:10.1007/s11120-006-9093-5

Gardebien, F., Thangudu, R. R., Gontero, B., & Offmann, B. (2006). Construction of a 3D model of CP12, a protein linker. *Journal of Molecular Graphics and Modelling, 25*(2), 186-195. doi:10.1016/j.jmgm.2005.12.003

Geck, M. K., & Hartman, F. C. (2000). Kinetic and mutational analyses of the regulation of phosphoribulokinase by thioredoxins. *Journal of Biological Chemistry, 275*(24), 18034-18039. doi:10.1074/jbc.M001936200

Gould, S. B., Waller, R. F., & McFadden, G. I. (2008). Plastid evolution. *Annual Review of Plant Biology, 59*(1), 491-517. doi:10.1146/annurev.arplant.59.032607.092915

Graciet, E., Gans, P., Wedel, N., Lebreton, S., Camadro, J.-M., & Gontero, B. (2003a). The small protein CP12: a protein linker for supramolecular complex assembly. *Biochemistry, 42*(27), 8163-8170. doi:10.1021/bi034474x

Graciet, E., Lebreton, S., Camadro, J.-M., & Gontero, B. (2003b). Characterization of native and recombinant A_4 glyceraldehyde 3-phosphate dehydrogenase. *European Journal of Biochemistry, 270*(1), 129-136. doi:10.1046/j.1432-1033.2003.03372.x

Graciet, E., Lebreton, S., & Gontero, B. (2004). Emergence of new regulatory mechanisms in the Benson–Calvin pathway via protein–protein interactions: A glyceraldehyde-3-phosphate dehydrogenase/CP12/phosphoribulokinase complex. *Journal of Experimental Botany, 55*(400), 1245-1254. doi:10.1093/jxb/erh107

Gray, M. W., & Boer, P. H. (1988). Organization and expression of algal (*Chlamydomonas reinhardtii*) mitochondrial DNA. *Philosophical Transactions of the Royal Society of London. Series B, Biological Sciences, 319*(1193), 135-147.

Greiner, A., Kelterborn, S., Evers, H., Kreimer, G., Sizova, I., & Hegemann, P. (2017). Targeting of photoreceptor genes in *Chlamydomonas reinhardtii* via zinc-finger nucleases and CRISPR/Cas9. *The Plant Cell, 29*(10), 2498. doi:10.1105/tpc.17.00659

Groben, R., Kaloudas, D., Raines, C. A., Offmann, B., Maberly, S. C., & Gontero, B. (2010). Comparative sequence analysis of CP12, a small protein involved in the formation of a Calvin cycle complex in photosynthetic organisms. *Photosynthesis Research, 103*(3), 183-194. doi:10.1007/s11120-010-9542-z

Hahn, A., Vonck, J., Mills, D. J., Meier, T., & Kühlbrandt, W. (2018). Structure, mechanism, and regulation of the chloroplast ATP synthase. *Science, 360*(6389), eaat4318. doi:10.1126/science.aat4318

Hajihashemi, S., Noedoost, F., Geuns, J. M. C., Djalovic, I., & Siddique, K. H. M. (2018). Effect of cold stress on photosynthetic traits, carbohydrates, morphology, and anatomy in nine cultivars of *Stevia rebaudiana*. *Frontiers in Plant Science, 9*, 1430. doi:10.3389/fpls.2018.01430

Hare, P. D., Cress, W. A., & Van Staden, J. (1998). Dissecting the roles of osmolyte accumulation during stress. *Plant, Cell & Environment, 21*(6), 535-553. doi:10.1046/j.1365-3040.1998.00309.x

Harris, E. H. (1989). 8 - Organelle Heredity. In E. H. Harris (Ed.), *The Chlamydomonas Sourcebook* (pp. 299-350). San Diego: Academic Press.

Hashida, S.-N., & Kawai-Yamada, M. (2019a). Inter-organelle NAD metabolism underpinning light responsive NADP dynamics in plants. *Frontiers in Plant Science, 10*(960). doi:10.3389/fpls.2019.00960

Hashida, S. N., & Kawai-Yamada, M. (2019b). Inter-organelle NAD metabolism underpinning light responsive NADP dynamics in plants. *Frontiers in Plant Science, 10*, 960. doi:10.3389/fpls.2019.00960

Heidarvand, L., & Maali-Amiri, R. (2013). Physio-biochemical and proteome analysis of chickpea in early phases of cold stress. *Journal of Plant Physiology, 170*(5), 459-469. doi:10.1016/j.jplph.2012.11.021

Heldt, H.-W., & Piechulla, B. (2011). 6 - The Calvin cycle catalyzes photosynthetic CO_2 assimilation. In H.-W. Heldt & B. Piechulla (Eds.), *Plant Biochemistry (Fourth Edition)* (pp. 163-191). San Diego: Academic Press.

Hirasawa, M., Schürmann, P., Jacquot, J.-P., Manieri, W., Jacquot, P., Keryer, E., Hartman, F. C., & Knaff, D. B. (1999). Oxidation-reduction properties of chloroplast thioredoxins, ferredoxin: thioredoxin reductase, and thioredoxin f-regulated enzymes. *Biochemistry, 38*(16), 5200-5205. doi:10.1021/bi982783v

Holmgren, A., & Bjornstedt, M. (1995). [21] Thioredoxin and thioredoxin reductase. In *Methods in Enzymology* (Vol. 252, pp. 199-208). San Diego: Academic Press.

Howard, T. P., Fryer, M. J., Singh, P., Metodiev, M., Lytovchenko, A., Obata, T., Fernie, A. R., Kruger, N. J., Quick, W. P., Lloyd, J. C., & Raines, C. A. (2011a). Antisense suppression of the small chloroplast protein CP12 in tobacco alters carbon partitioning and severely restricts growth. *Plant Physiology, 157*(2), 620-631. doi:10.1104/pp.111.183806

Howard, T. P., Lloyd, J. C., & Raines, C. A. (2011b). Inter-species variation in the oligomeric states of the higher plant Calvin cycle enzymes glyceraldehyde-3-phosphate dehydrogenase and phosphoribulokinase. *Journal of Experimental Botany, 62*(11), 3799-3805. doi:10.1093/jxb/err057

Howard, T. P., Metodiev, M., Lloyd, J. C., & Raines, C. A. (2008). Thioredoxin-mediated reversible dissociation of a stromal multiprotein complex in response to changes in light availability. *Proceedings of the National Academy of Sciences, 105*(10), 4056. doi:10.1073/pnas.0710518105

Huner, N. P., Oquist, G., Hurry, V. M., Krol, M., Falk, S., & Griffith, M. (1993). Photosynthesis, photoinhibition and low temperature acclimation in cold tolerant plants. *Photosynthesis Research, 37*(1), 19-39. doi:10.1007/BF02185436

Huner, N. P. A., Öquist, G., & Melis, A. (2003). Photostasis in plants, green algae and cyanobacteria: the role of light harvesting antenna complexes. In B. R. Green & W. W. Parson (Eds.), *Light-Harvesting Antennas in Photosynthesis. Advances in Photosynthesis and Respiration* (Vol. 13). Dordrecht: Springer.

Huner, N. P. A., Öquist, G., & Sarhan, F. (1998). Energy balance and acclimation to light and cold. *Trends in Plant Science, 3*(6), 224-230. doi:10.1016/S1360-1385(98)01248-5

Huppe, H. C., de Lamotte-Guéry, F., Jacquot, J. P., & Buchanan, B. B. (1990). The ferredoxin-thioredoxin system of a green alga, Chlamydomonas reinhardtii : Identification and characterization of thioredoxins and ferredoxin-thioredoxin reductase components. *Planta, 180*(3), 341-351. doi:10.1007/bf00198785

Hutchison, R. S., Groom, Q., & Ort, D. R. (2000). Differential effects of chilling-induced photooxidation on the redox regulation of photosynthetic enzymes. *Biochemistry, 39*(22), 6679-6688. doi:10.1021/bi0001978

Itakura, A. K., Chan, K. X., Atkinson, N., Pallesen, L., Wang, L., Reeves, G., Patena, W., Caspari, O., Roth, R., Goodenough, U., McCormick, A. J., Griffiths, H., & Jonikas, M. C. (2019). A rubisco-binding protein is required for normal pyrenoid number and starch sheath morphology in *Chlamydomonas reinhardtii*. *Proceedings of the National Academy of Sciences, 116*(37), 18445. doi:10.1073/pnas.1904587116

Ivanov, A. G., Morgan, R. M., Gray, G. R., Velitchkova, M. Y., & Huner, N. P. A. (1998). Temperature/light dependent development of selective resistance to photoinhibition of photosystem I. *FEBS Letters, 430*(3), 288-292. doi:10.1016/S0014-5793(98)00681-4

Janmohammadi, M., Zolla, L., & Rinalducci, S. (2015). Low temperature tolerance in plants: Changes at the protein level. *Phytochemistry, 117*, 76-89. doi:10.1016/j.phytochem.2015.06.003

Jiang, X., & Stern, D. (2009). Mating and tetrad separation of *Chlamydomonas reinhardtii* for genetic analysis. *Journal of Visualized Experiments*(30), 1274. doi:10.3791/1274

Kaiser, W. M., & Bassham, J. A. (1979). Carbon metabolism of chloroplasts in the dark: Oxidative pentose phosphate cycle versus glycolytic pathway. *Planta, 144*(2), 193-200. doi:10.1007/BF00387270

Kazemi-Shahandashti, S. S., & Maali-Amiri, R. (2018). Global insights of protein responses to cold stress in plants: Signaling, defence, and degradation. *Journal of Plant Physiology, 226*, 123-135. doi:10.1016/j.jplph.2018.03.022

Kindle, K. L. (1990). High-frequency nuclear transformation of Chlamydomonas reinhardtii. *Proceedings of the National Academy of Sciences, 87*(3), 1228. doi:10.1073/pnas.87.3.1228

Kirchsteiger, K., Ferrández, J., Pascual, M. B., González, M., & Cejudo, F. J. (2012). NADPH thioredoxin reductase C is localized in plastids of photosynthetic and nonphotosynthetic tissues and is involved in lateral root formation in *Arabidopsis The Plant Cell, 24*(4), 1534-1548. doi:10.1105/tpc.111.092304

Kirchsteiger, K., Pulido, P., González, M., & Cejudo, F. J. (2009). NADPH Thioredoxin reductase C controls the redox status of chloroplast 2-Cys peroxiredoxins in *Arabidopsis thaliana*. *Molecular Plant, 2*(2), 298-307. doi:10.1093/mp/ssn082

Kobayashi, D., Tamoi, M., Iwaki, T., Shigeoka, S., & Wadano, A. (2003). Molecular characterization and redox regulation of phosphoribulokinase from the cyanobacterium *Synechococcus sp. PCC 7942*. *Plant and Cell Physiology, 44*(3), 269-276. doi:10.1093/pcp/pcg048

König, J., Muthuramalingam, M., & Dietz, K.-J. (2012). Mechanisms and dynamics in the thiol/disulfide redox regulatory network: transmitters, sensors and targets. *Current Opinion in Plant Biology, 15*(3), 261-268. doi:10.1016/j.pbi.2011.12.002

Koornneef, M., & Meinke, D. (2010). The development of *Arabidopsis* as a model plant. *The Plant Journal, 61*(6), 909-921. doi:10.1111/j.1365-313X.2009.04086.x

Kosuge, K., Tokutsu, R., Kim, E., Akimoto, S., Yokono, M., Ueno, Y., & Minagawa, J. (2018). LHCSR1-dependent fluorescence quenching is mediated by excitation energy transfer from LHCII to photosystem I in *Chlamydomonas reinhardtii*. *Proceedings of the National Academy of Sciences of the United States of America, 115*(14), 3722-3727. doi:10.1073/pnas.1720574115

Kruger, N. J., & von Schaewen, A. (2003). The oxidative pentose phosphate pathway: structure and organisation. *Current Opinion in Plant Biology, 6*(3), 236-246. doi:10.1016/S1369-5266(03)00039-6

Lapina, T., Zalutskaya, Z., Anikina, A., & Ermilova, E. (2013). Accumulation and export of glycerol in unicellular green alga *Chlamydomonas reinhardtii*. *Biological Communications, 0*(2), 36–40.

Launay, H., Barré, P., Puppo, C., Zhang, Y., Maneville, S., Gontero, B., & Receveur-Bréchot, V. (2018). Cryptic disorder out of disorder: Encounter between conditionally disordered CP12 and glyceraldehyde-3-phosphate dehydrogenase. *Journal of Molecular Biology, 430*(8), 1218-1234. doi:10.1016/j.jmb.2018.02.020

Laurent, T. C., Moore, E. C., & Reichard, P. (1964). Enzymatic synthesis of deoxyribonucleotides. IV. Isolation and characterization of thioredoxin, the hydorgen donor from *Escherichia coli Journal of Biological Chemistry, 239*, 3436-3444.

Lebreton, S., Andreescu, S., Graciet, E., & Gontero, B. (2006). Mapping of the interaction site of CP12 with glyceraldehyde-3-phosphate dehydrogenase from *Chlamydomonas reinhardtii*. *The FEBS Journal, 273*(14), 3358-3369. doi:10.1111/j.1742-4658.2006.05342.x

Lebreton, S., & Gontero, B. (1999). Memory and imprinting in multienzyme complexes. Evidence for information transfer from glyceraldehyde-3-phosphate dehydrogenase to phosphoribulokinase under reduced state in *Chlamydomonas reinhardtii*. *Journal of Biological Chemistry, 274*(30), 20879-20884. doi:10.1074/jbc.274.30.20879

Lebreton, S., Gontero, B., Avilan, L., & Ricard, J. (1997). Memory and imprinting effects in multienzyme complexes--II. Kinetics of the bienzyme complex from *Chlamydomonas reinhardtii* and hysteretic activation of chloroplast oxidized phosphoribulokinase. *European Journal of Biochemistry, 246*(1), 85-91. doi:10.1111/j.1432-1033.1997.t01-2-00085.x

Lebreton, S., Graciet, E., & Gontero, B. (2003). Modulation, via protein-protein interactions, of glyceraldehyde-3-phosphate dehydrogenase activity through redox phosphoribulokinase regulation. *Journal of Biological Chemistry, 278*(14), 12078-12084. doi:10.1074/jbc.M213096200

Lemaire, S. D., Collin, V., Keryer, E., Issakidis-Bourguet, E., Lavergne, D., & Miginiac-Maslow, M. (2003). *Chlamydomonas reinhardtii*: a model organism for the study of the thioredoxin family. *Plant Physiology and Biochemistry, 41*(6), 513-521. doi:10.1016/S0981-9428(03)00079-2

Lemaire, S. D., Michelet, L., Zaffagnini, M., Massot, V., & Issakidis-Bourguet, E. (2007). Thioredoxins in chloroplasts. *Current Genetics, 51*(6), 343-365. doi:10.1007/s00294-007-0128-z

Lennon, B. W., Williams, C. H., & Ludwig, M. L. (2000). Twists in catalysis: alternating conformations of *Escherichia coli* thioredoxin reductase. *Science, 289*(5482), 1190. doi:10.1126/science.289.5482.1190

Li, A. D., & Anderson, L. E. (1997). Expression and characterization of pea chloroplastic glyceraldehyde-3-phosphate dehydrogenase composed of only the B-subunit. *Plant Physiology, 115*(3), 1201-1209. doi:10.1104/pp.115.3.1201

Li, K., Qiu, H., Zhou, M., Lin, Y., Guo, Z., & Lu, S. (2018). Chloroplast Protein 12 expression alters growth and chilling tolerance in tropical forage *Stylosanthes guianensis (*Aublet) Sw. *Frontiers in Plant Science, 9*(1319). doi:10.3389/fpls.2018.01319

Li, L., Peng, H., Tan, S., Zhou, J., Fang, Z., Hu, Z., Gao, L., Li, T., Zhang, W., & Chen, L. (2020). Effects of early cold stress on gene expression in *Chlamydomonas reinhardtii*. *Genomics, 112*(2), 1128-1138. doi:10.1016/j.ygeno.2019.06.027

Li, X., Patena, W., Fauser, F., Jinkerson, R. E., Saroussi, S., Meyer, M. T., Ivanova, N., Robertson, J. M., Yue, R., Zhang, R., Vilarrasa-Blasi, J., Wittkopp, T. M., Ramundo, S., Blum, S. R., Goh, A., Laudon, M., Srikumar, T., Lefebvre, P. A., Grossman, A. R., & Jonikas, M. C. (2019). A genome-wide algal mutant library and functional screen identifies genes required for eukaryotic photosynthesis. *Nature Genetics, 51*(4), 627-635. doi:10.1038/s41588-019-0370-6

Li, X., Zhang, R., Patena, W., Gang, S. S., Blum, S. R., Ivanova, N., Yue, R., Robertson, J. M., Lefebvre, P. A., Fitz-Gibbon, S. T., Grossman, A. R., & Jonikas, M. C. (2016). An indexed, mapped mutant library enables reverse genetics studies of biological processes in *Chlamydomonas reinhardtii The Plant Cell, 28*(2), 367-387. doi:10.1105/tpc.15.00465

Livingston, D. P., & Henson, C. A. (1998). Apoplastic sugars, fructans, fructan exohydrolase, and invertase in winter oat: responses to second-phase cold hardening. *Plant Physiology, 116*(1), 403. doi:10.1104/pp.116.1.403

Long, S. P., Humphries, S., & Falkowski, P. G. (1994). Photoinhibition of photosynthesis in nature. *Annual Review of Plant Physiology and Plant Molecular Biology, 45*(1), 633-662. doi:10.1146/annurev.pp.45.060194.003221

López-Calcagno, P. E., Howard, T. P., & Raines, C. A. (2014). The CP12 protein family: A thioredoxin-mediated metabolic switch? *Frontiers in Plant Science, 5*, 9-9. doi:10.3389/fpls.2014.00009

López-Calcagno, P. E., Omar Abuzaid, A., Lawson, T., & Anne Raines, C. (2017). *Arabidopsis* CP12 mutants have reduced levels of phosphoribulokinase and impaired function of the Calvin-Benson cycle. *Journal of Experimental Botany, 68*(9), 2285-2298. doi:10.1093/jxb/erx084

Machida, T., Kato, E., Ishibashi, A., Ohashi, N., Honjoh, K.-i., & Miyamoto, T. (2007). Molecular characterization of low-temperature-inducible NTR-C in *Chlorella vulgaris*. *Nucleic Acids Symposium Series, 51*(1), 463-464. doi:10.1093/nass/nrm232

Maeda, H., & Dudareva, N. (2012). The shikimate pathway and aromatic amino acid biosynthesis in plants. *Annual Review of Plant Biology, 63*(1), 73-105. doi:10.1146/annurev-arplant-042811-105439

Maikova, A., Zalutskaya, Z., Lapina, T., & Ermilova, E. (2016). The HSP70 chaperone machines of *Chlamydomonas* are induced by cold stress. *Journal of Plant Physiology, 204*, 85-91. doi:10.1016/j.jplph.2016.07.012

Marri, L., Pesaresi, A., Valerio, C., Lamba, D., Pupillo, P., Trost, P., & Sparla, F. (2010). *In vitro* characterization of *Arabidopsis* CP12 isoforms reveals common biochemical and molecular properties. *Journal of Plant Physiology, 167*(12), 939-950. doi:10.1016/j.jplph.2010.02.008

Marri, L., Thieulin-Pardo, G., Lebrun, R., Puppo, R., Zaffagnini, M., Trost, P., Gontero, B., & Sparla, F. (2014). CP12-mediated protection of Calvin–Benson cycle enzymes from oxidative stress. *Biochimie, 97*, 228-237. doi:10.1016/j.biochi.2013.10.018

Marri, L., Trost, P., Pupillo, P., & Sparla, F. (2005). Reconstitution and properties of the recombinant glyceraldehyde-3-phosphate dehydrogenase/CP12/phosphoribulokinase supramolecular complex of *Arabidopsis*. *Plant Physiology, 139*(3), 1433-1443. doi:10.1104/pp.105.068445

Marri, L., Trost, P., Trivelli, X., Gonnelli, L., Pupillo, P., & Sparla, F. (2008). Spontaneous assembly of photosynthetic supramolecular complexes as mediated by the intrinsically unstructured protein CP12. *Journal of Biological Chemistry, 283*(4), 1831-1838. doi:10.1074/jbc.M705650200

Marri, L., Zaffagnini, M., Collin, V., Issakidis-Bourguet, E., Lemaire, S. D., Pupillo, P., Sparla, F., Miginiac-Maslow, M., & Trost, P. (2009). Prompt and easy activation by specific thioredoxins of calvin cycle enzymes of Arabidopsis thaliana associated in the GAPDH/CP12/PRK supramolecular complex. *Molecular Plant, 2*(2), 259-269. doi:10.1093/mp/ssn061

Martin, W., & Kowallik, K. V. (1999). Annotated English translation of Mereschkowsky's 1905 paper 'Über Natur und Ursprung der Chromatophoren im Pflanzenreiche'. *European Journal of Phycology, 34*(3), 287-295.

Matsumura, H., Kai, A., Maeda, T., Tamoi, M., Satoh, A., Tamura, H., Hirose, M., Ogawa, T., Kizu, N., Wadano, A., Inoue, T., & Shigeoka, S. (2011). Structure basis for the regulation of glyceraldehyde-3-phosphate dehydrogenase activity via the intrinsically disordered protein CP12. *Structure, 19*(12), 1846-1854. doi:10.1016/j.str.2011.08.016

Maul, J. E., Lilly, J. W., Cui, L., dePamphilis, C. W., Miller, W., Harris, E. H., & Stern, D. B. (2002). The *Chlamydomonas reinhardtii* plastid chromosome: Islands of genes in a sea of repeats. *The Plant Cell, 14*(11), 2659-2679. doi:10.1105/tpc.006155

McConnell, E. W., Werth, E. G., & Hicks, L. M. (2018). The phosphorylated redox proteome of *Chlamydomonas reinhardtii*: Revealing novel means for regulation of protein structure and function. *Redox biology, 17*, 35-46. doi:10.1016/j.redox.2018.04.003

McFadden, G. I., & van Dooren, G. G. (2004). Evolution: Red algal genome affirms a common origin of all plastids. *Current Biology, 14*(13), R514-516. doi:10.1016/j.cub.2004.06.041

Mehler, A. H. (1951). Studies on reactions of illuminated chloroplasts. I. Mechanism of the reduction of oxygen and other Hill reagents. *Archives of Biochemistry and Biophysics, 33*(1), 65-77. doi:10.1016/0003-9861(51)90082-3

Melis, A. (1998). Photostasis in plants. In T. P. Williams & A. B. Thistle (Eds.), *Photostasis and Related Phenomena*. Boston, MA.: Springer.

Merchant, S. S., Prochnik, S. E., Vallon, O., Harris, E. H., Karpowicz, S. J., Witman, G. B., Terry, A., Salamov, A., Fritz-Laylin, L. K., Maréchal-Drouard, L., Marshall, W. F., Qu, L.-H., Nelson, D. R., Sanderfoot, A. A., Spalding, M. H., Kapitonov, V. V., Ren, Q., Ferris, P., Lindquist, E., Shapiro, H., Lucas, S. M., Grimwood, J., Schmutz, J., Cardol, P., Cerutti, H., Chanfreau, G., Chen, C.-L., Cognat, V., Croft, M. T., Dent, R., Dutcher, S., Fernández, E., Fukuzawa, H., González-Ballester, D., González-Halphen, D., Hallmann, A., Hanikenne, M., Hippler, M., Inwood, W., Jabbari, K., Kalanon, M., Kuras, R., Lefebvre, P. A., Lemaire, S. D., Lobanov, A. V., Lohr, M., Manuell, A., Meier, I., Mets, L., Mittag, M., Mittelmeier, T., Moroney, J. V., Moseley, J., Napoli, C., Nedelcu, A. M., Niyogi, K., Novoselov, S. V., Paulsen, I. T., Pazour, G., Purton, S., Ral, J.-P., Riaño-Pachón, D. M., Riekhof, W., Rymarquis, L., Schroda, M., Stern, D., Umen, J., Willows, R., Wilson, N., Zimmer, S. L., Allmer, J., Balk, J., Bisova, K., Chen, C.-J., Elias, M., Gendler, K., Hauser, C., Lamb, M. R., Ledford, H., Long, J. C., Minagawa, J., Page, M. D., Pan, J., Pootakham, W., Roje, S., Rose, A., Stahlberg, E., Terauchi, A. M., Yang, P., Ball, S., Bowler, C., Dieckmann, C. L., Gladyshev, V. N., Green, P., Jorgensen, R., Mayfield,

S., Mueller-Roeber, B., Rajamani, S., Sayre, R. T., Brokstein, P., Dubchak, I., Goodstein, D., Hornick, L., Huang, Y. W., Jhaveri, J., Luo, Y., Martínez, D., Ngau, W. C. A., Otillar, B., Poliakov, A., Porter, A., Szajkowski, L., Werner, G., Zhou, K., Grigoriev, I. V., Rokhsar, D. S., & Grossman, A. R. (2007). The *Chlamydomonas* genome reveals the evolution of key animal and plant functions. *Science, 318*(5848), 245. doi:10.1126/science.1143609

Mereschkowsky, C. (1905). Über Natur und Ursprung der Chromatophoren im Pflanzenreiche. *Biologisches Centralblatt*

25(18), 593-604.

Meyer, Y., Reichheld, J. P., & Vignols, F. (2005). Thioredoxins in *Arabidopsis* and other plants. *Photosynthesis Research, 86*(3), 419-433. doi:10.1007/s11120-005-5220-y

Michalska, J., Zauber, H., Buchanan, B. B., Cejudo, F. J., & Geigenberger, P. (2009). NTRC links built-in thioredoxin to light and sucrose in regulating starch synthesis in chloroplasts and amyloplasts. *Proceedings of the National Academy of Sciences, 106*(24), 9908. doi:10.1073/pnas.0903559106

Michelet, L., Zaffagnini, M., Morisse, S., Sparla, F., Pérez-Pérez, M. E., Francia, F., Danon, A., Marchand, C., Fermani, S., Trost, P., & Lemaire, S. (2013). Redox regulation of the Calvin–Benson cycle: something old, something new. *Frontiers in Plant Science, 4*(470). doi:10.3389/fpls.2013.00470

Miguez, F., Fernandez-Marin, B., Becerril, J. M., & Garcia-Plazaola, J. I. (2017a). Diversity of winter photoinhibitory responses: A case study in co-occurring lichens, mosses, herbs and woody plants from subalpine environments. *Physiologia Plantarum, 160*(3), 282-296. doi:10.1111/ppl.12551

Miguez, F., Schiefelbein, U., Karsten, U., Garcia-Plazaola, J. I., & Gustavs, L. (2017b). Unraveling the photoprotective response of lichenized and free-living green algae (trebouxiophyceae, chlorophyta) to photochilling stress. *Frontiers in Plant Science, 8*, 1144. doi:10.3389/fpls.2017.01144

Mittag, M. (2009). The Function of Circadian RNA-Binding Proteins and Their cis-Acting Elements in Microalgae. *Chronobiology International, 20*(4), 529-541. doi:10.1081/CBI-120022411

Moon, J. C., Lee, S., Shin, S. Y., Chae, H. B., Jung, Y. J., Jung, H. S., Lee, K. O., Lee, J. R., & Lee, S. Y. (2015). Overexpression of *Arabidopsis* NADPH-dependent thioredoxin reductase C (AtNTRC) confers freezing and cold shock tolerance to plants. *Biochemical and Biophysical Research Communications, 463*(4), 1225-1229. doi:10.1016/j.bbrc.2015.06.089

Moore, E. C., Reichard, P., & Thelander, L. (1964). Enzymatic synthesis of deoxyribonucleotides. V. Purification and properties of thioredoxin reductase from *Escherichia coli Journal of Biological Chemistry, 239*, 3445-3452.

Morgan-Kiss, R. M., Priscu, J. C., Pocock, T., Gudynaite-Savitch, L., & Huner, N. P. (2006). Adaptation and acclimation of photosynthetic microorganisms to permanently cold environments. *Microbiology and Molecular Biology Reviews, 70*(1), 222-252. doi:10.1128/MMBR.70.1.222-252.2006

Müller, P., Li, X. P., & Niyogi, K. K. (2001). Non-photochemical quenching. A response to excess light energy. *Plant Physiology, 125*(4), 1558-1566. doi:10.1104/pp.125.4.1558

Mulo, P. (2011). Chloroplast-targeted ferredoxin-NADP+ oxidoreductase (FNR): Structure, function and location. *Biochimica et Biophysica Acta (BBA) - Bioenergetics, 1807*(8), 927-934. doi:10.1016/j.bbabio.2010.10.001

Murata, N., Takahashi, S., Nishiyama, Y., & Allakhverdiev, S. I. (2007). Photoinhibition of photosystem II under environmental stress. *Biochim Biophys Acta, 1767*(6), 414-421. doi:10.1016/j.bbabio.2006.11.019

Naranjo, B., Mignée, C., Krieger-Liszkay, A., Hornero-Méndez, D., Gallardo-Guerrero, L., Cejudo, F. J., & Lindahl, M. (2016). The chloroplast NADPH thioredoxin reductase C, NTRC, controls non-photochemical quenching of light energy and photosynthetic electron transport in *Arabidopsis*. *Plant, Cell & Environment, 39*(4), 804-822. doi:10.1111/pce.12652

Nechushtai, R., Conlan, A. R., Harir, Y., Song, L., Yogev, O., Eisenberg-Domovich, Y., Livnah, O., Michaeli, D., Rosen, R., Ma, V., Luo, Y., Zuris, J. A., Paddock, M. L., Cabantchik, Z. I., Jennings, P. A., & Mittler, R. (2012). Characterization of *Arabidopsis* NEET reveals an ancient role for NEET proteins in iron metabolism. *The Plant Cell, 24*(5), 2139-2154. doi:10.1105/tpc.112.097634

Née, G., Zaffagnini, M., Trost, P., & Issakidis-Bourguet, E. (2009). Redox regulation of chloroplastic glucose-6-phosphate dehydrogenase: A new role for f-type thioredoxin. *FEBS Letters, 583*(17), 2827-2832. doi:10.1016/j.febslet.2009.07.035

Nelson, N., & Junge, W. (2015). Structure and energy transfer in photosystems of oxygenic photosynthesis. *Annual Review of Biochemistry, 84*(1), 659-683. doi:10.1146/annurev-biochem-092914-041942

Neuhaus, H. E., & Emes, M. J. (2000). Non-photosynthetic metabolism in plastids. *Annual Review of Plant Physiology and Plant Molecular Biology, 51*(1), 111-140. doi:10.1146/annurev.arplant.51.1.111

Neupert, J., Karcher, D., & Bock, R. (2009). Generation of *Chlamydomonas* strains that efficiently express nuclear transgenes. *The Plant Journal, 57*(6), 1140-1150. doi:10.1111/j.1365-313X.2008.03746.x

Neusius, D. (2015). *The role of NTRC for chloroplast gene expression.* (Master). Ludwig Maximilians University Munich, Germany.

Nickelsen, J., & Kück, U. (2000). The unicellular green alga *Chlamydomonas reinhardtii* as an experimental system to study chloroplast RNA metabolism. *Naturwissenschaften, 87*(3), 97-107. doi:10.1007/s001140050686

Nikkanen, L., Toivola, J., & Rintamäki, E. (2016). Crosstalk between chloroplast thioredoxin systems in regulation of photosynthesis. *Plant, Cell & Environment, 39*(8), 1691-1705. doi:10.1111/pce.12718

O'Kane, D., Gill, V., Boyd, P., & Burdon, R. (1996). Chilling, oxidative stress and antioxidant responses in *Arabidopsis thaliana* callus. *Planta, 198*(3), 371-377. doi:10.1007/BF00620053

Oesterhelt, C., Klocke, S., Holtgrefe, S., Linke, V., Weber, A. P. M., & Scheibe, R. (2007). Redox regulation of chloroplast enzymes in *Galdieria sulphuraria* in view of eukaryotic evolution. *Plant and Cell Physiology, 48*(9), 1359-1373. doi:10.1093/pcp/pcm108

Ohad, I., Siekevitz, P., & Palade, G. E. (1967). Biogenesis of chloroplast membranes : I. Plastid dedifferentiation in a dark-grown algal mutant (*Chlamydomonas reinhardi*). *Journal of Cell Biology, 35*(3), 521-552. doi:10.1083/jcb.35.3.521

Ojeda, V., Pérez-Ruiz, J. M., & Cejudo, F. J. (2018). The NADPH-dependent thioredoxin reductase C-2-cys peroxiredoxin redox system modulates the activity of thioredoxin-x in *Arabidopsis* chloroplasts. *Plant and Cell Physiology, 59*(10), 2155-2164. doi:10.1093/pcp/pcy134

Oxborough, K., & Baker, N. R. (1997). Resolving chlorophyll a fluorescence images of photosynthetic efficiency into photochemical and non-photochemical components – calculation of qP and F_v/F_m; without measuring F_o. *Photosynthesis Research, 54*(2), 135-142. doi:10.1023/A:1005936823310

Pascual, M. B., Mata-Cabana, A., Florencio, F. J., Lindahl, M., & Cejudo, F. J. (2011). A comparative analysis of the NADPH thioredoxin reductase C-2-Cys peroxiredoxin system from plants and cyanobacteria. *Plant Physiology, 155*(4), 1806-1816. doi:10.1104/pp.110.171082

Pérez-Pérez, M. E., Mauriès, A., Maes, A., Tourasse, N. J., Hamon, M., Lemaire, S. D., & Marchand, C. H. (2017). The deep thioredoxome in *Chlamydomonas reinhardtii*: New insights into redox regulation. *Molecular Plant, 10*(8), 1107-1125. doi:10.1016/j.molp.2017.07.009

Perez-Ruiz, J. M., Gonzalez, M., Spinola, M. C., Sandalio, L. M., & Cejudo, F. J. (2009). The quaternary structure of NADPH thioredoxin reductase C is redox-sensitive. *Molecular Plant, 2*(3), 457-467. doi:10.1093/mp/ssp011

Pérez-Ruiz, J. M., Naranjo, B., Ojeda, V., Guinea, M., & Cejudo, F. J. (2017). NTRC-dependent redox balance of 2-Cys peroxiredoxins is needed for optimal function of the photosynthetic apparatus. *Proceedings of the National Academy of Sciences, 114*(45), 12069. doi:10.1073/pnas.1706003114

Pérez-Ruiz, J. M., Spínola, M. C., Kirchsteiger, K., Moreno, J., Sahrawy, M., & Cejudo, F. J. (2006). Rice NTRC is a high-efficiency redox system for chloroplast protection against oxidative damage. *The Plant Cell, 18*(9), 2356. doi:10.1105/tpc.106.041541

Petersen, J. r., Teich, R., Becker, B., Cerff, R. d., & Brinkmann, H. (2006). The GapA/B gene duplication marks the origin of streptophyta (charophytes and land plants). *Molecular Biology and Evolution, 23*(6), 1109-1118. doi:10.1093/molbev/msj123

Pohlmeyer, K., Paap, B. K., Soll, J., & Wedel, N. (1996). CP12: A small nuclear-encoded chloroplast protein provides novel insights into higher-plant GAPDH evolution. *Plant Molecular Biology, 32*(5), 969-978. doi:10.1007/BF00020493

Porter, M. A., Stringer, C. D., & Hartman, F. C. (1988). Characterization of the regulatory thioredoxin site of phosphoribulokinase. *Journal of Biological Chemistry, 263*(1), 123-129. doi:10.1016/S0021-9258(19)57366-5

Puerto-Galán, L., Pérez-Ruiz, J. M., Guinea, M., & Cejudo, F. J. (2015). The contribution of NADPH thioredoxin reductase C (NTRC) and sulfiredoxin to 2-Cys peroxiredoxin overoxidation in Arabidopsis thaliana chloroplasts. *Journal of Experimental Botany, 66*(10), 2957-2966. doi:10.1093/jxb/eru512

Pupillo, P., & Piccari, G. G. (1973). The effect of NADP on the subunit structure and activity of spinach chloroplast glyceraldehyde-3-phosphate dehydrogenase. *Archives of Biochemistry and Biophysics, 154*(1), 324-331. doi:10.1016/0003-9861(73)90064-7

Puyaubert, J., & Baudouin, E. (2014). New clues for a cold case: nitric oxide response to low temperature. *Plant, Cell & Environment, 37*(12), 2623-2630. doi:10.1111/pce.12329

Ran, F. A., Cong, L., Yan, W. X., Scott, D. A., Gootenberg, J. S., Kriz, A. J., Zetsche, B., Shalem, O., Wu, X., Makarova, K. S., Koonin, E. V., Sharp, P. A., & Zhang, F. (2015). *In vivo* genome editing using *Staphylococcus aureus* Cas9. *Nature, 520*(7546), 186-191. doi:10.1038/nature14299

Rappsilber, J., Ishihama, Y., & Mann, M. (2003). Stop and go extraction tips for matrix-assisted laser desorption/ionization, nanoelectrospray, and LC/MS sample pretreatment in proteomics. *Analytical Chemistry, 75*(3), 663-670. doi:10.1021/ac026117i

Reichheld, J.-P., Meyer, E., Khafif, M., Bonnard, G., & Meyer, Y. (2005). AtNTRB is the major mitochondrial thioredoxin reductase in *Arabidopsis thaliana*. *FEBS Letters, 579*(2), 337-342. doi:10.1016/j.febslet.2004.11.094

Renaut, J., Hausman, J.-F., & Wisniewski, M. E. (2006). Proteomics and low-temperature studies: bridging the gap between gene expression and metabolism. *Physiologia Plantarum, 126*(1), 97-109. doi:10.1111/j.1399-3054.2006.00617.x

Richter, A. S., Peter, E., Rothbart, M., Schlicke, H., Toivola, J., Rintamäki, E., & Grimm, B. (2013). Posttranslational influence of NADPH-dependent thioredoxin reductase C on enzymes in tetrapyrrole synthesis *Plant Physiology, 162*(1), 63-73. doi:10.1104/pp.113.217141

Rocha, A. G., & Vothknecht, U. C. (2013). Identification of CP12 as a novel calcium-binding protein in chloroplasts. *Plants, 2*(3). doi:10.3390/plants2030530

Ruelland, E., & Miginiac-Maslow, M. (1999). Regulation of chloroplast enzyme activities by thioredoxins: activation or relief from inhibition? *Trends Plant Sci, 4*(4), 136-141. doi:10.1016/s1360-1385(99)01391-6

Salomé, P. A., & Merchant, S. S. (2019). A series of fortunate events: introducing *Chlamydomonas* as a reference organism. *The Plant Cell, 31*(8), 1682. doi:10.1105/tpc.18.00952

Sanghera, G. S., Wani, S. H., Hussain, W., & Singh, N. B. (2011). Engineering cold stress tolerance in crop plants. *Current Genomics, 12*(1), 30-43. doi:10.2174/138920211794520178

Savitch, L. V., Massacci, A., Gray, G. R., & Huner, N. P. A. (2000). Acclimation to low temperature or high light mitigates sensitivity to photoinhibition: roles of the Calvin cycle and the Mehler reaction. *Functional Plant Biology, 27*(3), 253-264. doi:10.1071/PP99112

Scagliarini, S., Trost, P., & Pupillo, P. (1998). The non-regulatory isoform of NAD(P)-glyceraldehyde-3-phosphate dehydrogenase from spinach chloroplasts. *Journal of Experimental Botany, 49*(325), 1307-1315. doi:10.1093/jxb/49.325.1307

Scheibe, R., Baalmann, E., Backhausen, J. E., Rak, C., & Vetter, S. (1996). C-terminal truncation of spinach chloroplast NAD(P)-dependent glyceraldehyde-3-phosphate dehydrogenase prevents inactivation and reaggregation. *Biochimica et Biophysica Acta (BBA) - Protein Structure and Molecular Enzymology, 1296*(2), 228-234. doi:10.1016/0167-4838(96)00074-X

Scheibe, R., Wedel, N., Vetter, S., Emmerlich, V., & Sauermann, S.-M. (2002). Co-existence of two regulatory NADP-glyceraldehyde-3-P dehydrogenase complexes in higher plant chloroplasts. *European Journal of Biochemistry, 269*(22), 5617-5624. doi:10.1046/j.1432-1033.2002.03269.x

Schulz, E., Tohge, T., Zuther, E., Fernie, A. R., & Hincha, D. K. (2016). Flavonoids are determinants of freezing tolerance and cold acclimation in *Arabidopsis thaliana*. *Scientific Reports, 6*(1), 34027. doi:10.1038/srep34027

Schürmann, P., & Buchanan, B. B. (2008). The ferredoxin/thioredoxin system of oxygenic photosynthesis. *Antioxidants & Redox Signaling, 10*(7), 1235-1274. doi:10.1089/ars.2007.1931

Schürmann, P., & Jacquot, J. P. (2000). Plant thioredoxin systems revisted. *Annual Review of Plant Physiology and Plant Molecular Biology, 51*(1), 371-400. doi:10.1146/annurev.arplant.51.1.371

Serrato, A. J., Perez-Ruiz, J. M., Spinola, M. C., & Cejudo, F. J. (2004). A novel NADPH thioredoxin reductase, localized in the chloroplast, which deficiency causes hypersensitivity to abiotic stress in *Arabidopsis thaliana*. *Journal of Biological Chemistry, 279*(42), 43821-43827. doi:10.1074/jbc.M404696200

Shen, J.-R. (2015). The structure of photosystem II and the mechanism of water oxidation in photosynthesis. *Annual Review of Plant Biology, 66*(1), 23-48. doi:10.1146/annurev-arplant-050312-120129

Shimogawara, K., Fujiwara, S., Grossman, A., & Usuda, H. (1998). High-efficiency transformation of *Chlamydomonas reinhardtii* by electroporation. *Genetics, 148*(4), 1821-1828.

Singh, P., Kaloudas, D., & Raines, C. A. (2008). Expression analysis of the *Arabidopsis* CP12 gene family suggests novel roles for these proteins in roots and floral tissues. *Journal of Experimental Botany, 59*(14), 3975-3985. doi:10.1093/jxb/ern236

Sonoike, K. (2011). Photoinhibition of photosystem I. *Physiologia Plantarum, 142*(1), 56-64. doi:10.1111/j.1399-3054.2010.01437.x

Sparla, F., Pupillo, P., & Trost, P. (2002). The C-terminal extension of glyceraldehyde-3-phosphate dehydrogenase subunit B acts as an autoinhibitory domain regulated by thioredoxins and nicotinamide adenine dinucleotide. *Journal of Biological Chemistry, 277*(47), 44946-44952. doi:10.1074/jbc.M206873200

Spínola, M. C., Pérez-Ruiz, J. M., Pulido, P., Kirchsteiger, K., Guinea, M., González, M., & Cejudo, F. J. (2008). NTRC new ways of using NADPH in the chloroplast. *Physiologia Plantarum, 133*(3), 516-524. doi:10.1111/j.1399-3054.2008.01088.x

Steponkus, P. L. (1984). Role of the plasma membrane in freezing injury and cold acclimation. *Annual Review of Plant Physiology, 35*(1), 543-584. doi:10.1146/annurev.pp.35.060184.002551

Stitt, M., & Hurry, V. (2002). A plant for all seasons: alterations in photosynthetic carbon metabolism during cold acclimation in Arabidopsis. *Current Opinion in Plant Biology, 5*(3), 199-206. doi:10.1016/S1369-5266(02)00258-3

Strand, Å., Hurry, V., Henkes, S., Huner, N., Gustafsson, P., Gardeström, P., & Stitt, M. (1999). Acclimation of *Arabidopsis* leaves developing at low temperatures. Increasing cytoplasmic volume accompanies increased activities of enzymes in the Calvin cycle and in the sucrose-biosynthesis pathway. *Plant Physiology, 119*(4), 1387. doi:10.1104/pp.119.4.1387

Suzuki, N., & Mittler, R. (2006). Reactive oxygen species and temperature stresses: A delicate balance between signaling and destruction. *Physiologia Plantarum, 126*(1), 45-51. doi:10.1111/j.0031-9317.2005.00582.x

Szyszka-Mroz, B., Cvetkovska, M., Ivanov, A. G., Smith, D. R., Possmayer, M., Maxwell, D. P., & Hüner, N. P. A. (2019). Cold-adapted protein kinases and thylakoid remodeling impact energy distribution in an antarctic psychrophile. *Plant Physiology, 180*(3), 1291-1309. doi:10.1104/pp.19.00411

Taiz, L., & Zeiger, E. (1998). In *Plant Physiology* (Vol. 2nd Edition). Sunderland, Massachusetts: Sinauer Associates Publishers.

Takeda, T., Yokota, A., & Shigeoka, S. (1995). Resistance of photosynthesis to hydrogen peroxide in algae. *Plant and Cell Physiology, 36*(6), 1089-1095. doi:10.1093/oxfordjournals.pcp.a078852

Tamoi, M., Ishikawa, T., Takeda, T., & Shigeoka, S. (1996a). Enzymic and molecular characterization of NADP-dependent glyceraldehyde-3-phosphate dehydrogenase from *Synechococcus PCC 7942*: Resistance of the enzyme to hydrogen peroxide. *The Biochemical journal, 316 (Pt 2)*(Pt 2), 685-690. doi:10.1042/bj3160685

Tamoi, M., Ishikawa, T., Takeda, T., & Shigeoka, S. (1996b). Molecular characterization and resistance to hydrogen peroxide of two fructose-1,6-bisphosphatases from *SynechococcusPCC 7942*. *Archives of Biochemistry and Biophysics, 334*(1), 27-36. doi:10.1006/abbi.1996.0425

Tamoi, M., Kanaboshi, H., Miyasaka, H., & Shigeoka, S. (2001). Molecular mechanisms of the resistance to hydrogen peroxide of enzymes involved in the Calvin cycle from halotolerant *Chlamydomonas sp. W80*. *Archives of Biochemistry and Biophysics, 390*(2), 176-185. doi:10.1006/abbi.2001.2375

Tamoi, M., Miyazaki, T., Fukamizo, T., & Shigeoka, S. (2005). The Calvin cycle in cyanobacteria is regulated by CP12 via the NAD(H)/NADP(H) ratio under light/dark conditions. *The Plant Journal, 42*(4), 504-513. doi:10.1111/j.1365-313X.2005.02391.x

Tamoi, M., Murakami, A., Takeda, T., & Shigeoka, S. (1998). Acquisition of a new type of fructose-1,6-bisphosphatase with resistance to hydrogen peroxide in cyanobacteria: molecular characterization of the enzyme from *Synechocystis PCC 6803*. The nucleotide sequence data for fructose-1,6-

bisphosphatase reported in this paper will appear in the GSDB, DDBJ, EMBL, and NCBI nucleotide sequence databases with the accession numbers D89973. *Biochimica et Biophysica Acta (BBA) - Protein Structure and Molecular Enzymology, 1383*(2), 232-244. doi:10.1016/S0167-4838(97)00208-2

Tamoi, M., & Shigeoka, S. (2015). Diversity of regulatory mechanisms of photosynthetic carbon metabolism in plants and algae. *Bioscience, Biotechnology, and Biochemistry, 79*(6), 870-876. doi:10.1080/09168451.2015.1020754

Tardif, M., Atteia, A., Specht, M., Cogne, G., Rolland, N., Brugière, S., Hippler, M., Ferro, M., Bruley, C., Peltier, G., Vallon, O., & Cournac, L. (2012). PredAlgo: A New Subcellular Localization Prediction Tool Dedicated to Green Algae. *Molecular Biology and Evolution, 29*(12), 3625-3639. doi:10.1093/molbev/mss178

Terashima, I., Noguchi, K., Itoh-Nemoto, T., Park, Y.-M., Kuhn, A., & Tanaka, K. (1998). The cause of PSI photoinhibition at low temperatures in leaves of Cucumis sativus, a chilling-sensitive plant. *Physiologia Plantarum, 103*(3), 295-303. doi:10.1034/j.1399-3054.1998.1030301.x

Thalmann, M., & Santelia, D. (2017). Starch as a determinant of plant fitness under abiotic stress. *New Phytologist, 214*(3), 943-951. doi:10.1111/nph.14491

The Arabidopsis Genome Initiative. (2000). Analysis of the genome sequence of the flowering plant *Arabidopsis thaliana*. *Nature, 408*(6814), 796-815. doi:10.1038/35048692

Thomashow, M. F. (1999). Plant cold acclimation: freezing tolerance genes and regulatory mechanisms. *Annual Review of Plant Physiology and Plant Molecular Biology, 50*, 571-599. doi:10.1146/annurev.arplant.50.1.571

Thompson, L. R., Zeng, Q., Kelly, L., Huang, K. H., Singer, A. U., Stubbe, J., & Chisholm, S. W. (2011). Phage auxiliary metabolic genes and the redirection of cyanobacterial host carbon metabolism. *Proceedings of the National Academy of Sciences, 108*(39), E757. doi:10.1073/pnas.1102164108

Thormählen, I., Meitzel, T., Groysman, J., Öchsner, A. B., von Roepenack-Lahaye, E., Naranjo, B., Cejudo, F. J., & Geigenberger, P. (2015). Thioredoxin f1 and NADPH-dependent thioredoxin reductase C have overlapping functions in regulating photosynthetic metabolism and plant growth in response to varying light conditions *Plant Physiology, 169*(3), 1766-1786. doi:10.1104/pp.15.01122

Thormählen, I. N. A., Ruber, J., Von Roepenack-Lahaye, E., Ehrlich, S.-M., Massot, V., HÜMmer, C., Tezycka, J., Issakidis-Bourguet, E., & Geigenberger, P. (2013). Inactivation of thioredoxin f1 leads to decreased light activation of ADP-glucose pyrophosphorylase and altered diurnal starch turnover in leaves of *Arabidopsis* plants. *Plant, Cell & Environment, 36*(1), 16-29. doi:10.1111/j.1365-3040.2012.02549.x

Timperio, A. M., Egidi, M. G., & Zolla, L. (2008). Proteomics applied on plant abiotic stresses: role of heat shock proteins (HSP). *Journal of Proteomics, 71*(4), 391-411. doi:10.1016/j.jprot.2008.07.005

Toivola, J., Nikkanen, L., Dahlström, K., Salminen, T., Lepistö, A., Vignols, F., & Rintamäki, E. (2013). Overexpression of chloroplast NADPH-dependent thioredoxin reductase in *Arabidopsis* enhances leaf growth and elucidates in vivo function of reductase and thioredoxin domains. *Frontiers in Plant Science, 4*(389). doi:10.3389/fpls.2013.00389

Tompa, P., & Fuxreiter, M. (2008). Fuzzy complexes: polymorphism and structural disorder in protein-protein interactions. *Trends in Biochemical Sciences, 33*(1), 2-8. doi:10.1016/j.tibs.2007.10.003

Trost, P., Fermani, S., Marri, L., Zaffagnini, M., Falini, G., Scagliarini, S., Pupillo, P., & Sparla, F. (2006). Thioredoxin-dependent regulation of photosynthetic glyceraldehyde-3-phosphate

dehydrogenase: autonomous vs. CP12-dependent mechanisms. *Photosynthesis Research, 89*(2), 263-275. doi:10.1007/s11120-006-9099-z

Tyanova, S., Temu, T., Sinitcyn, P., Carlson, A., Hein, M. Y., Geiger, T., Mann, M., & Cox, J. (2016). The Perseus computational platform for comprehensive analysis of proteomics data. *Nature Methods, 13*(9), 731-740. doi:10.1038/nmeth.3901

Upchurch, R. G. (2008). Fatty acid unsaturation, mobilization, and regulation in the response of plants to stress. *Biotechnology Letters, 30*(6), 967-977. doi:10.1007/s10529-008-9639-z

Uversky, V. N. (2002). Natively unfolded proteins: a point where biology waits for physics. *Protein Science, 11*(4), 739-756. doi:10.1110/ps.4210102

Valledor, L., Furuhashi, T., Hanak, A. M., & Weckwerth, W. (2013). Systemic cold stress adaptation of *Chlamydomonas reinhardtii*. *Molecular & Cellular Proteomics, 12*(8), 2032-2047. doi:10.1074/mcp.M112.026765

Vasilikiotis, C., & Melis, A. (1994). Photosystem II reaction center damage and repair cycle: chloroplast acclimation strategy to irradiance stress. *Proceedings of the National Academy of Sciences of the United States of America, 91*(15), 7222-7226. doi:10.1073/pnas.91.15.7222

Vaultier, M. N., Cantrel, C., Vergnolle, C., Justin, A. M., Demandre, C., Benhassaine-Kesri, G., Cicek, D., Zachowski, A., & Ruelland, E. (2006). Desaturase mutants reveal that membrane rigidification acts as a cold perception mechanism upstream of the diacylglycerol kinase pathway in *Arabidopsis* cells. *FEBS Letters, 580*(17), 4218-4223. doi:10.1016/j.febslet.2006.06.083

Vizcaino, J. A., Csordas, A., del-Toro, N., Dianes, J. A., Griss, J., Lavidas, I., Mayer, G., Perez-Riverol, Y., Reisinger, F., Ternent, T., Xu, Q. W., Wang, R., & Hermjakob, H. (2016). 2016 update of the PRIDE database and its related tools. *Nucleic Acids Research, 44*(D1), D447-456. doi:10.1093/nar/gkv1145

Wang, H., Gau, B., Slade, W. O., Juergens, M., Li, P., & Hicks, L. M. (2014). The global phosphoproteome of *Chlamydomonas reinhardtii* reveals complex organellar phosphorylation in the flagella and thylakoid membrane. *Molecular & Cellular Proteomics, 13*(9), 2337-2353. doi:10.1074/mcp.M114.038281

Wang, X., Li, W., Li, M., & Welti, R. (2006). Profiling lipid changes in plant response to low temperatures. *Physiologia Plantarum, 126*(1), 90-96. doi:10.1111/j.1399-3054.2006.00622.x

Wedel, N., & Soll, J. (1998). Evolutionary conserved light regulation of Calvin cycle activity by NADPH-mediated reversible phosphoribulokinase/CP12/ glyceraldehyde-3-phosphate dehydrogenase complex dissociation. *Proceedings of the National Academy of Sciences, 95*(16), 9699. doi:10.1073/pnas.95.16.9699

Wedel, N., Soll, J., & Paap, B. K. (1997). CP12 provides a new mode of light regulation of Calvin cycle activity in higher plants. *Proceedings of the National Academy of Sciences, 94*(19), 10479. doi:10.1073/pnas.94.19.10479

Wenderoth, I., Scheibe, R., & von Schaewen, A. (1997). Identification of the cysteine residues involved in redox modification of plant plastidic glucose-6-phosphate dehydrogenase. *Journal of Biological Chemistry, 272*(43), 26985-26990. doi:10.1074/jbc.272.43.26985

Wulff, R. P., Lundqvist, J., Rutsdottir, G., Hansson, A., Stenbaek, A., Elmlund, D., Elmlund, H., Jensen, P. E., & Hansson, M. (2011). The activity of barley NADPH-dependent thioredoxin reductase C is independent of the oligomeric state of the protein: tetrameric structure determined by cryo-electron microscopy. *Biochemistry, 50*(18), 3713-3723. doi:10.1021/bi200058a

Wunder, T., Oh, Z. G., & Mueller-Cajar, O. (2019). CO_2-fixing liquid droplets: Towards a dissection of the microalgal pyrenoid. *Traffic, 20*(6), 380-389. doi:10.1111/tra.12650

Yamano, T., Iguchi, H., & Fukuzawa, H. (2013). Rapid transformation of *Chlamydomonas reinhardtii* without cell-wall removal. *Journal of Bioscience and Bioengineering, 115*(6), 691-694. doi:10.1016/j.jbiosc.2012.12.020

Zalutskaya, Z. M., Skryabina, U. S., & Ermilova, E. V. (2019). Generation of hydrogen peroxide and transcriptional regulation of antioxidant enzyme expression in *Chlamydomonas reinhardtii* under hypothermia. *Russian Journal of Plant Physiology, 66*(2), 223-230. doi:10.1134/S1021443719020171

Zandalinas, S. I., Song, L., Sengupta, S., McInturf, S. A., Grant, D. G., Marjault, H.-B., Castro-Guerrero, N. A., Burks, D., Azad, R. K., Mendoza-Cozatl, D. G., Nechushtai, R., & Mittler, R. (2020). Expression of a dominant-negative AtNEET-H89C protein disrupts iron–sulfur metabolism and iron homeostasis in *Arabidopsis*. *The Plant Journal, 101*(5), 1152-1169. doi:10.1111/tpj.14581

Zapponi, M. C., Iadarola, P., Stoppini, M., & Ferri, G. (1993). Limited proteolysis of chloroplast glyceraldehyde-3-phosphate dehydrogenase (NADP) from *Spinacia oleracea*. *374*(1-6), 395-402. doi:doi:10.1515/bchm3.1993.374.1-6.395

Zhang, R., Patena, W., Armbruster, U., Gang, S. S., Blum, S. R., & Jonikas, M. C. (2014). High-throughput genotyping of green algal mutants reveals random distribution of mutagenic insertion sites and endonucleolytic cleavage of transforming DNA. *The Plant Cell, 26*(4), 1398. doi:10.1105/tpc.114.124099

Zhang, Y., Launay, H., Schramm, A., Lebrun, R., & Gontero, B. (2018). Exploring intrinsically disordered proteins in *Chlamydomonas reinhardtii*. *Scientific Reports, 8*(1), 6805. doi:10.1038/s41598-018-24772-7

Zheng, Y., Xue, C., Chen, H., He, C., & Wang, Q. (2020). Low-temperature adaptation of the snow alga *Chlamydomonas nivalis* is associated with the photosynthetic system regulatory process. *Frontiers in Microbiology, 11*, 1233. doi:10.3389/fmicb.2020.01233

Zhu, X., Liu, S., Sun, L., Song, F., Liu, F., & Li, X. (2018). Cold tolerance of photosynthetic electron transport system is enhanced in wheat plants grown under elevated CO_2. *Frontiers in Plant Science, 9*(933). doi:10.3389/fpls.2018.00933

Zrenner, R., Stitt, M., Sonnewald, U., & Boldt, R. (2006). Pyrimidine and purine biosyntheis and degradation in plants. *Annual Review of Plant Biology, 57*(1), 805-836. doi:10.1146/annurev.arplant.57.032905.105421

VI. APPENDIX

VI.1. Supplemental Figures

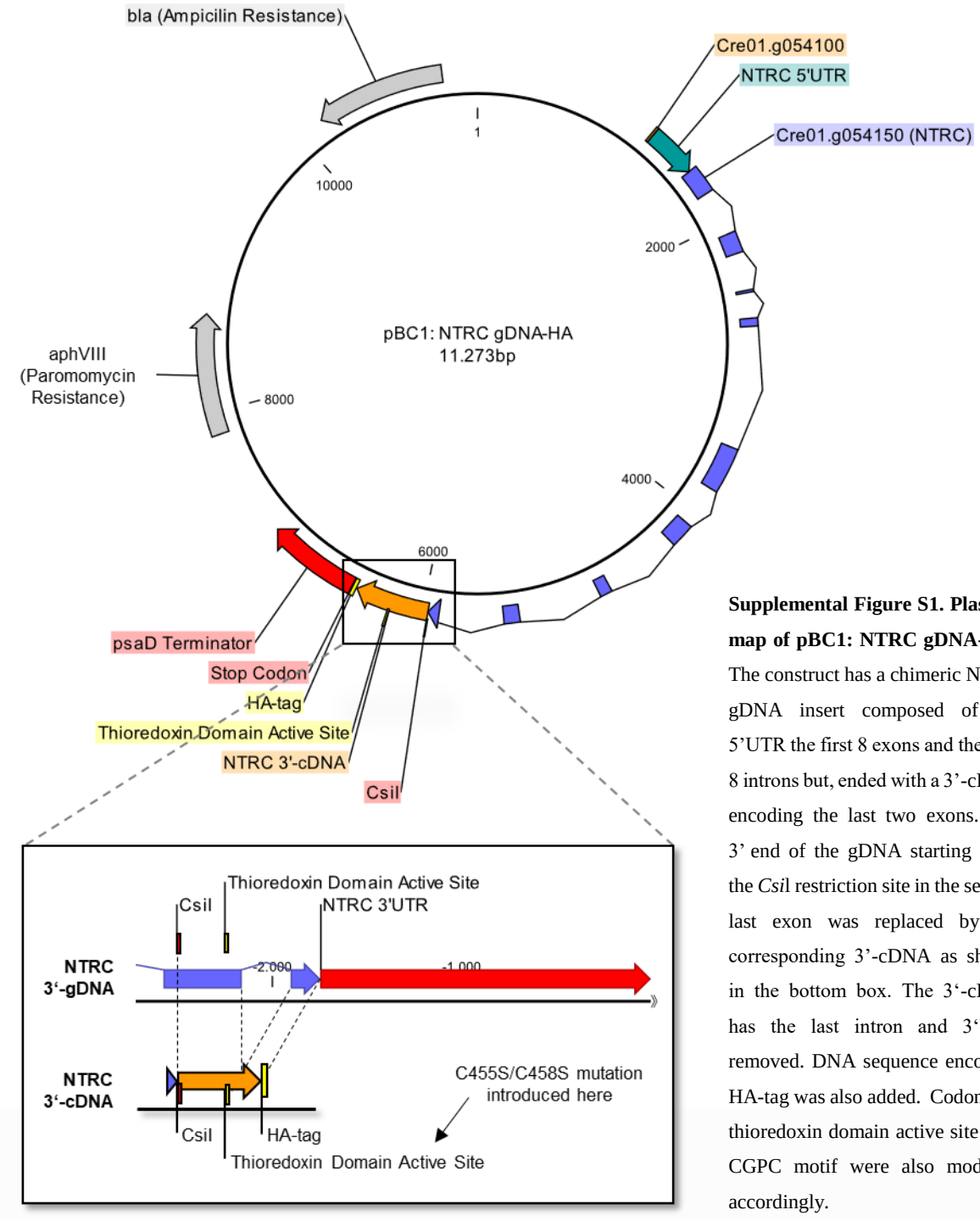

Supplemental Figure S1. Plasmid map of pBC1: NTRC gDNA-HA. The construct has a chimeric NTRC gDNA insert composed of the 5'UTR the first 8 exons and the first 8 introns but, ended with a 3'-cDNA encoding the last two exons. The 3' end of the gDNA starting from the *CsiI* restriction site in the second last exon was replaced by the corresponding 3'-cDNA as shown in the bottom box. The 3'-cDNA has the last intron and 3'UTR removed. DNA sequence encoding HA-tag was also added. Codons for thioredoxin domain active site –the CGPC motif were also modified accordingly.

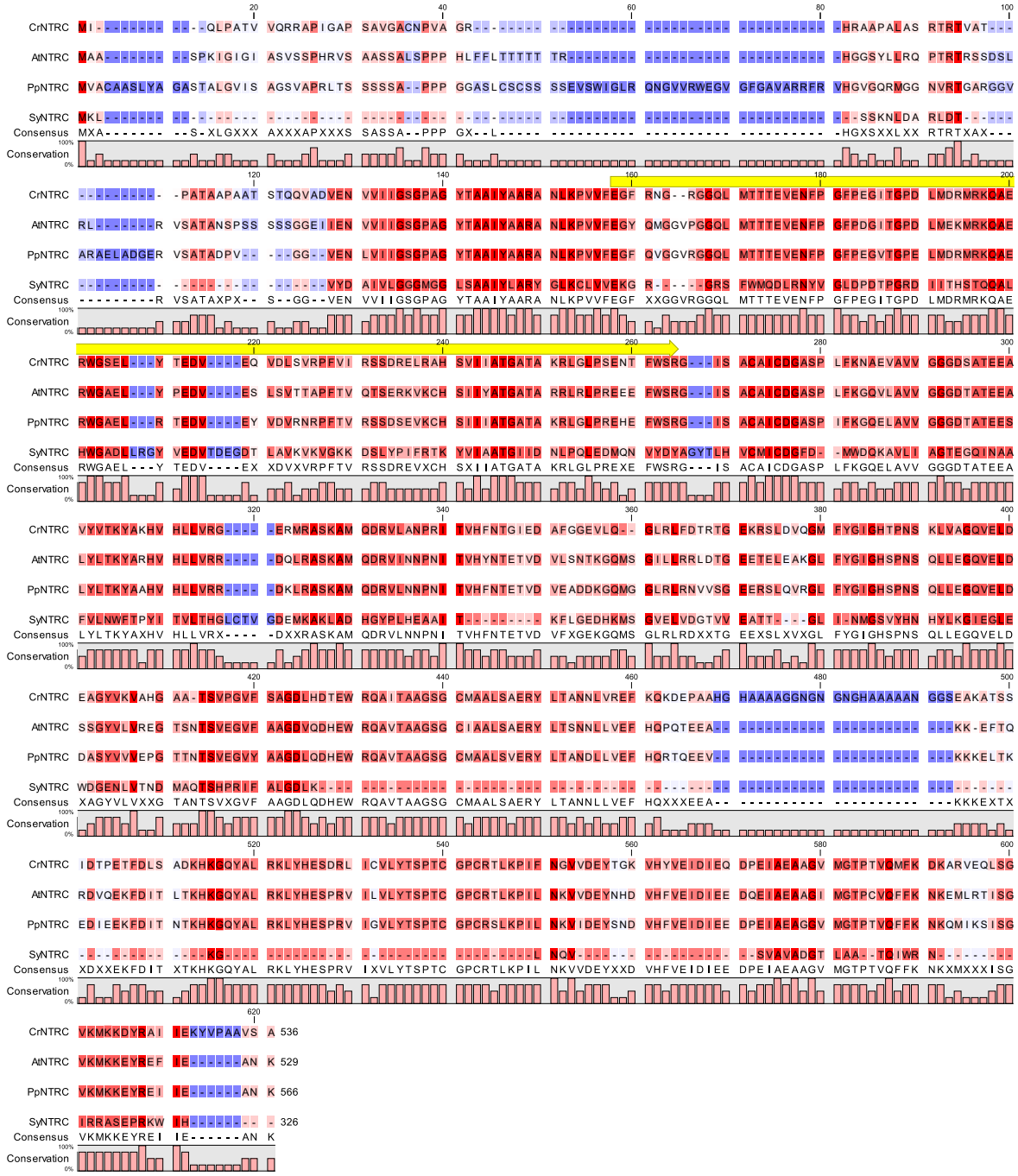

Supplemental Figure S2: The consensus amino acid (aa) sequence of NTRC among *C. reinhardtii*, *A. thaliana*, *Physcomitrella patens* and *Synechocystis sp.* PCC 6803. Sequences are aligned by using CLC Main Workbench software (Qiagen). Highly conserved aa's are highlighted in red while the reverse is in blue. The eukaryotic NTRC aa sequences of the microalga, plant and moss were retrieved from the Phytozome v12 (https://phytozome.jgi.doe.gov/pz/portal.html) with gene loci identifier: Cre01.g054150, AT2G41680 and Pp3c20_5530 respectively, whereas that of the cyanobacterium was retrieved from the CyanoBase (http://genome.microbedb.jp/cyanobase/) with accession code: Slr0600. The fragment (yellow region) corresponding to the CrNTRC aa position number 93 to 190 (counted from the N-terminus) with a total length of 98 aa, was synthesized and used as antigen for antiserum production.

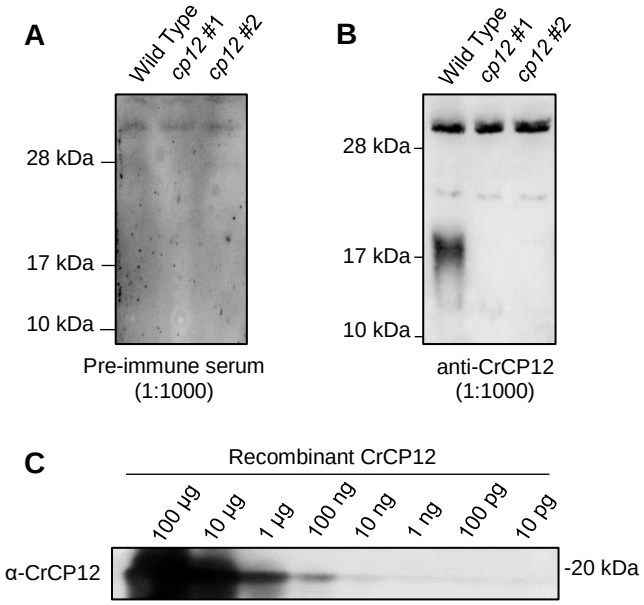

Supplemental Figure S3. Specificity and sensitivity tests for antiserum against CrCP12. **A – B,** Specificity test for CrCP12 antiserum. 50 µg of each soluble protein extract of *cp12* knockout mutants and the wild type strains of was separated by SDS PAGE followed by immunoblot analysis using pre-immune serum (A) or CrCP12 antiserum (B) derived from rabbit. **C,** Sensitivity test for CrCP12 antiserum. Different dosages of recombinant CrCP12 proteins ranging from 10 pg to 100 µg were used in the test.

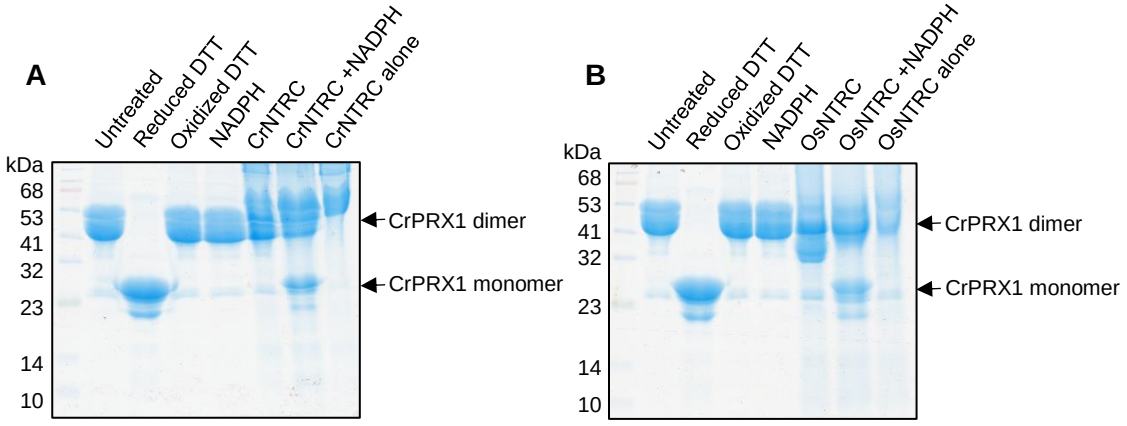

Supplemental Figure S4. Redox reactivity tests for recombinant CrNTRC and OsNTRC proteins. 2-Cys peroxiredoxin (PRX1) is a known redox target of NTRC, and hence was used as a positive control to test for redox reactivities of recombinant NTRC proteins of *C. reinhardtii* and *O. sativa*. 100 µg recombinant CrPRX1 proteins, were either treated or 30 mM of NADPH, 150 µg NTRC recombinant proteins or combination of both. Plain buffer solution was used as untreated control, while treatment with 5 mM of either reduced or oxidized DTT served as positive and negative controls respectively. The reaction mixes were then incubated for 1.5 hours at 37 °C before proceeding to non-reducing SDS-PAGE followed by Coomassie blue staining.

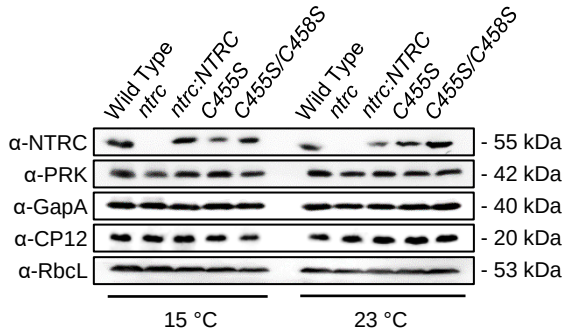

Supplemental Figure S5. Immunoblot analysis comparing PRK, GapA and CP12 proteins in *C. reinhardtii* strains of different *NTRC* genetic status, grown at 15 °C and 23 °C. Proteins were extracted from cultures which had been grown in TAP medium under 30 µE/m^2/s light at 23 °C or 15 °C for 48 hours. Equal RbcL levels indicate even loadings. Shown blot were representative from three repeated experiments with similar results.

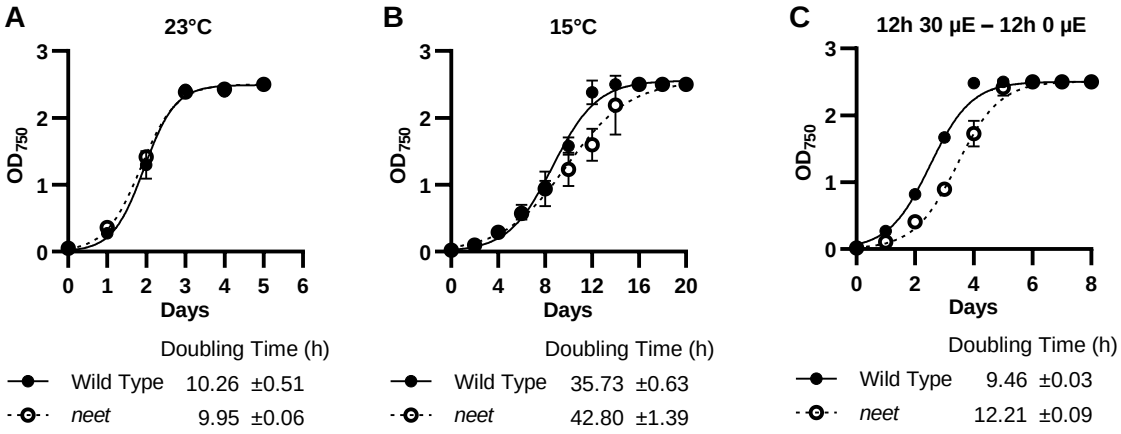

Supplemental Figure S6. Growth studies of *neet* knockout mutant of *C. reinhardtii*. Growth curves of wild type CC-406 and *neet* mutant strains of *C. reinhardtii* in TAPS medium under different conditions. OD_{750} was read every day or every other day until the saturation reached. Curves were plotted using GraphPad Prism v8, and doubling times were derived. All data presented are means and standard deviation of biological triplicates. **A – B,** Microalgal growths under continuous light of 30 µE/m^2/s, at 23 °C and 15 °C, respectively. **C,** Growths under cycle of 12-hour switching between 30 µE/m^2/s light and absolute dark, at room temperature.

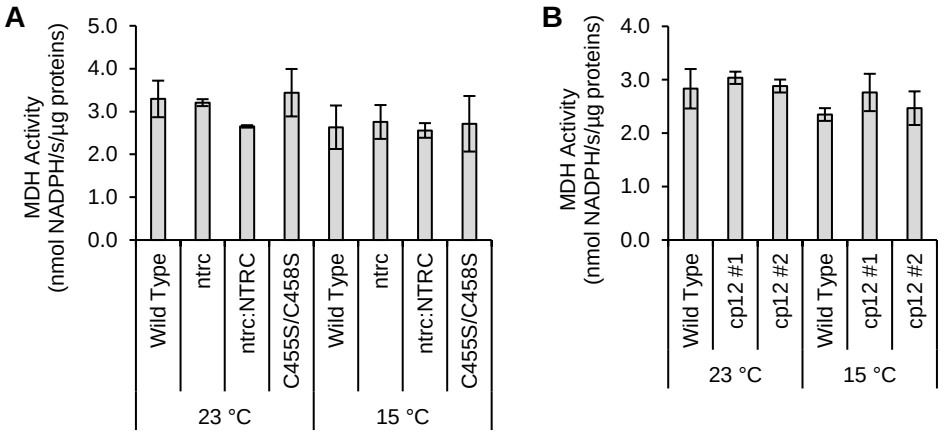

Supplemental Figure S7. Malate dehydrogenase (MDH) activity assays. A – B, *ntrc* and *cp12* mutants of *C. reinhardtii* cultured in TAP and TAPS medium, respectively, under 30 µE/m^2/s light at 23 °C or 15 °C for 48 hours. Soluble proteins were then extracted from these cultures for MDH enzyme activity measurement. Data presented are means and standard deviation of technical triplicates. The experiments have been repeated once with similar results obtained.

VI.1. Supplemental Tables

Supplemental Table S1. List of suppliers for materials and equipment.

Supplier	Address
Agrisera	Agrisera AB, Vännäs, Sweden
AppliChem	AppliChem GmbH, Darmstadt, Germany
Biosigma	Biosigma S.p.A., Cona (VE), Italy
Biogenes	BioGenes GmbH, Berlin, Germany
Bio-Rad Laboratories	Bio-Rad Laboratories GmbH, Feldkirchen, Germany
Biozym Scientific	Biozym Scientific GmbH, Hessisch Oldendorf, Germany
Bandelin Electronics	Bandelin Electronic GmbH & Co. KG, Berlin, Germany
Bruker Daltonik	Bruker Corporation, Billerica, USA
Carl Roth	Carl Roth GmbH + Co. KG, Karlsruhe, Germany
VWR	VWR International GmbH, Bruchsal, Germany
GE Healthcare	GE Healthcare GmbH, Munich, Germany
Integrated DNA Technologies	Integrated DNA Technologies Inc., Coralville, USA
Macherey-Nagel	Macherey-Nagel GmbH & Co. KG, Düren, Germany
Merck Milipore	Merck KGaA, Darmstadt, Germany
Microfluidics	Microfluidics, Westwood, Massachusetts, USA
Molecular Devices	Molecular Devices, San Jose, USA
Nepa Gene	Nepa Gene Co. Ltd., Chiba, Japan
New England Biolabs	New England Biolabs GmbH, Frackfurt am Main, Germany
NIPPON Genetics	NIPPON Genetics Europe GmbH, Düren, Germany
Photo Systems Instruments	Photo Systems Instruments spol. s.r.o., Drasov, Czech Republic
Pineda	Pineda Antikörper-Service, Berlin, Germany
Qiagen	Qiagen GmbH, Hilden, Germany
Roche	Roche Diagnostics GmbH, Mannheim, Germany
Sarstedt	Sarstedt AG & Co. KG, Nümbrecht, Germany
SERVA Electrophoresis	SERVA Electrophoresis GmbH, Heidelberg, Germany
Sigma-Aldrich	Sigma-Aldrich Chemie GmbH, Munich, Germany
Stratagene	Stratagene California, San Diego, USA
Thermo Fisher Scientific	Thermo Fisher Scientific Inc., Waltham, USA

Supplemental Table S2. List of oligonucleotides with their respective sequences used in the study. Fw and Rv are abbreviations for forward and reverse respectively. Restriction sites are underlined. Codes given are corresponding to the internal primer library of AG Nickelsen. All oligonucleotides were ordered from Sigma-Aldrich.

Codes	Oligonucleotides	Primer Sequences (5' → 3')
For generations of *C. reinhardtii* NTRC mutants:		
P-2227	NTRC cDNA Fw	GGATTCCATATGATGATACAGCTACCTGCAACAG
P-2228	NTRC cDNA-HA Rv	CGGAATTCTTAGGCGTAGTCCGGCACGTCGTAGGGGTA AGATCTCGCGGACACGGCGGC
P-2237	C455S primer	GGCAGGGCCCGGACGTGG
P-2240	C458S primer	GTGCGGGCCCTCCCGCAC
For knockout via CRISPR/Cas9 in *C. reinhardtii:*		
P-2891	FLAG Fw	GACTACAAAGACGATGACGACAAG
P-2892	CP12 short locus Fw	TCATATACAGGACTGCGCCG
P-2893	CP12 short locus Rv	AATTCAGGCCGGCTACTCAC
P-2894	CP12 long locus Fw	CCGGCGACAAACACACTATTAC
P-2895	CP12 long locus Rv	CGCCACTCAACCACCTAGTT
P-2896	NEET long locus Rv	TACCCACTGCACACCACACA
P-2897	NEET short locus Rv	ACCTTCTCCTCAGACTTCCG
P-2898	NEET short locus Fw	CTGCCCCTTTGCCCATTTAAG
P-2366	Flag-3xStop-EMX1 Fw	GACTACAAAGACGATGACGACAAGCTAATTAGCTAAG CCTCCCCAAAGCCTGGCCAGGGCTAATTAGCTAACTT GTCGTCATCGTCTTTGTAGTC
P-2367	Flag-3xStop-EMX1 Rv	GACTACAAAGACGATGACGACAAGTTAGCTAATTAGC CCTGGCCAGGCTTTGGGGAGGCTTAGCTAATTAGCTT GTCGTCATCGTCTTTGTAGTC
For recombinant protein syntheses:		
P-2885	CrNTRC cDNA Fw	CGCCATATGATGATACAGCTACCTGCAACAGTTGTGC
P-2884	CrNTRC cDNA Rv	CGCCTCGAGTCACGCGGACACGGCG
P-2888	CrCP12 cDNA Fw	CGCCATATGATGCAGCCCGCTGCGAG
P-2843	CrCP12 cDNA Rv	CGCCTCGAGTTAATCCTCGTAGACGCGGCACT
P-2932	AtCP12 cDNA Fw	CGCCATATGATGGCAACTATAGCTACTGGTCT
P-2854	AtCP12 cDNA Rv	CGCCTCGAGTCAGTTGTCGTAAGTACGGC
P-2887	CrPRX1 cDNA Fw	CGCCATATGATGGCCGCTCTGCAGTCTGC
P-2933	CrPRX1 cDNA Rv	CGCCTCGAGTTACACGGCAGAGAAGTACTCCTTGGA
P-1798	CrNTRC cDNA (98aa) Fw	GGATCCGAGGGCTTCCGCAATGGT
P-1799	CrNTRC cDNA (98aa) Rv	GAATTCTTACCGGCTCCAGAAGGTGTTC

Supplemental Table S3. Plasmids used in this study.

Plasmids	Description	Source/ Reference
pBeloBAC11: PTQ7836	Bacterial Artificial Chromosome (BAC) library plasmid containing *C. reinhardtii* NTRC gDNA	Clemson University Genetics Institute
pBC1	Plasmid vector used for protein expression in *C. reinhardtii* contains a paromomycin resistance cassette	Neupert et al. (2009)
pBC1: NTRC gDNA	pBC1 vector containing the wild-type *C. reinhardtii* NTRC gDNA	Generated in this work
pBC1: NTRC cDNA-HA	pBC1 vector containing the wild-type *C. reinhardtii* NTRC cDNA with HA-tag coding sequence.	Generated in this work
pBC1: NTRC cDNA (C455S)-HA	pBC1 vector containing the point-mutated *C. reinhardtii* NTRC cDNA, leading to the expression of a HA-tagged NTRC with C455S mutation	Generated in this work
pBC1: NTRC cDNA (C455S/C458S)-HA	pBC1 vector containing the point-mutated *C. reinhardtii* NTRC cDNA, leading to the expression of a HA-tagged NTRC with C455S and C458S mutations	Generated in this work
pBC1: NTRC gDNA-HA	pBC1 vector containing the wild-type *C. reinhardtii* NTRC gDNA with HA-tag coding sequence.	Generated in this work
pBC1: NTRC gDNA (C455S)-HA	pBC1 vector containing the point-mutated *C. reinhardtii* NTRC gDNA, leading to the expression of a HA-tagged NTRC with C455S mutation	Generated in this work
pBC1: NTRC gDNA (C455S/C458S)-HA	pBC1 vector containing the point-mutated *C. reinhardtii* NTRC gDNA, leading to the expression of a HA-tagged NTRC with C455S and C458S mutations	Generated in this work
pET-28b-Sumo	Plasmid vector used for the expression of recombinant 6xHis/Sumo fusion proteins in *E. coli*, contains a kanamycin resistance cassette	Bepperling et al. (2012)
pET-28b: CrNTRC-His	pET-28b vector containing the *C. reinhardtii* NTRC cDNA, used for the overexpression of recombinant His-tagged CrNTRC proteins in *E. coli*	Generated in this work
pET-28b: CrCP12-His	pET-28b vector containing the *C. reinhardtii* CP12 cDNA, used for the overexpression of recombinant His-tagged CrCP12 proteins in *E. coli*	Generated in this work
pET-28b: AtCP12-2-His	pET-28b vector containing the *A. thaliana* CP12-2 cDNA, used for the overexpression of recombinant His-tagged AtCP12-2 proteins in *E. coli*	Generated in this work
pET-28b: CrPRX1-His	pET-28b vector containing the *C. reinhardtii* PRX1 cDNA, used for the overexpression of recombinant His-tagged CrPRX1 proteins in *E. coli*	Generated in this work
pQE-30: OsNTRC	pQE-30 vector containing the *O. sativa* NTRC cDNA, used for the overexpression of recombinant His-tagged OsNTRC proteins in *E. coli,* also contains an ampicillin resistance cassette	Provided by Prof. Cejudo (Serrato et al., 2004)
pMal-c5x	Plasmid vector used for the expression of recombinant MBP fusion proteins in *E. coli*, contains an ampicillin resistance cassette	GE Healthcare
pMal: CrNTRC (98 aa)	pMal-c5x vector containing a part of the *C. reinhardtii* NTRC cDNA, used for the overexpression of recombinant MBP-tagged CrNTRC proteins (98 aa) in *E. coli*	Generated by Dr. Daniel Neusius

Autotrophic Growth (HSM, 23 °C)

Growth Doubling	30 µE/m2/s		100 µE/m2/s	
Time (hours)	Mean	SD	Mean	SD
Wild Type	40.20	3.31	23.18	0.71
ntrc	59.52	6.35	24.52	0.83
ntrc: NTRC	40.00	3.03	22.75	0.49
C455S	61.12	0.54	24.01	2.99
C455S/C458S	65.99	2.79	25.58	2.19

Supplemental Table S4. Low light phenotype of *C. reinhardtii ntrc* knockout and cysteine-substituted strains. Liquid cultures of the strains were grown in HSM at 23 °C under 30 µE/m^2/s or 100 µE/m^2/s. Cell densities were recorded every second day as OD_{750} to derive doubling times. Averages and standard deviations (SD) were calculated from biological triplicates.

Cold & High Light Stress (15 °C, 100 µE/m^2/s)

Growth Doubling	TAP		HSM	
Time (hours)	Mean	SD	Mean	SD
Wild Type	23.77	2.57	33.33	0.27
ntrc	54.82	4.44	58.00	8.77
ntrc:NTRC	21.44	0.82	30.00	1.56
C455S	51.02	5.67	59.91	5.53
C455S/C458S	64.19	6.92	52.33	4.26

Supplemental Table S5. Growth studies of *C. reinhardtii ntrc* knockout and cysteine-substituted strains under cold and high light stress. Liquid cultures of the strains were grown at 15 °C, 100 µE/m^2/s, in TAP or HSM. Cell densities were recorded every second day as OD_{750} to derive doubling times. Averages and standard deviations (SD) were calculated from biological triplicates.

Supplemental Table S6. Table presenting potential NTRC interaction partners of interest pulled down in HA-based NTRC co-IP assay.

Phytoyome Accession Number	Protein Candidates	30µE/m²/s Light			Redox Dependency		# of Cysteine	Size (kDa)	Functional Catogories	Chloroplast Transit Peptide
		23°C	23°C	15°C						
		HSM	TAP	TAP	C455S	C455S/C458S				
Cre06.g257601	2-Cys Peroxiredoxin (PRX1)	x	x	x	↓	↓↓	2	25.9	Oxidative Stress	x
Cre15.g641600	Predicted Protein_A8JHI9	x	x	x	–	–	9	14.1	Unknown	–
Cre02.g104300	Uncharacterized Protein_A8I4C6	–	–	x	↑	–	11	58.0		Mitochondrial
Cre01.g050550	Predicted Protein_A8HND3 -- CrNEET	–	–	x	–	↓↓	3	10.5		x
Cre10.g447950	Predicted Protein_A8HZF9 -- Rab25	–	–	x	–	–	2	21.5		x
Cre10.g436550	Low CO2 inducible protein (LCI5 or EPYC1)	x	x	x	↑	–	0	32.3	Carbon Fixation	x
Cre08.g380250	Calvin cycle protein (CP12)	–	–	x	↓	↓↓	4	14.0		x
Cre07.g328150	Protein Disulphide Isomerase (PDI4)	x	x	–	↓	↓↓	10	48.5	Protein Metabolism	–
Cre06.g250100	Heat Shock Protein 70B (HSP70B)	–	–	x	–	–	3	72.0		x
Cre06.g273700	PSII stability/assembly factor (HCF136)	–	–	x	–	–	1	32.6		x
Cre07.g352850	Plastid Ribosomal Protein L32 (PRPL32)	x	–	–	–	–	0	10.6		x
Cre10.g435300	Aspartyl aminopeptidase-like protein (AAP1)	x	–	–	–	–	8	60.4		x
Cre03.g158900	Pyruvate Dehydrogenase E2 (DLA2)	x	–*	x	–	–	2	63.0	Lipid Metabolism	x
Cre08.g359350	Biotin Carboxylase (AccC)	–	–	x	–	–	7	52.0		x
Cre01.g037850	Acetyl-coA biotin carboxyl carrier (BCC2/AccB)	x	–	–	–	–	4	24.3		x

The study was conducted using *C. reinhardtii* cultured in three different growth conditions as indicated in the table. 'x' marks binding to NTRC and the arrows indicate quantitative changes in binding enrichment detected by mass spectrometry due to single or double cysteine mutations in the CGPC motif of NTRC protein. The existence of chloroplast transit peptide is predicted by using PredAlgo online tool (http://lobosphaera.ibpc.fr/cgi-bin/predalgodb2.perl?page=main). * Despite a lacking signal in MS, DLA2 was detected by western blot analysis under these conditions (data not shown). A full set of the MS data can be accessed online, refer to section II.12 for instruction.

LIST OF ABBREVIATIOBS

1,3BPGA	1,3-bisphosphoglycerate
3PGA	3-phosphoglycerate
3'UTR	3'-unstranslated region
5'UTR	5'-unstranslated region
A_2B_2-GAPDH	GAPDH heterotetramer composed of 2 GapA and 2 GapB subunits
A_4-GAPDH	GAPDH homotetramer composed of 4 GapA subunits
aa	amino acids
ADP	adenosine diphosphate
AGPase	ADP-glucose pyrophosphorylase
APX	ascorbate peroxidase
At or *A. thaliana*	*Arabidopsis thaliana*
ATP	adenosine triphosphate
C or Cys	cysteine
Cas9	caspase 9
CCM	CO_2-concentrating mechanism
cDNA	complementary DNA
CGPC	cysteine-glycine-proline-cysteine motif
CKABP	2-carboxy-3-keto-1,5-bisphosphoribotol
CP12	Calvin Cycle Protein 12
Cr or *C. reinhardtii*	*Chlamydomonas reinhardtii*
CRISPR	Clustered Regularly Interspaced Short Palindromic Repeats
C-terminus	carboxyl-terminus
CTE	C-terminal extension
DNA	deoxyribonucleic acid
DTT	dithiothreitol
E4P	erythrose-4-phosphate
ECL	enhanced chemiluminescence
EDTA	ethylenediaminetetraacetic acid
ETC	electron transport chain
FBPase	fructose 1,6-bisphosphatase
FLAG	epitope with peptide sequence: DYKDDDDK
F_m	maximum fluorescence in the dark-adapted state
$F_{m\text{-}Lss}$	maximum fluorescence in light-adapted steady state
FNR	ferredoxin-$NADP^+$ reductase

F_o	minimum fluorescence
F_v	viable fluorescence
G6P	glucose 6-phosphate
GapA	GAPDH subunit A
GapB	GAPDH subunit B
GAP	glyceraldehyde 3-phosphate
GAPDH	glyceraldehyde 3-phosphate dehydrogenase
Gly	glycine
gRNA	guide RNA
GSNO	S-nitrosoglutathione
GSSG	glutathione disulfide
HA	human influenza hemagglutinin
His	histidine
HRP	horseradish peroxidase
HSM	high salt minimal medium
HSP	heat shock proteins
IDP	intrinsically disordered protein
IP	immunoprecipitation
K_d	dissociation constant
LC-MS	liquid chromatography-tandem mass spectrometry
LDH	lactate dehydrogenase
LHC	light harvesting complex
MBP	maltose binding protein
MDH	malate dehydrogenase
mRNA	messenger RNA
mt	mating type
NAD^+	oxidized nicotinamide adenine dinucleotide
NADH	reduced nicotinamide adenine dinucleotide
$NADP^+$	oxidized nicotinamide adenine dinucleotide phosphate
NADPH	reduced nicotinamide adenine dinucleotide phosphate
NPQ	non-photochemical quenching
Ni-NTA	nickel-charged nitrilotriacetic acid
N-terminus	NH_2- or amino-terminus
NTR	NADPH-thioredoxin reductase
NTRC	NADPH-dependent thioredoxin reductase C
OD_{750}	optical density at 750nm wavelength

oligo-dT	oligo-deoxythymine
OPPP	oxidative pentose phosphate pathway
Os or *O. sativa*	*Oryza sativa*
Ox	oxidized
PAGE	polyacrylamide gel electrophoresis
PCR	polymerase chain reaction
PK	pyruvate kinase
PRK	phosphoribulokinase
PRX1	2-Cys peroxiredoxin
PSI	photosystem I
PSII	photosystem II
PsaD	PSI reaction center subunit II
PGK	phosphoglycerate kinase
pmf	proton motive force
Pp	*Physcomitrella patens*
Pro	proline
Rd	reduced
RNA	ribonucleic acid
RNAi	RNA interference
ROS	reactive oxygen species
Ru5P	ribulose-5-phosphate
R5P	ribose-5-phosphate
Rubisco	ribulose-1,5-bisphosphate carboxylase/oxygenase
RuBP	ribulose-1,5-bisphosphate
S or Ser	serine
SBPase	sedoheptulose-1,7-bisphosphate
SEC	size exclusion chromatography
Sp	*Streptococcus pyogenes*
Sy	*Synechocystis sp.* PCC 6803
TAP	tris-acetate-phosphate medium
TAPS	tris-acetate-phosphate medium + 1 % sorbitol
TBS	tris-buffered saline
T-DNA	transfer-DNA of the tumour-inducing agrobacterial plasmid
TEM	transmission electron micrograph
Trx or TR	thioredoxin
Xu5P	xylulose-5-phosphate

ACKNOWLEDGEMENT

First of all, I would like to thank Prof. Dr. Joerg Nickelsen, the core-supervisor of this research project for providing valuable guidance and supports to me over the past 4 years. Next, I really appreciate the collaboration with AG Geigenberger. Prof. Dr. Peter Geigenberger and Verena Leitz not only provided constructive opinions during our discussions but also shared protocols and materials for the enzyme activity assays. Verena has also contributed to preparing the *A. thaliana* samples for the gel filtration assay and conducting other related studies of NTRC and CP12 in *A. thaliana* which are not presented in this thesis. Dr. Daniel Neusius's efforts in generating the NTRC antiserum and doing some other preliminary studies of NTRC (data not shown) during the early state of the project, are deeply appreciated as well. I am also grateful to Dr. Giada Marino's contribution in performing mass spectrometry analysis for the NTRC co-IP eluates.

Further, I would also like to thank Prof. Dr. Krishna K. Niyogi and Prof. Dr. Renate Scheibe for their generous gifts of *ntrc* knockout mutant strain of *C. reinhardtii* and antisera against PRK and GAPDH, respectively. It was really nice that Prof. Peter Hegemann shared with us CRISPR/Cas9 protocol for *C. reinhardtii* established in his lab. Thanks to PD Dr. Alexandra-Viola Bohne, with her precious advice, I saved lots of time in doing bioinformatic analysis for the whole bunch of NTRC binding candidates. She also proofread the first draft of this thesis and advised in the writing. Also, my gratitude to SFB-TRR175 (The Green Hub: Central Coordinator of Acclimation in Plants) for funding the research. I am also thankful to the Graduate School Life Sciences Munich (LSM) program of LMU, and its previous and current coordinators – Francisca Rosa Mende and Nadine Hamze, for organizing lectures and useful workshops as well as giving assistance in the administration stuffs.

I would also like to thank my colleagues, Korbinian Dischinger, Dr. Annabel Mechela and Julia Hamm for their patient cares especially in German translation for letters, online information as well as the abstract of this thesis, helping me to survive through the past 4 years with my poor command of German language. Korbinian was also a good teacher, tutoring me with my homework for German language courses. Yet, my German is still very bad. I am sorry, I have been impersistent in learning the language, though I do like your country and you people a lot! I also very much appreciate that Karin and Simone Boos, the lab technicians cum managers have maintained everything in the lab in a good order. Thanks also to the other pervious and current members of the big family of AG Nickelsen – Dr. Montserrat Jarquin, Dr. Steffen Heinz, and Matthias Ostermeier for being nice, friendly, and more importantly fun and humorous! I appreciate our friendships.

Lastly, I would like to reiterate that without supports from all of you, it is impossible to bring my doctoral study to fruition. I do have had a good time in Germany. Thank you.

EIDESSTATTLICHE ERKLÄRUNG

Eidesstattliche Erklärung

Ich versichere hiermit an Eides statt, dass die vorgelegte Dissertation von mir selbständing und ohne unerlaubte Hilfe angefertigt ist.

I hereby declare that the submitted dissertation has been prepared by myself independently, without unauthorized help.

München, den 09 August 2021 _____

Jing Tsong Teh

Erklärung

Hiermit erkläre ich, dass die Dissertation nicht ganz oder in wesentlichen Teilen einer anderen Prüfungskommission vorgelegt worden ist. Des Weiteren habe ich mich nicht anderweitig einer Doktorprüfung ohne Erfolg unterzogen.

I hereby declare that this dissertation has not been submitted in whole or in part to any other examination committee. Furthermore, I have never taken any other doctoral examination.

München, den 09 August 2021 _____

Jing Tsong Teh